UNIVERSIDADE FEDERAL DE MINAS GERAIS

Escola de Engenharia

Programa de Pós-graduação em Engenharia Metalúrgica, Materiais e de Minas

Nelson Henrique Jardim Freire

Novel flow electrodes for increased ion removal rate and energy consumption reduction in flow-electrode capacitive deionization

Belo Horizonte

2023

Nelson Henrique Jardim Freire

Novel flow electrodes for increased ion removal rate and energy consumption reduction in flow-electrode capacitive deionization

Tese de doutorado apresentado ao Programa de Pós-Graduação em Engenharia Metalúrgica, Materiais e de Minas da Escola de Engenharia da Universidade Federal de Minas Gerais, como requisito parcial para obtenção do Grau de Doutor em Engenharia Metalúrgica, Materiais e de Minas.

Orientadora: Prof.a Virginia Sampaio Teixeira Ciminelli

Coorientador: Prof. Luciano Andrey Montoro

Belo Horizonte

2023

UNIVERSIDADE FEDERAL DE MINAS GERAIS
ESCOLA DE ENGENHARIA
Programa de Pós-Graduação em Engenharia
Metalúrgica, Materiais e de Minas

PPGEM
UFMG

A tese intitulada **"Novel Flow Electrodes for Increased Ion Removal Rate and Energy Consumption Reduction in Flow-electrode Capacitive Deionization"**, área de concentração: Tecnologia Mineral, apresentada pelo candidato <u>**Nelson Henrique Jardim Freire**</u>, para obtenção do grau de Doutor em Engenharia Metalúrgica, Materiais e de Minas, foi aprovada pela comissão examinadora constituída pelos seguintes membros:

Documento assinado digitalmente
VIRGINIA SAMPAIO TEIXEIRA CIMINELLI
Data: 13/11/2023 13:39:45-0300
Verifique em https://validar.iti.gov.br

Dra. Virginia Sampaio Teixeira Ciminelli
Orientadora (UFMG)
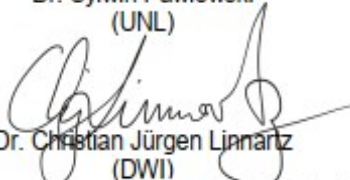
Documento assinado digitalmente
LUCIANO ANDREY MONTORO
Data: 15/11/2023 22:02:18-0300
Verifique em https://validar.iti.gov.br

Dr. Luciano Andrey Montoro
Coorientador (UFMG)

Sylwin
Pawlowski

Digitally signed by Sylwin Pawlowski
DN: cn=Sylwin Pawlowski, o, ou=LAQV-
FCT-NOVA,
email=s.pawlowski@fct.unl.pt, c=PT
Date: 2023.11.14 16:07:04 Z

Dr. Sylwin Pawlowski
(UNL)

Dr. Christian Jürgen Linnartz
(DWI)

Documento assinado digitalmente
SONIA DENISE FERREIRA ROCHA
Data: 13/11/2023 16:43:07-0300
Verifique em https://validar.iti.gov.br

Dra. Sônia Denise Ferreira Rocha
(UFMG)

Documento assinado digitalmente
DANIEL MAJUSTE
Data: 13/11/2023 16:01:24-0300
Verifique em https://validar.iti.gov.br

Dr. Daniel Majuste
(UFMG)

Documento assinado digitalmente
EDUARDO HENRIQUE MARTINS NUNES
Data: 15/11/2023 17:51:20-0300
Verifique em https://validar.iti.gov.br

Coordenador do Programa de Pós-Graduação em
Engenharia Metalúrgica, Materiais e de Minas/UFMG

Belo Horizonte, 09 de novembro de 2023

Agradecimentos

Agradeço a toda minha família pelo incentivo e ajuda. Agradeço em especial a minha mãe, pelo orgulho, exemplo e apoio incondicional, e a minha avó por todo o carinho. Ao meu avô (in Memorian), pelo exemplo devida.

Aos amigos de toda a vida, por estarem presentes mesmo com a distância. À Natália, por me aguentar sempre, e por sempre me incentivar. À Flávia, por todo o cuidado e apoio que sempre me deu, e foi fundamental para que eu chegasse aqui.

Aos novos amigos de Aachen: Siqi, Waralee, Felipe, Marcela, Eleni, Leandro, Valerinha e Meike por toda ajuda e companheirismo nessa jornada em Aachen. A amizade de vocês é muito especial.

Sou imensamente grato à minha orientadora Prof.ª Virginia Ciminelli, pelo exemplo de excelência e dedicação. Por me fazer crescer enquanto pesquisador e aluno desde o meu trabalho de conclusão de curso no bacharelado, pelas críticas que me fizeram buscar melhorar e pelo tempo dedicada à minha pesquisa e desenvolvimento desta tese. Ao meu coorientador Prof. Luciano Montoro, pelos vários ensinamentos e por todo seu tempo e paciência nas minhas questões científicas. Ao Prof. Daniel Majuste, por todo apoio e ensinamento no bacharelado, mestrado e outros projetos que trabalhamos juntos. Os ensinamentos de vocês foram fundamentais para que eu chegasse até aqui.

À Prof.ª Andreia Bicalho por toda a ajuda durante a pandemia e pelas análises difração de raios X. Ao Prof. Paulo Brandão pelas análises de Espectrocospia no Infravermelho. Ao Prof. Eduardo Nunes por se disponibilizar diversas vezes para analisar minhas amostras, pelos ensinamentos científicos, e por ajudar a todos os alunos sempre. Ao Prof. Vicente Buono e ao seu laboratório por todos os cafés, conselhos e apoio.

Aos amigos do Laboratório de Hidrometalurgia pelo convívio prazeroso, longas conversas, trocas de conhecimento, cafés e lanches. Agradeço principalmente a Taiane, Marina, Saulo, Poliana, Tamiris, Victor, Nathanael, Thaiara, Daísa e Eric pelo ótimo tempo juntos. Obrigado ao Eric por aceitar continuar no projeto enquanto me ausentei no doutorado sanduíche. À Taiane, um imenso obrigado pelas longas horas extras no laboratório, companhia, discussões científicas e colaborações. À Ilda por espalhar alegria pelo laboratório e pela disponibilidade em nos ajudar, e por me ensinar a fazer pão de queijo à distância. À Claudia Caldeira e Christina Salvador pela presteza e disponibilidade em ajudar sempre. À Patrícia e, Hellen e Filipe pelas análises químicas e inúmeros ajudas para manter o laboratório funcionando sempre.

Resumo

A separação e a remoção de íons da água são essenciais para atender às restrições cada vez maiores de emissões de poluentes de águas residuais e reutilização de água. Além disso, novas tecnologias são necessárias para fornecer água potável aos locais em áreas afetadas pela seca. Por fim, os íons normalmente descartados nas águas residuais podem ser recuperados como subprodutos em operações industriais. A deionização capacitiva por eletrodo de fluxo (FCDI) é uma das técnicas que atrai a atenção devido às possíveis vantagens em relação às tecnologias estabelecidas, como a remoção específica de íons, a operação contínua e o tratamento de água com alta salinidade. Uma das principais desvantagens da FCDI é a maior resistência elétrica do eletrodo de fluxo em comparação aos eletrodos estáticos típicos. Algumas tentativas de usar outros materiais, como os análogos de azul da Prússia, resultaram em um desempenho de dessalinização ainda pior devido à menor condutividade desses materiais em relação aos sólidos à base de carbono. Portanto, este trabalho se concentrou na redução do consumo de energia e no aumento da produtividade do FCDI, melhorando a transferência de carga no sistema. O desempenho da dessalinização obtido com os eletrodos modificados é comparado ao do FCDI com polpas de carvão ativado (CA). A aplicação do hexacianoferrato de níquel (NiHCF) como material ativo no eletrodo de fluxo foi estudada juntamente com o cianeto de ferro $[Fe(CN)_6]^{3-}$ como mediador redox. Os eletrodos de fluxo com NiHCF e o mediador redox apresentaram o dobro da corrente em comparação com os eletrodos de fluxo típicos com CA. Em comparação com o sistema em que o mediador redox também é adicionado ao eletrodo de fluxo com CA, o sistema com NiHCF e mediador redox também apresentou correntes mais altas e mais estáveis durante a dessalinização. Devido à melhora da performance de dessalinização com a adição de um mediador redox aos eletrodos de fluxo com CA, o cloreto de ferro (Fe-Cl), o citrato de ferro (Fe-Cit) e o carvão ativado também foram investigados. Foi demonstrado que, mesmo na concentração de 0,05 M de Fe-Cl, a taxa de dessalinização é maior do que a das polpas de CA. Além disso, um efeito sinérgico é observado quando o CA e o Fe-Cl são misturados. A taxa de dessalinização é aumentada em até 100% para a mistura de CA - 0,2 M de Fe-Cl. A adição de citrato férrico em concentrações de 0,2 M aumentou a dessalinização em 23%. Foi demonstrado que a adição de pares redox é uma estratégia relevante para melhorar o desempenho do FCDI, o que provavelmente o tornará mais competitivo em relação a outras tecnologias.

Palavras-chave: flow electrodes; flow-electrode capacitive deionization; separação eletroquímica; dessalinização.

Abstract

The separation and removal of ions from water is essential to comply with increasingly restricted wastewater pollutant emissions and water reuse. Furthermore, new technologies are necessary to provide the locals with quality water in drought-affected areas. Finally, ions usually discharged in the wastewater can be recovered as valuable by-products in industrial operations. Flow electrode capacitive deionization FCDI is one of the techniques attracting attention due to potential advantages relative to the established technologies, such as specific ion removal, continuous operation, and the treatment of high salinity water streams. One major drawback of FCDI is the higher electrical resistance of the flow electrode compared to typical static electrodes. Few attempts to use other materials, such as Prussian-Blue Analogs, resulted in even worse desalination performance due to the lower conductivity of these materials relative to carbon-based materials. Hence, this work focused on reducing energy consumption and increasing the productivity of FCDI by improving the charging transfer in the system. The desalination performance achieved with the modified electrodes is compared to that of typical FCDI with activated carbon (AC) slurries. The application of nickel hexacyanoferrate (NiHCF) as an active material in the flow electrode was studied along with ferricyanide $[Fe(CN)_6]^{3-}$ as a redox mediator. The flow electrodes with NiHCF and a redox mediator showed twice the current compared to typical flow electrodes with AC. Compared to the system where the redox mediator is also added to the AC flow electrode, the system with NiHCF and redox mediator also showed higher and more stable currents during desalination. Due to the improvement of adding a redox mediator to AC- flow electrodes, iron chloride (Fe-Cl), iron citrate (Fe-Cit), and activated carbon were also investigated. It is demonstrated that even at a concentration of 0.05 M Fe-Cl, the desalination rate is higher than AC-only slurries. Also, a synergetic effect is observed when AC and Fe-Cl are mixed. The desalination rate is enhanced up to 100% for the AC - 0.2 M of Fe-Cl mixture, and the addition of ferric citrate at concentrations of 0.2 M increased desalination by 23%. It is demonstrated that adding redox couples is a relevant strategy to improve the FCDI performance, and this will likely make it more competitive against other technologies.

Keywords: flow electrodes; flow-electrode capacitive deionization; electrochemical separation; desalination.

List of Figures

List of Tables

List of acronyms

AC – Activated Carbon

AEM – Anion Exchange Membrane

ATR – Attenuated Total Reflectance

CDI – Capacitive Deionization

CEM – Cation Exchange Membrane

CuHCF – Copper Hexacyanoferrate

FCDI – Flow-Electrode Capacitive Deionization

Fe-Cl – Iron Chloride

Fe-Cit – Iron Citrate

FT-IR – Fourier Transform Infra-Red spectroscopy

ICC – Isolated closed-cycle

ICP-OES – Inductively Coupled Plasma Optical Emission Spectrometry

MCDI – Membrane Capacitive Deionization

NiHCF – Nickel Hexacyanoferrate

RM – Redox Mediator

SCC – Short-circuited closed cycle

SEM – Scanning Electron Microscopy

SM – Single Module

XRD – X-Ray Diffraction

Summary

1 Introdução

Prevê-se que a demanda global de água aumente em cerca de 55% nos próximos cinquenta anos, o que levará ao estresse hídrico no planeta (Ma et al., 2020). Atualmente, 4,0 bilhões de pessoas sofrem de escassez severa durante alguma parte do ano (Mekonnen e Hoekstra, 2016), e é cada vez mais necessário produzir água potável de fontes não convencionais, como água subterrânea e água do mar (Jones et al., 2019). No entanto, essas duas fontes têm elevada quantidade de sal e muitas vezes são inadequadas para a agricultura e o consumo humano. O estado da arte da dessalinização é a osmose inversa, mas esse processo é mais eficiente para o tratamento de água em concentrações mais altas de sal, sendo menos eficiente para tratar água salobra. Para água salobra, por exemplo, foi demonstrado recentemente que outra técnica, chamada eletrodiálise, é energeticamente mais eficiente do que a osmose inversa para concentrações de até 3 g L^{-1} de NaCl (Patel et al., 2021). Além disso, a osmose inversa e a eletrodiálise têm alto consumo de energia, variando de 0,2 kWh m^{-3} e 1,2 kWh m^{-3}, dependendo da produtividade, da remoção de sal, da concentração de sal na água de alimentação e da recuperação de energia no caso da osmose inversa. Além disso, tanto a eletrodiálise quanto a osmose inversa são tecnologias maduras e estão próximas de sua eficiência máxima esperada.

Dessa forma, é relevante desenvolver novas tecnologias para lidar com a questão da escassez de água. Assim, uma nova tecnologia chamada de deionização capacitiva (CDI) tem atraído grande interesse nos últimos anos, principalmente devido ao seu menor consumo de energia - 0,4 kWh m^{-3} (Suss et al., 2015). O ciclo operacional de uma célula CDI consiste em aplicar uma diferença de potencial entre dois eletrodos, que geralmente são feitos de carvões ativados devido à sua grande área de superfície específica. Os cátions presentes na solução são atraídos para o eletrodo carregado negativamente, e os ânions são atraídos para o eletrodo carregado positivamente até a saturação completa da superfície disponível nos eletrodos. A polaridade da célula é então invertida para que os íons sejam dessorvidos, gerando um efluente de alta concentração de sal. Embora o CDI seja interessante do ponto de vista energético, ele tem uma importante desvantagem, pois tem um ciclo operacional intermitente - uma etapa de carga para a adsorção e uma etapa de descarga para a dessorção. A operação intermitente e a baixa capacidade de adsorção devido à pequena dimensão dos eletrodos impedem que o CDI seja aplicado em escala industrial.

Recentemente, uma nova arquitetura foi desenvolvida como uma alternativa ao ciclo intermitente das células CDI. Em vez de ter dois eletrodos com carvão ativado, os eletrodos

agora consistem em uma suspensão aquosa de carvão ativado. Essa suspensão pode ser então armazenada em tanques fora da célula, e o limite de adsorção de sal não está mais ligado à área de superfície do carvão ativado, mas sim ao volume total de suspensão disponível (Jeon et al., 2013; Ma et al., 2018). Além disso, os eletrodos de fluxo podem ser regenerados continuamente fora da célula. A mudança da operação intermitente para a contínua representará um desenvolvimento significativo, considerando as aplicações comerciais. Essa nova arquitetura é conhecida como deionização capacitiva por eletrodo de fluxo (FCDI).

Embora o FCDI tenha demonstrado a viabilidade da dessalinização contínua, essa tecnologia ainda está em sua infância, e vários desafios precisam ser resolvidos antes que o FCDI possa ser introduzida no mercado. Ainda é necessário entender melhor os parâmetros que afetam as células FCDI para melhorar o seu desempenho:

i. Consumo de energia: O FCDI sofre com a baixa condutividade intrínseca nos eletrodos de fluxo e com o consumo de energia no bombeamento da suspensão de carvão ativado.

ii. Estabilidade de operação e aplicações: Apenas alguns estudos avaliaram a operação do FCDI por um período prolongado - 2 semanas. Além disso, o FCDI tem se concentrado mais na dessalinização, e outras aplicações podem ser exploradas.

iii. Recuperação de água: a recuperação de água é um parâmetro essencial no processo de dessalinização, e o FCDI tem se mostrado vantajosa em relação a outros processos de membrana. Ainda é necessário entender os fatores que influenciam a recuperação de água no FCDI.

iv. Custos de capital: Como o FCDI é uma tecnologia nova, faltam testes em escala piloto. Além disso, estudos recentes modificaram a célula FCDI para criar um desenho que pode ser mais facilmente escalonado e reduzir os custos da montagem da célula.

Este projeto aborda alguns dos problemas do FCDI e visa desenvolver ainda mais esta técnica e ampliar sua aplicabilidade. Especificamente, procuramos reduzir o consumo de energia da FCDI adicionando aditivos nos eletrodos de fluxo para melhorar a transferência de carga e, consequentemente, reduzir a resistência elétrica dos eletrodos de fluxo. Além disso, um novo material eletroativo é testado no eletrodo de fluxo para aumentar a taxa de dessalinização e reduzir a viscosidade da suspensão, reduzindo o consumo de energia.

1.1 Objetivos

O principal objetivo deste projeto é reduzir o consumo de energia e aumentar a produtividade da deionização capacitiva por eletrodos de fluxo modificando os eletrodos de fluxo para melhorar sua transferência de carga. Os objetivos específicos são:

i. Investigar o análogo de azul da Prússia, o hexacianoferrato de níquel (NiHCF) como material ativo no eletrodo de fluxo. Identificar o par redox adequado para atuar como mediador redox (RM) para melhorar a transferência de carga no eletrodo de fluxo.

ii. Melhorar a transferência de carga em eletrodos de fluxo de carbono ativado usando cloreto de ferro e citrato de ferro como pares redox. Determinar o efeito da concentração de ferro solúvel e do pH dos eletrodos de fluxo em experimentos de dessalinização.

1.2 Estrutura da tese e organização

Esta tese está organizada em cinco capítulos. Os Capítulos 1 e 2 contextualizam o trabalho e apresenta brevemente a deionização capacitiva por eletrodo de fluxo. Em seguida, são apresentadas as principais lacunas na literatura e os objetivos da tese. O Capítulo 3 apresenta uma revisão da literatura sobre o desenvolvimento do FCDI, suas principais aplicações e as modificações propostas para melhorar a condutividade do eletrodo de fluxo.

O Capítulo 4 apresenta a aplicação do hexacianoferrato de níquel (NiHCF) como um material ativo no eletrodo de fluxo. É demonstrado que o NiHCF pode ser usado no eletrodo de fluxo se um mediador redox for adicionado ao eletrólito. Esse trabalho foi enviado como um manuscrito, "Enhanced desalination performance with flow electrodes based on nickel hexacyanoferrate and redox mediator".

O Capítulo 5 apresenta a aplicação de pares redox à base de ferro para melhorar os eletrodos de fluxo de carbono ativado típicos usados nas células FCDI. Foi demonstrado que o cloreto de ferro é um reagente interessante devido ao seu baixo custo e à melhoria na taxa de dessalinização em comparação com os eletrodos de fluxo FCDI típicos. Em seguida, também foi demonstrado que o citrato de ferro pode melhorar o desempenho de dessalinização da célula. Este capítulo foi enviado como um manuscrito intitulado "Flow electrode capacitive deionization with iron-based redox electrolyte".

Os Capítulos 6 e 7 destacam os principais resultados obtidos por esta pesquisa e sugere tópicos para investigações futuras. O Apêndice A e o Apêndice B fornecem informações e

figuras adicionais para os Capítulos 4 e 5, respectivamente. Essas figuras foram enviadas como material suplementar para os manuscritos correspondentes.

2 Introduction

The global water demand is projected to increase by around 55% in the next fifty years, which will lead to water stress on the planet (Ma et al., 2020). Currently, 4.0 billion people experience severe scarcity during some part of the year (Mekonnen and Hoekstra, 2016), and it is increasingly necessary to produce drinking water from unconventional sources such as groundwater and seawater (Jones et al., 2019). However, these two sources have a large amount of salt and often are unsuitable for agriculture and human consumption. The state of the art of desalination is reverse osmosis, but this process is more efficient for water treatment in higher salt concentrations, being less efficient to treat brackish water. For brackish water, for example, it was demonstrated recently that another technique called electrodialysis is more energetically efficient than reverse osmosis for concentration up to 3 g L^{-1} of NaCl (Patel et al., 2021). In addition, reverse osmosis and electrodialysis have high energy consumption, ranging from 0.2 kWh m^{-3} to 1.2 kWh m^{-3} depending on productivity, salt removal, the salt concentration in the feedwater, and energy recovery in the case of reverse osmosis. Furthermore, both electrodialysis and reverse osmosis are mature technologies, and they are close to their maximum expected efficiency.

In this way, it is relevant to develop new technologies to address the issue of water scarcity. Thus, a new technology called capacitive deionization (CDI) has attracted great interest in recent years, mainly due to its lower energy consumption – 0.4 kWh m^{-3} (Suss et al., 2015). The operating cycle of a CDI cell consists of applying a potential difference between two electrodes, which are usually made of activated carbons due to their large specific surface area. The cations present in the solution are attracted to the negatively charged electrode, and anions are attracted to the positively charged electrode until complete saturation of the area available in the electrodes. The cell's polarity is then reversed so that the ions are desorbed, generating an effluent of high salt concentration. Although the CDI is interesting from an energetic point of view, it has a significant disadvantage since it has an intermittent operating cycle – one charge step for the adsorption and a discharge step for desorption. The intermittent operation and low adsorption capacity due to the small dimension of the electrodes prevent the CDI from being applied on an industrial scale.

Recently, a new architecture was developed as an alternative to the intermittent cycle of the CDI cells. Instead of having two electrodes with activated carbon, the electrodes now consist of an aqueous suspension of activated carbon. This suspension can then be stored in tanks

outside the cell, and the salt adsorption limit is no longer linked to the surface area of the activated carbon but rather to the total suspension volume available (Jeon et al., 2013; Ma et al., 2018). Furthermore, the flow electrodes can be continuously regenerated outside the cell. The change from intermittent to continuous operation will represent a significant development considering commercial applications. This new architecture is known as flow-electrode capacitive deionization (FCDI).

Although FCDI has demonstrated the feasibility of continuous desalination, this technology is still in its infancy, and several challenges must be resolved before FCDI can be introduced in the market. It is still necessary to understand better parameters that affect FCDI cells to improve performance:

i. Energy consumption: FCDI suffers from intrinsic low conductivity in the flow-electrodes and pumping energy dissipation associated with electrode circulation.

ii. Operation stability and applications: Only a few studies have evaluated the operation of FCDI for an extended period – 2 weeks. Furthermore, FCDI has focused more on desalination, and many applications can be explored.

iii. Water recovery[1]: Water recovery is an essential parameter in the desalination process, and FCDI has been claimed to have an advantage relative to other membrane processes. Understanding the factors that influence superior water recovery on FCDI is still necessary.

iv. Capital costs: As FCDI is a new technology, pilot-scale tests are lacking. Also, recent studies have modified the typical FCDI cell to create a design that may be easier to scale up and reduce the costs of the cell assembly.

This project addresses some FCDI issues discussed to develop the technique further and extend its applicability. Specifically, we seek to reduce the energy consumption of FCDI by adding additives in the flow electrodes to improve the charge transfer and, consequently, reduce the electrical resistance of the flow electrodes. Also, new electroactive material is tested in the flow electrode to increase the desalination rate and reduce the suspension's viscosity, reducing energy consumption.

---

[1] Water recovery is the ratio of the volume of treated water produced by the total volume of water fed into the process (the brine plus treated water).

2.1   Objectives

The main objective of this project is to reduce energy consumption and increase the water production of Flow-Electrode Capacitive Deionization by modifying the flow electrodes to improve their charging transfer capability. The specific objectives are:

i.   Investigate Prussian blue analogs nickel hexacyanoferrate (NiHCF) as active material in the flow-electrode. Identify suitable redox couple to act as redox mediators (RM) to improve the charge transfer in flow electrode.

ii.   Improve charge transfer on activated carbon flow electrodes using iron chloride and iron citrate as redox couples. Determine the effect of soluble iron concentration and pH of flow electrodes in desalination experiments.

2.2   Thesis structure and organization

This thesis is organized into five chapters. Chapter 1 and 2 contextualize the work and briefly presents flow electrode capacitive deionization. Then, the main gaps in the literature and the thesis objectives are presented. Chapter 3 presents a literature review of the FCDI development, its main applications, and the proposed modifications to improve the flow electrode conductivity.

Chapter 4 presents the application of nickel hexacyanoferrate (NiHCF) as an active material in the flow electrode. It is demonstrated that NiHCF can be used in the flow electrode if a redox mediator is added to the electrolyte. This work was submitted as a manuscript, "Enhanced desalination performance with flow electrodes based on nickel hexacyanoferrate and redox mediator".

Chapter 5 presents the application of iron-based redox couples to improve typical activated carbon flow electrodes used in FCDI cells. It was shown that iron chloride is an interesting reactant due to its low cost and improvement in the desalination rate compared to typical FCDI flow electrodes. Then, it is also demonstrated that iron citrate can enhance the desalination performance of the cell. This chapter was submitted as a manuscript entitled "Flow electrode capacitive deionization with iron-based redox electrolyte".

Chapter 6 and 7 highlight the main results obtained by this research and suggests topics for future investigations. Appendix A and Appendix B provide additional information and figures for Chapters 4 and 5, respectively. Those pictures were submitted as supplementary material for the corresponding manuscripts.

3 Literature Review

3.1 Capacitive Deionization

Developing sustainable technologies for water desalination and recovering valuable chemicals from water and wastewater is a major technological challenge. CDI has emerged over the years as a robust, energy-efficient, and cost-effective technology for desalination and removal of ionic species from water (Porada et al., 2013; Suss et al., 2015). A typical CDI cell consists of two porous electrodes, usually made of carbon materials. These electrodes are separated by an open channel or a porous dielectric material, and the feed water flows between the electrodes. The operational cycle of CDI desalination has two steps: First, an electrical potential is applied (typically 0.6 – 1.4 V) between the electrodes, which become charged on their electrical double layer. Thus, the ions present in the feed water migrate to the electrode's pores, and then those ions adsorb at the double layer in a process known as electrosorption. This step results in a stream of water with a lower salt concentration than the feed. The removed ions are kept in the double layer of the electrodes until the discharging step. For this step, the electrical potential is either removed or reversed – the positive electrode becomes negative and vice-versa – and the ions are released from the pores, and the electrodes are regenerated, producing a concentrated brine stream. Figure 3.1 presents the steps of CDI desalination schematically.
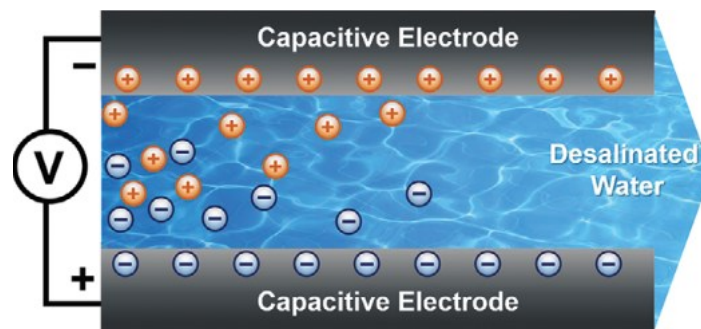
Figure 3.1 – Schematic picture of capacitive deionization cell. The anode adsorbs anions, and the cathode adsorbs cations (Li et al., 2020).

CDI has attracted research interest due to some advantages compared to reverse osmosis and distillation-based systems. First, CDI can remove salt at relatively low voltages and consequently has low energy consumption, and high pressure and heat systems are not required

as in other techniques. Second, the minor constituent of the solution – the salt ions – is removed, whereas, in other techniques, water is removed. Finally, CDI operates similarly to an electrochemical supercapacitor, and the energy spent during the charge step can be, in principle, partially recovered in the discharge step.

A significant part of CDI's development is devoted to improving its electrode materials. As the principle of salt removal is based on the materials' capacitance, it is necessary to have materials with a high specific area to increase the salt removal capacity. Typical materials applied in CDI cells are activated carbons and carbon aerogels, but many other carbon-based materials, such as graphene, carbon nanotubes, and mesoporous carbons, have been evaluated. The structure of those materials must balance the requirement of fast ion transport within the macropores and high microporosity to increase the specific surface area and capacitance. Currently, CDI research is dedicated to further optimizing the pore size distribution and chemical composition of already-known carbons and expanding to novel materials.

Another current research in the CDI field aims to broaden its range of applications. While CDI was conceived for desalination applications, it became clear after some time that the CDI's static electrodes have a limited electrosorption capacity, which restricted its use for the desalination of brackish water – salinity of 1 - 10 g L^{-1}. However, as desalinated water production moves from seawater to inland, brackish water sources such as groundwater from naturally saline aquifers, rivers, wastewater from human activities, and industrial process and irrigation return flow become essential water sources (Pan et al., 2020). Furthermore, water treatment often aims to remove hazardous species that, even at low concentrations, present environmental and health problems. Common techniques applied to decontaminate those water streams are, for example, electrodialysis, nanofiltration, reverse osmosis, crystallization and adsorption, among others. Thus, CDI research focused on removing several charged chemical species from water. Hence, more complex systems – not only deionized water and NaCl – were evaluated. To exemplify, CDI was investigated for water softening applications to remove hard water minerals such as Ca and Mg (Seo et al., 2010). Further studies investigated the feasibility of removal of more hazardous elements, such as As(III) and As(V) (Fan et al., 2017, 2016), Cr(III) (Gaikwad and Balomajumder, 2018, 2017a, 2017b), Cu^{2+} (Huang et al., 2014), F^- (Tang et al., 2016), Ni^{2+} (Liu et al., 2017; C. Wang et al., 2021), NO_3^-, Pb(II) species (Zheng et al., 2017), PO_4^{3+} , Zn^{2+} (Liu et al., 2017). Most studies successfully remove those contaminants from water – as expected since those are charged species – along with other ions in water. However, in several cases, just one specific ion needs to be removed from the effluent. Hence,

CDI studies also developed carbon materials with heteroatoms such as N, Fe, or S and functionalized carbon materials with Fe_2O_3 particles or chemical functional groups such as carboxyl and phosphate (R. Chen et al., 2020) to target specific species. This field seems to be an attractive advantage of CDI, as nanofiltration, electrodialysis, and reverse osmosis are not selective processes.

Although CDI has demonstrated its capability and the feasibility of its applications, there is a lack of studies comparing CDI directly with other techniques for a specific application. CDI is in its infancy, and only two companies – Voltea in the Netherlands and EST Corp. in China – produce CDI cells for industrial and commercial applications. Furthermore, a debate on whether CDI is more efficient than reverse osmosis in energy consumption for brackish water desalination is still ongoing. The primary drawback of RO is the high energy costs of this process. Typically, the total energy requirement for brackish water desalination using reverse osmosis is approximately $0.8 - 2.5$ kWh m^{-3}, depending on the salinity and effluent requirement. By incorporating energy recovery devices, the overall energy consumption can be as low as 0.4 – 0.7 kWh m^{-3}. On the other hand, the energy consumption of CDI is reported to be as low as 0.1^{2} kWh m^{-3} up to 1.5 kWh m^{-3} (Pan et al., 2020).

However, a fair comparison between desalination technologies is difficult. The performance of those systems in terms of energy consumption is affected by several process parameters, such as water recovery, initial salt concentration, and desalination rate (Hawks et al., 2019). A theoretical study claimed that CDI would consume more energy than RO at any given salt concentration. Even with further improvements in the cell, CDI would not overcome the RO (Qin et al., 2019). However, another study criticized the model and parameters used in the latter study, arguing that the authors underestimated the energy efficiency of CDI and used unrealistic physical phenomena in their model (Ramachandran et al., 2019). Later on, CDI cell with ion exchange membranes[3] was compared to RO (Porada et al., 2020). Depending on the water recovery and salt rejection, the RO or CDI can present better performance. It was shown, for instance, that for the effluent of 2g L^{-1}, MCDI cells can be more efficient than RO if the cell is set to achieve a high water recovery of about 95% (Porada et al., 2020). Then, it can be concluded that CDI can be compared to RO for brackish water in terms of energy consumption

---

[2] Voltea's Industrial System (IS12) can produce purified water with the energy consumption of 0.1 - 0.2 kWh m^{-3} (Voltea, 2015).
[3] This type of CDI cell is better presented later in this text.

and that the specific water treatment requirements may dictate which technology may be used[4]. Furthermore, CDI research is still developing new cell architectures to improve the process performance regarding salt adsorption capacity, desalination rate, and energy consumption. Of course, these CDI cells variations have their advantages and drawbacks, and their current status will be briefly presented in the following section.

3.1.1 Architectures of Capacitive Deionization

Blair and Murphy developed the first type of CDI cell in 1960, the so-called flow-by architecture. The cell consisted of two flat parallel electrodes separated by a thin water chamber by which the water flows, Figure 3.2A. The direction of water flow is parallel to the carbon electrodes and perpendicular to the electrical field. The first studies that followed this pioneering work also used the same type of cell, which today is still one of the most studied architecture. This type of cell has a simple design and no ion exchange membranes that increase the cost of the cell. Flow-by and other CDI architectures are shown in Figure 3.2.

---

[4] Several factors affect the choise of a water treatment technology. Besides the energy consumption, capital costs and operational cost play an important role in this decision. As CDI has few data regarding its ecnonomical aspects and few data in the literature, these aspects are not discussed here.
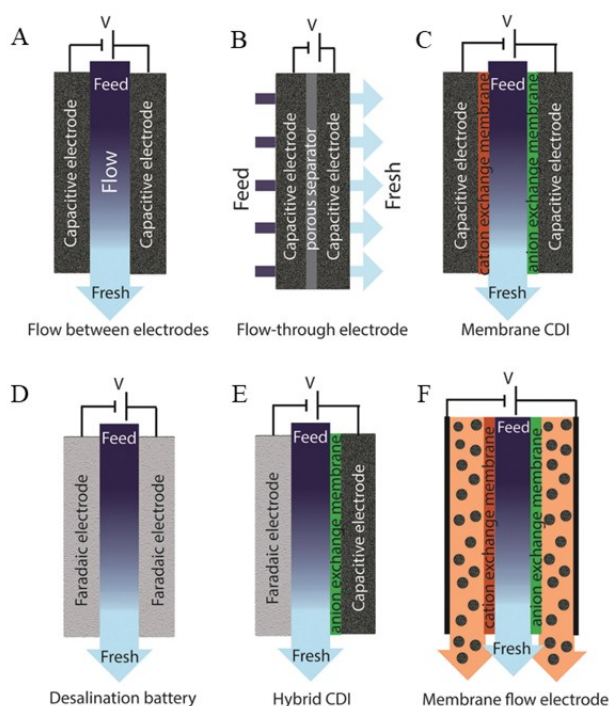
Figure 3.2 – (A) – (C) CDI architectures with activated carbon. (D) Desalination battery. (E) Hybrid CDI. (F) Flow-electrode CDI. Adapted from (Suss et al., 2015).

Another type of CDI is called flow-through CDI or flow-through electrode, shown in Figure 3.2B. The water is pumped through the carbon electrodes in this architecture – parallel to the electric field. The first advantage over the typical CDI cell is the absence of a separator or spacer channel between the electrodes. This feature allows shorter electrode distance and reduces ionic resistance, potentially allowing faster desalination. Usually, the spacer's thickness ranges from 0.2 to 0.5 mm in a flow-by cell, whereas in flow-through, the electrode separation can be as thin as 0.01mm. However, this cell requires multi-scale porous electrodes: macrometer-scale porous to allow water permeation and micrometer-scale porous to increase salt removal capacity.

A relevant variation of CDI called membrane capacitive deionization (MCDI) was proposed by (Lee et al., 2006), as shown in Figure 3.2C. This architecture utilizes ion exchange membranes (IEM) between the water channel and the electrodes. Thus, like an electrodialysis cell, the feed water flows between an anion exchange membrane (AEM) and a cation exchange membrane (CEM). Usually, the membranes are typical commercial IEM placed on top of the respective electrode. However, in some studies, an in-house membrane is directly coated onto the electrode, allowing thinner membranes to be used, which benefits the system as the overall electrical resistance decreases (Kim and Choi, 2010). At first, the use of IEM in CDI cells was

controversial, as IEM are relatively expensive, and the absence of IEM in the system would be a significant advantage of CDI. However, further studies revealed that using IEM improves charge efficiency due to the blockage of co-ions – ions with the same charge as the local electrode – mitigating parasitic current in the cell. For instance, it was shown that for NaCl concentrations ranging from 100 – 200 mM, the energy consumption per ion (kT) could be twice as high for the CDI (50 kT) compared to MCDI (25 kT). Furthermore, it is possible to tailor the membrane to be selective for specific ions, as demonstrated for Na^+ over Mg^{2+} (Sahin et al., 2020) and nitrate removal (Mubita et al., 2020). Thus, the possibility of tailoring the membranes for selective ion removal and the more energetic efficiency make this architecture attractive in the view of practical applications.

Another type of desalination cell that has attracted interest cannot be classified as capacitive deionization as their work principle relies on faradaic reactions instead of capacitive reactions (Figure 3.2D). Those cells are called desalination batteries, as the active materials are typically used in batteries, and the chemical reactions involve cation insertion or chemical conversion (Nam et al., 2021; Suss and Presser, 2018). The advantages of desalination batteries over standard capacitive technologies are that battery materials are more easily tuned to react with a specific ion, allowing the selective removal of ions without membranes. Furthermore, faradaic electrodes do not suffer from co-ion currents as porous carbon materials do, and the capacity of battery materials is usually much higher than the capacity of carbon materials. Thus, battery materials are, in principle, capable of removing more ions than capacitive materials, and, therefore, those materials can be applied to desalinate high salinity streams.

For instance, Cl^- has been removed from water by reacting with metallic silver and bismuth electrodes, forming their respective chlorides. The removal of cations was demonstrated by using materials such as $NaMnO_2$, $Na_3V_2(PO_4)_3$, $NaTi_2(PO_4)_3$, Copper hexacyanoferrate (CuHCF), nickel hexacyanoferrate (NiHCF), and iron hexacyanoferrate (FeHCF). The main drawback of desalination batteries is that the electrodes typically exhibit lower salt removal rates than the carbon electrodes applied on CDI. Also, the capacity fading of those materials, especially in neutral solutions, remains to be improved. Hybrid CDI is an electrochemical cell that combines CDI and desalination batteries Figure 3.2E. One electrode is made of typical battery materials and is usually applied to insert cations, whereas the other electrode is made of porous carbon to adsorb anions from the solution.

Finally, another CDI architecture is based on a different concept where the electrodes are not solid materials but, instead, are carbon flow-electrodes – also known as carbon slurry

electrodes Figure 3.2F. This architecture's application and further development is the main focus of this thesis, and it is further discussed in detail in the next section.

3.2 Flow-Electrode Capacitive Deionization

Flow-electrodes were first reported in 1966 (Porada et al., 2013); however, they did not find applications and were treated as a scientific curiosity. After several years, and considering the vast development in the material science field, flowable suspension-type electrodes[5] have gained attention in the last decade, as they offer scalability and flexibility under operation for conventional energy storage, mainly in stationary applications where the weight and size of electrodes are not a concern (Akuzum et al., 2020). In flow-electrodes, electrochemically active solid particles are mixed with liquid electrolytes to form a biphasic ionically and electrically conductive suspension. During operation, suspensions are pumped through an electrochemical cell, where voltage is applied. Then, the solid particles are electrically charged either through direct contact with the current collectors or through interparticle charge percolation networks that can facilitate electron transport away from the current collectors.

In 2011, flow-electrodes containing insertion materials – $LiCoO_2$, $LiFePO_4$, and $Li_4Ti_5O_{12}$ – were first used to increase the specific capacity of redox-flow batteries (Duduta et al., 2011). The authors called this new type of battery a semi-solid flow battery. Later on, flow electrodes were also evaluated as electrodes in an electrochemical capacitor using activated carbon as active material, and the authors named it an electrochemical flow capacitor (Presser et al., 2012). The main objective of the flow-electrode is to decouple the charge capacity from the size of the electrode. The capacity in flow-electrodes depends on the total volume of the electrode, and since the suspension is stored outside the reactor, a pseudo-infinite storage capacity is possible. Those pioneer studies demonstrated the feasibility of the concept of the flow-electrodes, and since then, several studies have investigated the application of electroactive suspensions in energy storage systems (Campos et al., 2013; Dennison et al., 2014; Duduta et al., 2011; Hatzell et al., 2013; Presser et al., 2012; Zhao et al., 2015).

Following the innovation of electrochemical flow-capacitors and semi-solid flow batteries, the concept of a CDI cell with flow-electrodes – called flow-electrode capacitive deionization (FCDI) – was presented in 2013 (Jeon et al., 2013). This new CDI architecture has advantages over the typical CDI cells. First, the FCDI cell does not require a discharge step within the same

---

[5] Also known as suspension electrodes, semi-solid electrodes, slurry electrodes.

cell – as the other CDI variations do – and can operate continuously. Second, the adsorption capacity is no longer coupled with the electrode size since electroactive suspended materials are kept in reservoirs. Thus, FCDI exhibits better desalination efficiency in high-concentration solutions – compared to typical CDI cells – due to the pseudo-infinite ion adsorption capacity of the flow-electrodes. FCDI employs the same architecture as MCDI cells, except for the electrode part, as shown in Figure 3.3.
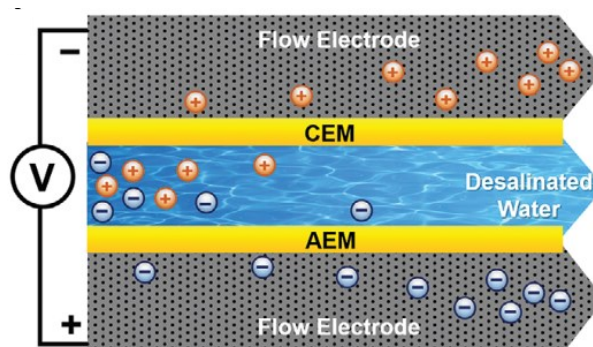
Figure 3.3 – Scheme of a flow-electrode capacitive deionization cell. Ion exchange membranes separate the flow channel from the flow-electrodes (Li et al., 2020).

The flow-electrode in the FCDI cell typically consists of a suspension of activated carbon particles that flows through a serpentine channel carved on the current collector, usually made of graphite. The purpose of the serpentine is to increase the residence time of the carbon suspension and effectively charge the particles. By applying an electrical voltage between the current collectors, the carbon particles inside the anode become positively charged, and the particles inside the cathode become negatively charged, as in semi-solid flow batteries and electrochemical flow capacitors. However, instead of ion exchange between the anodic and cathodic compartments, the saltwater flows in a spacer between the two ion exchange membranes and cations and anions of the feed water permeate the ion exchange membranes to neutralize the charges in the electrode compartment. Besides removing ions due to the charge neutrality, it was shown that there is also an electrodialytic contribution in FCDI, as the electric field created in the current collectors attracted the counter-ions. However, this effect has been shown to present a minor effect in the FCDI desalination process (Ma et al., 2018; Nativ et al., 2017), as the potential is much lower than the electrodialysis process – typically 1.2 - 2.4 V.

Despite the potential advantages of FCDI over the CDI cells, mainly continuous operation and treatment of high salt concentration in the feedwater, fundamental problems must be

addressed to improve the FCDI. The flow-electrodes have low electrical conductivity – 0.1 - 1.0 mS cm^{-1} (Petek et al., 2016) – due to the non-homogenous mixture condition, whereas film electrodes present about 1000 mS cm^{-1} (Ramachandran et al., 2019). In this way, several studies have been conducted to enhance the electronic conductivity by increasing the electroactive partible concentration or adding additives in the flow-electrode. These strategies will be discussed later. Besides improving the flow-electrodes, FCDI studies aim to improve desalination capability, electrochemical characterization of the cell and development of mathematical models, and evaluation of other applications involving contaminants removal and resource recovery (e.g., lithium from brines and N, P compounds for agriculture applications) as well. Those topics will be presented later in this text. First, the configurations of FCDI cells that have been evaluated in the literature are discussed in the next section.

3.2.1   Operational modes of Flow-Electrode Capacitive Deionization

An FCDI cell can operate in different configurations concerning the circulation of the carbon suspension and the circulation of the feed stream. Regarding the feed, the system can be operated in a continuous mode – usually called single-pass – so the solution to be treated enters the cell and produces desalinated water. The other option is the batch mode, where a fixed volume of solution is recirculated in the system, i.e., the desalinated water returns to the container where the feed solution is stored. The batch mode setup generally produces effluents with lower salt concentrations than the continuously operating system (Shin et al., 2021). On the other hand, a continuous operation is more interesting than a batch process on an industrial scale due to the more facile operation. Thus, the most recent studies in the literature have focused more on evaluating the performance of the FCDI on a single-pass configuration (Dahiya and Mishra, 2020; Ha et al., 2020; Shin et al., 2021)

Considering the setup of the flow-electrodes, the FCDI can be operated in three different ways. The first mode is called Isolated closed-cycle (ICC), and there are two storage containers for the carbon suspension. While in one container, the suspension is pumped and recirculated in the cathodic compartment, in the other container, the suspension is pumped into the anodic compartment (Jeon et al., 2013), as shown in Figure 3.4A.
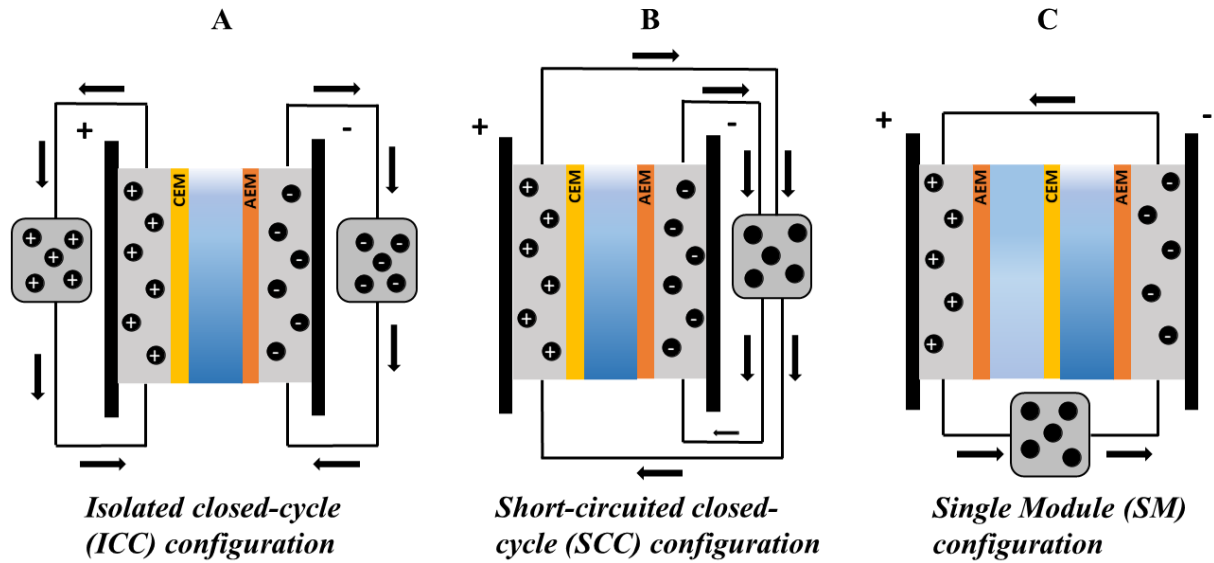
Figure 3.4 – Schematic representations of operational modes of FCDI. (A) Isolated closed-cycle; (B) Short-circuited closed-cycle, (C) Single Module.

The second configuration used to operate the FCDI is called Short-circuit closed-cycle (SCC). There is only one reservoir with carbon suspension in this mode, which is pumped in separate hoses for the cathodic and anodic compartments. The two flows return to the same container when leaving the cell, as presented in Figure 3.4B (Jeon et al., 2014).

Finally, the third configuration is called Single-Module (SM)[6]. This setup resembles an electrodialysis cell, as there are two water streams: a diluate and a concentrate, as shown in Figure 3.4C. The former corresponds to the feed stream, where ions are removed, and the latter is the channel that receives the removed ions, creating a water brine stream with a higher salt concentration than the feed stream. In the SM setup, the flow-electrode is kept in one reservoir, as in the SCC. However, the carbon suspension enters one electrode compartment, then directly flows to the other electrode, and only then it goes back to the reservoir (Rommerskirchen et al., 2020a, 2015). Fewer studies about this configuration are available in the literature, and some of its applications will be discussed later. These configurations are relevant in FCDI performance as they determine the overall energy consumption, desalination rate, and the principle of operation of the FCDI cell.

---

[6] There is a divergence of the name of this configuration in the literature and in some studies this setup is called Single Cycle (SC).

The ICC and SCC modes were compared in both single-pass and batch experiments under constant current (CC) and constant voltage (CV) (Luo et al., 2020). It is worth mentioning that the experiments were carried out for just 1 h – 1 h adsorption in the SCC mode and 30 min adsorption, and 30 min desorption in the ICC mode. Therefore, the results did not demonstrate the adsorption capacity of ICC and SCC. However, it was possible to compare the different configurations regarding energy consumption and average salt removal rate (ASRR).

First, comparing the batch mode in both SCC and ICC in constant voltage operation, it is observed that the electrical current slightly decreases during the desalination step in both setups. This deterioration of performance occurs as the concentration of the feed stream in batch mode decreases over time, and the ohmic drop in the spacer becomes higher due to the lower salt concentration. In addition, the performance deteriorates faster in the ICC than in SCC, as the activated carbon surface becomes saturated in the ICC as the electrodes are not discharged after each cycle inside the cell. In contrast, the flow-electrodes in the SCC mode are mixed, and theoretically, the activated carbon is constantly regenerated.

On the other hand, comparing ICC and SCC in single-pass mode and constant voltage operation, the current response during desalination is quite different in the ICC and SCC setup. For instance, in ICC, the current constantly decreases over time due to carbon saturation. Instead, in the SCC, the current remains constant during all the experiments. Another study also observed this behavior, where single-pass ICC and SCC were compared for water softening in CC (He et al., 2018). The results demonstrated a faster loss of desalination performance in the ICC/single-pass than that shown more recently (Luo et al., 2020). The different rates are likely ascribed to different experimental conditions. In the study of (He et al., 2018), the feed water contained 2 g L^{-1} of NaCl, the flow electrode in the reservoir had approximately 100 ml, and the experiments were run for 80 min. In contrast, the study of (Luo et al., 2020) used a lower salt concentration in the feed – 1 g L^{-1} – and twice the volume of the flow electrode – 200 mL. Furthermore, the experiment was shorter, just 30 min. Hence, it can be concluded that the current decreases over time when a constant voltage is applied in ICC mode and single-pass.

Another relevant issue is the overall energy consumption for desalination. (He et al., 2018) compared the energy consumption considering the energy recovery in the ICC – not possible in the SCC – to make a fairer comparison. The authors say that the SCC is more energetically

efficient, even considering the energy recovery[7] in the ICC mode. Another drawback observed in the ICC mode is the pH change in the flow-electrodes. Due to faradaic reactions, the pH in the anode decreases, and the pH of the cathode increases. Thus, higher pH in the cathode could lead to salt precipitation inside the cathodic flow-electrode.

To sum up, although only a few studies directly compared the ICC and SCC performance, it can be concluded that the ICC has the disadvantage of a faster loss of salt removal rate. It is observed that the cell voltage constantly increases in CC operation and, consequently, higher energy consumption per volume of treated solution is needed. Further drawbacks of ICC include the requirement of another cell to run the desorption cycle and the chance of salt precipitation due to the pH increase in the flow-electrode. Hence, by now, it seems that the SCC is more promising for further FCDI developments. Besides the operational modes, the efficiency of the FCDI process can be affected by several variables, which will be discussed in the following section.

3.2.2 Optimization of the operational parameters of FCDI

In addition to the operational configurations of the FCDI cell, several process variables such as the applied potential, salinity of the feedwater, the feedwater flow rate, flow-electrode flow rate, and total carbon in the flow-electrode play a role in the desalination process. For instance, productivity, average salt removal rate (ASRR), and volumetric energy consumption, among other responses, are all affected by operational variables. The effect of those variables alone, i.e., only changing one variable while keeping the others constant, is understood.

The increase in cell voltage or electrical current increases the driving force for ions removal as the charge in the carbon particles increases, and more ions are adsorbed. The electrical dialytic contribution – the migration of ions due to the electric field – has a minor effect on FCDI (Ma et al., 2018). Cell voltage values ranging from 0.8 V up to 4.8 V are reported in the literature (Tran et al., 2022). However, voltages higher than 1.23 V are expected to decrease the energy efficiency as faradaic reactions may be triggered over this voltage. For instance, it was reported that desalination of feed water containing 3 g L^{-1} at 1.2 V has a charge efficiency of approximately 100 %, and it drops down to 70 % when the voltage is increased to 2.4 V (Tang et al., 2020).

---

[7] The energy recovery in ICC mode has reported values that range from 3 to 35%. The main loses are the related to the flow-electrode and membrane resistance. In this way, further improvements in the cell design may provide higher energy recoveries in the ICC system.

The concentration of carbon in flow-electrode is a critical factor in FCDI cells as the ohmic resistance of the flow-electrode is high and, consequently, has a relevant impact on FCDI performance. The carbon content varies largely in the literature, ranging from 5 % to 35 % wt of active material. The higher the carbon content, the lower the resistance of the flow electrode, as more particles interact with the current collector, and a better percolation between the carbon particles is achieved (Rommerskirchen et al., 2019). However, the carbon content is often between 5 and 10 %, as the concentration of solids increases the flow-electrode's viscosity, which impacts the applicability of flow electrodes as the pumping energy increases, and there is more risk of clogging in the flow channels.

Regarding the flow-electrode flow rate, a study that performed electrochemical impedance spectroscopy showed that increasing the flow rate from 12 to 100 mL min^{-1} decreases the cell's impedance (Rommerskirchen et al., 2019). Two distinguished phenomena were attributed to the lower impedance. First, as the flow rate increases, more particles are likely to transfer charge with the current collector. Second, the increase in flow rate was also responsible for a better charge percolation between the carbon particles.

An optimization study of the feed water salt concentration and applied potential was performed by (Tang et al., 2020) . The authors systematically evaluated the influence of applied potential – 1.2 - 2.4 V – and electrolyte concentration – ~ 3 g L^{-1} – 30 g L^{-1} of NaCl– in the SCC/batch mode. It is relevant to mention that the flow electrodes consisted of a constant carbon loading of 7.41 % wt. Also, the flow rates of feed water and flow-electrodes were kept constant at 10 ml min^{-1} and 25 ml min^{-1}, respectively.

Increasing the applied potential from 1.2 to 2.4 V (Tang et al., 2020) showed a positive shift in the ASRR for all feed concentrations. However, considering the feed concentration of 2.9 g L^{-1} and 5.8 g L^{-1}, there is a slight difference in the ASRR by increasing the applied potential from 1.6 V to 2.0 V. In higher feed concentrations – 11.7 g L^{-1} and 29 g L^{-1} – it can be seen a relevant increase in ASRR as the cell potential is increased. The authors did not explain those results and did not show the NaCl concentration of the water exiting the cell, only the concentration of the feed water reservoir. However, at concentrations of 2.9 g L^{-1} and 5.8 g L^{-1}, the increase in the cell voltage likely did not result in a more significant increase in ASRR due to a low salt concentration in the spacer, reaching almost a complete depletion of salt. Consequently, a concentration polarization in the spacer channel was developed.

Another study evaluated several feed hydraulic retention times[8] (HRT) and applied current densities (He et al., 2018). Several HRT and feed water concentrations of 2 g L^{-1} of NaCl in SCC/single-pass were investigated. As expected, the higher the HRT, the lower the NaCl concentration in the produced water. Furthermore, it was shown that the cell voltage increases linearly with the current in all HRT until a limit where the voltage sharply increases. As previously mentioned, this current density threshold may be related to a depletion of ions in the spacer and concentration overpotential. Thus, it can be concluded that the HRT affects the cell voltage energy consumption and productivity.

To conclude, it is possible to note that several operational parameters have a relevant impact on FCDI's energy consumption and ASRR. However, few studies investigated more than one variable, and only two investigated two variables together, and parameters such as carbon concentration and especially flow electrode flow rate are commonly neglected. As previously mentioned, those parameters were shown to affect the ASRR and energy consumption (Carmona-Orbezo and Dryfe, 2021; He et al., 2018; Rommerskirchen et al., 2019). In this way, evaluating the effect of more variables in the same study is relevant to improving the FCDI performance.

3.2.3 Application of Single-Module cells

The typical ICC and SCC architectures continuously increase the salt concentration in the flow-electrodes. Then, after some period of desalination, the electrodes must be desalinated. Other studies used two FCDI cells (Rommerskirchen et al., 2018) – one for desalination, producing freshwater, and another for removing the salt from the electrode, producing a concentrated brine –while some studies used micro filtration along with the FCDI cell (Zhang et al., 2019b). Those two concepts, of course, add more complexity and costly operation. To overcome this issue, a new architecture called Single-module makes desalination and restoration of the flow-electrodes in a single cell possible. The basic unit of a single module cell consists of two water channels: the desalinated stream and the concentrated stream (Figure 2.5). This cell has three membranes instead of two ion exchange membranes in CEM|AEM|CEM or AEM|CEM|AEM configuration. For instance, in the latter configuration, the anion is loaded on the positively charged flow-electrodes – the left-hand side compartment

---

[8] Hydraulic retention time refers to the time that the feed water stays inside the reactor. Most FCDI studies report flow rates instead of HRT, which makes difficult to compare the results in the literature. For instance, the same flow rate can represent different HRT depending on the size of the reactor.

– and is discharged in the negative electrode – the right-hand side compartment. Cations are transferred from the diluate channel to the concentrated stream to keep electroneutrality. Thus, desalination and electrode regeneration are possible using one single cell.
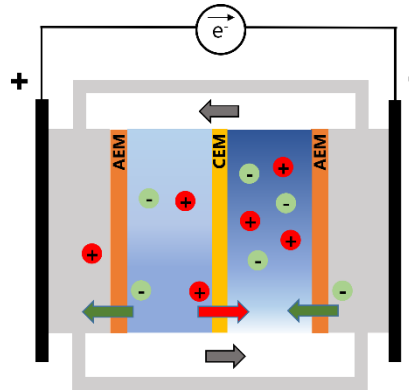
Figure 3.5 – Single-Module cell with two anion exchange membranes and one cation exchange membrane

To date, only a few studies have evaluated single-module cells for desalination. The first study demonstrated that this new cell could produce a diluate and concentrate stream (Rommerskirchen et al., 2015). High current efficiencies – near 100 % – were reported, and a significant improvement in energy consumption was achieved due to the combination of desalination and concentration in the same cell. However, this cell presents a lower desalination rate, as adding a new membrane and another spacer increases the overall cell resistance.

Thus, another study investigated the feasibility of increasing the number of cell pairs between the FCDI flow-electrodes (Rommerskirchen et al., 2020b). While more new cell pairs would increase the resistance, increasing the number of spacer channels allows desalination of a larger volume of water per cell. Besides, it is known that flow-electrodes are responsible for most cell resistance, around 0.33 – 0.4 Ω for 15 wt% activated carbon (Rommerskirchen et al., 2019). In contrast, the resistance of the spacer channel may range from 0.02 to 0.1 Ω[9], while ion exchange membranes account for 0.12 – 0.21 Ω (Rommerskirchen et al., 2020b). Thus, adding more cell pairs between the flow-electrode slightly increased the cell resistance but significantly decreased the energy per volume treated. The authors performed experiments using one, two, and three-cell pairs. The results demonstrated that with one cell pair, the energy

---

[9] The resistance of diluate channel varies according to the outlet salt concentration.

consumption was approximately 24 kWh m^{-3} with one pair, while with two and three pairs, the energy was reduced to 14 and 12 kWh m^{-3}, respectively. These findings demonstrated that the single-module configuration could significantly improve the FCDI by improving the energy per volume and dismissing another cell to regenerate the flow-electrode.

3.2.4   Single-module cells with faradaic reactions

Using the same design of an FCDI SM cell, a new concept of desalination cell was developed based on faradaic reactions instead of capacitive reactions. A solution containing the ferri-/ferrocyanide redox couple was recirculated directly from the cathode and anode, allowing continuous salt removal from the electrode (F. Chen et al., 2020). The principle is that symmetrical electrochemical cells could desalinate a water stream with lower applied voltage, as no product is formed in the electrochemical reaction. While the $Fe(CN)_6^{4-}$ is oxidized to $Fe(CN)_6^{3-}$ in the anode, the $Fe(CN)_6^{3-}$ is reduced to $Fe(CN)_6^{4-}$ in the cathode. In this way, the open circuit potential for this reaction is null. A relatively low cell voltage is required during the operation due to several ohmic drops such as in membranes, spacers, and slurry electrodes.

The experiments were carried out at constant current and with several equivalent molar concentrations of $Fe(CN)_6^{3-}$ and $Fe(CN)_6^{4-}$ (1, 2, 5, and 10 mM). The results demonstrated that 2 mM (1 mM of each species) increased cell voltage exponentially as the applied current was increased. However, for 5, 10, and 20 mM of electroactive species, the voltage increased slowly and almost linearly with the increase in the current density. Electrochemical analyses by Tafel plots showed that the exchange current density increased with the increase in the ferro/ferricyanide species concentration, although an increase from 10 mM to 20 mM did not significantly change the exchange current density. This shows that there might be a limit of a redox couple concentration that results in the best efficiency, and above this limit, there is no beneficial effect in the process.

Following the application of and symmetrical cell single-module cell with redox couples, two studies investigated systems with mixed activated carbon slurry and redox couple (Z. Wang et al., 2021; Wei et al., 2020). First, (Wei et al., 2020) evaluated the energy consumption per ion removed for flow electrodes with activated carbon only, ferro/ferricyanide – 20 mM of each species, and activated carbon plus ferro/ferricyanide. It could be seen that the energy was around 410 and 356 kJ mol^{-1} of removed ion for activated carbon and redox couple, respectively. However, when activated carbon and ferro/ferricyanide were mixed, the energy dropped to 103 kJ mol^{-1}. The same behavior was observed when the redox couple in the slurry

was V^{2+}/V^{3+} (Z. Wang et al., 2021). While the energy consumption was approximately 193 and 169 kJ mol^{-1} for the system with only vanadium and activated carbon, respectively, the combination of these materials dropped the energy to 103.26 kJ mol^{-1}. The addition of carbon nanotubes further reduces the energy to 73 kJ mol^{-1}. These results demonstrated that adding a redox couple in a slurry system improves the charge transfer of the system and consequently decreases the resistance of the flow-electrodes.

However, some drawbacks of those studies are the toxicity of ferro/ferricyanide and vanadium species, which eventually may contaminate the water stream. Also, ferro/ferricyanide readily precipitates when in contact with transition metals, such as iron, copper, nickel, and zinc, and, in this way, in some applications, those precipitates will likely foul the membrane. Regarding vanadium, besides its toxicity, it is a relatively expensive reactant. Thus, there is a need for different redox couples that can meet the requirements of a water desalination system. One option could be iron chloride, as explored in the present work, as iron has low toxicity, the reactant is relatively unexpensive, and chloride is already present in the system. As it will be shown, other iron-based species, such as iron citrate, are an interesting option as citrate has no risk to human health.

3.3   Applications of FCDI

FCDI has been evaluated for several applications besides NaCl removal. These applications include water softening (He et al., 2018), lithium extraction from brines (Ha et al., 2019), removal of ammonia (Fang et al., 2018; Zhang et al., 2019a), and phosphorous (Zhang et al., 2020) from wastewater, selective separation of monovalent and divalent cations (Nativ et al., 2018), and production of salts from double-displacement reactions (Linnartz et al., 2017). Recently, studies with an FCDI SM cell demonstrated that it is possible to recover ions from brines (60 g L^{-1}) producing an effluent of 120 g L^{-1} (Rommerskirchen et al., 2020b). All those previous studies are relevant as they demonstrated that FCDI could remove several micropollutants from water, and it is also capable of treating a broad range of salinity.

3.4   Materials for Flow-electrode capacitive deionization

The slurry electrodes are the fundamental component of FCDI cells. Thus, the chemical and physical characteristics of materials used in slurry electrodes are critical for electrode electrochemical and rheological behavior. In FCDI, carbon materials have been widely applied as active materials, mainly due to their electrical conductivity and relatively high specific

surface area. Typically activated carbons (AC) are preferable in those applications, as they have surface areas ranging from several hundred to 3000 m^2 g^{-1}. The advantage of this large specific surface area relies on the working principle of FCDI, where the ions are electrosorbed in the electrical double layer. Thus, the higher the surface area, the higher the available site for ion removal.

In slurry electrodes, the conductive solid particles that enter the flow cell become charged either through direct contact with the current collector or through interparticle percolation that allows electron transport away from the current collectors (Akuzum et al., 2020; Dennison et al., 2014; Liang et al., 2017; Rommerskirchen et al., 2019). Therefore, the flow electrodes present intrinsically lower electrical conductivity than typical solid electrodes. Two strategies are applied to overcome the low conductivity of flow-electrodes. The most straightforward strategy is to increase the content of conductive material in the suspension. However, increasing the solids concentration could result in clogging, and the suspension viscosity increases, requiring more energy to pump the slurry.

One strategy to increase the solids concentration in flow-electrode and avoid clogging is the oxidation of carbon before the experiments (Hatzell et al., 2015). Activated carbon was oxidized with nitric acid, and XPS analyses showed an increase in oxygen-containing groups, mainly COOH, C=O, and C-OH. The experiments comparing the performance of the pristine and oxidized AC using several loadings of AC (5 – 23 wt %) showed a slight increase in the cell voltage, likely due to a reduction in the conductivity of oxidized carbon. However, the oxidized carbon presented a better rheological performance. The flow-electrode mass loading was increased by nearly 40% (from 20 to 28 wt %) without sacrificing the viscosity.

Another way to improve flow-electrodes' conductivity is by adding materials that are better conductors than AC. Carbon black is commonly applied to enhance conductivity in batteries and electrochemical capacitors. The first study evaluating the addition of carbon black (CB) on the suspension used in FCDI demonstrated by Electrochemical Impedance Spectroscopy (EIS) analysis that the cell resistance dropped by approximately 25 % for the addition of 1.5 wt% of CB. The improvement caused by the CB was attributed to higher cell conductivity and not to a significant increase in the overall surface area. Since the study of (Liang et al., 2017), several studies have added carbon black as an additive.

Considering the active materials reported in FCDI literature, it can be noticed that most studies applied carbon-based materials, and the primary active material – responsible for salt adsorption – is commonly active carbon. In CDI, following the investigations mainly focused

on carbon materials, there was a shift in interest to faradaic materials for desalination (Li et al., 2020; Suss and Presser, 2018). The working principle of those materials can be intercalation[10] or conversion[11] reactions. Regarding the intercalation, typical cathode materials used in batteries, such as sodium manganese oxide, titanium oxide, and Prussian blue analogs, may be of interest due to their higher capacity compared to carbon materials. As active materials, Prussian blue analogs were applied in CDI (Porada et al., 2017; Kaustub Singh et al., 2020). Nickel hexacyanoferrate (NiHCF) was investigated as an electrode material to remove sodium and potassium, and it was found that NiHCF capacity is much higher than electrodes made of activated carbon (Porada et al., 2017). Owing to the interest in PBAs for batteries and recently for CDI, it would also be relevant to investigate its feasibility in an FCDI cell. The following section will discuss some aspects of PBA and its application on FCDI.

3.4.1 Prussian Blue Analogs and their application

Prussian blue (PB), or iron hexacyanoferrate, is a known compound since the 18th century (B. Wang et al., 2018). Initially, PB was produced accidentally and used as a blue pigment. Later in the 19th century, PB and its analogs were investigated as hydrogen storage materials, biosensors, and adsorbent materials to treat contaminated water (Paolella et al., 2017). Only recently, PB and its variants – Prussian blue analogs (PBA) – were reported as materials capable of reversible insertion and extraction of sodium and potassium ions, demonstrating great potential for battery application. The interest of PBA in batteries is due to several reasons. First, PBA can be synthesized by a simple coprecipitation method. Usually, one reactant is a ferricyanide salt, and the other is a salt of transition metal, commonly nitrate, chloride, or sulfate. Once the reactants are dissolved in water and then mixed, PBA readily precipitates. This method is simple compared to other synthesis methods and is expected to be cheap and easy to scale up. Another reason for using PBA as a battery electrode is its structure, as presented in Figure 3.6. The unit cell of PBA has an open framework, where Fe atoms are coordinated by C atoms, and the other transition metal is coordinated by N atoms. In principle, each unit cell allows the insertion of eight atoms of alkali or alkali-earth metals. Thus, high capacity is expected for this type of structure. Furthermore, the open cubic geometry and wide

---

[10] Intercalation is a process where guest ions are inserted into the host material lattice.
[11] Conversion reactions are presented in two types: (1) The alkali ion reacts with a transition metal compound, usually sulfide, oxides, fluorides, phosphates and nitrates, forming a new phase. (2) The alkali metal ion reacts with a chalcogens – S, Se, and Te – or halogens – Br, I – forming a new compound.

channels PBA have good ionic conduction and high-rate[12] capability. Finally, the structure presents minimal change during charge and discharge, which may preserve long cycling life.
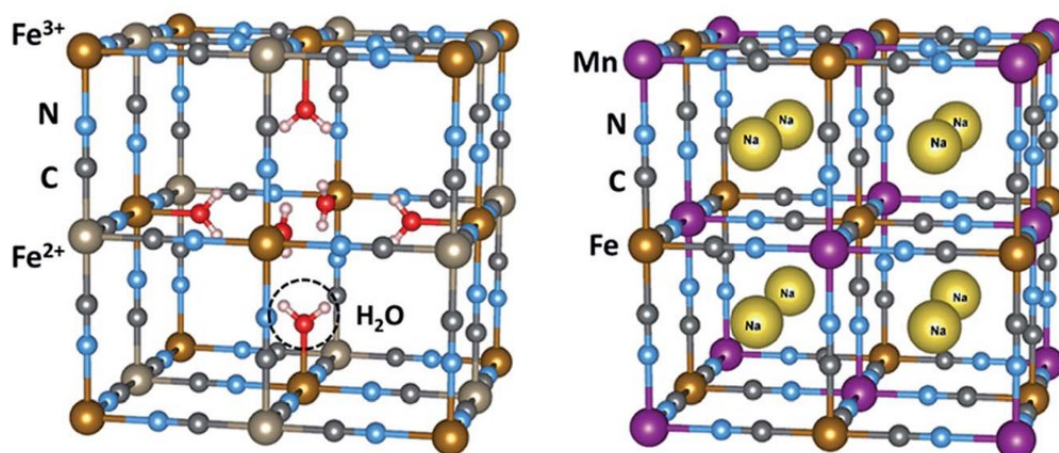
Figure 3.6 – (A) Unit cell of Prussian blue showing Fe^{3+} coordinated by N atoms and Fe^{2+} coordinated by C atoms. $[Fe(CN)_6]^{4-}$ vacancies are occupied by water molecules. (B) Structure of PBA showing intercalated sodium ions (Paolella et al., 2017).

The general formula of PBA is $A_xM_A[M_B(CN)_6]_z\cdot nH_2O$, where A is an alkali or alkali-earth metal intercalated in the structure to keep electroneutrality. The index 'x' ranges from 0 to 1. The number 0 represents the absence of the atom, and 1 represents the maximum capacity of the material. M_A is a transition metal coordinated by eight N atoms, and M_B[13] is a transition metal – usually Fe – coordinated by eight C atoms. The 'z' index represents the stoichiometry of the material, where $Fe(CN)_6$ vacancies in the structure are occupied by 'n' water molecules. The possibility of changing the M_A atom is relevant regarding the electrochemical properties of the material, as the intercalation potential and ionic conduction can be tuned in those materials.

Hence, several PBAs have been investigated for Li, Na, and K batteries. Among the PBA for intercalation of Na and K, the MnHCF, FeHCF, CoHCF, NiHCF, and CuHCF have been the most investigated PBAs due to their high capacity. However, regarding the application in water electrolytes, NiHCF and CuHCF are preferred since their reactions occur in the water decomposition voltage window (Wang et al., 2018). Furthermore, their application in water

---

[12] High-rate capability means how fast the material is able to intercalate/deintercalated ions in its structure.

[13] PB and PBA are usually iron hexacyanoferrates. However, the development of new materials produced PBA where the M_B atom can be several transition metals, such as cobalt, zinc and manganese. For the sake of clarity, just PBA that have M_B as iron are discussed here.

electrolytes has proven to successfully intercalate Li^+, Na^+, and K^+ ions in aqueous electrolytes (Wessells et al., 2012, 2011)

3.4.2 Prussian blue analogs application in FCDI

PBA analogs were recently evaluated as active materials in FCDI applications (Chang et al., 2019; Xu et al., 2021). CuHCF was investigated in an asymmetrical FCDI system in ICC configuration. One electrode consisted of activated carbon, while another mixture of CuHCF and carbon black as an additive. The total load of active material was approximately 5% solid, likely due to the high viscosity of this mixture. The performance of CuHCF was compared to a typical ICC system, with both anodic and cathodic suspensions containing active carbon and carbon black as additive. Electrochemical measurements with solid electrodes confirmed the faradaic behavior of the CuHCH, and galvanostatic charge and discharge curves demonstrated that the capacity of the CuHCF is higher than the AC. According to the electrochemical impedance spectroscopy data fitting, the cell with CuHCF has a lower equivalent resistance and a lower resistance attributed to the ion transfer between the membrane and the flow-electrode. Thus, considering the higher capacity and lower cell resistance with CuHCF, a better desalination performance was expected using this material. However, the desalination experiments showed that the setup with both AC/AC presented faster desalination in 1.2 and 1.6 V. In higher cell voltages – 2.0, 2.4, and 2.8V – the AC/PBA configuration has a faster desalination rate. Although the authors claimed that a cathode with CuHCF performs better in higher voltages, the salt removal rate is slightly higher for AC/PBA than AC/AC at cell voltages higher than 2.0 V. At 2.4 V, the difference is negligible, being only 0.05 mg cm^{-2} min^{-1}. This difference in salt removal rate is likely within an experimental. The authors measured the potential of each electrode using a platinum sheet as a reference. According to the authors, the potential of the cathode was too low for a faster intercalation reaction when the cell voltage was 1.2 V and 1.6 V (Chang et al., 2019). Thus, at higher cell voltages, the intercalation reaction kinetics is increased, and the CuHCF performs better than AC.

A second study using PBA as an electroactive material evaluated nickel hexacyanoferrate (NiHCF) (Xu et al., 2021). As in the previous study with CuHCF, the experiments were performed in ICC configuration, and the concentration of active material was approximately 5%. The effect of the voltage was investigated by shifting it between 1.2 and 2.8 V. A similar trend was observed regarding the salt removal rate in the AC/AC and AC/NiHCF cells. Only at 2.4 and 2.8 V the cell with AC/NiHCF has a higher desalination rate than the cell with AC/AC

(Xu et al., 2021). However, the difference was more significant at 2.4 V (while at 2.8 V the difference might be within the experimental error). After 3 hours of experiments, the Na^+ concentration in the cathodic compartment was measured. Considering the mass balance of Na^+, the cathode with NiCHF has a lower Na^+ ratio than the cathode with AC. Thus, it can be concluded that more Na^+ was intercalated in the NiHCF than adsorbed onto AC surface. Furthermore, the pH in the cathodic compartment after 3 hours of experiment varied from 7 to 12.5 with AC, while the increase in pH was lower with NiHCF (7 to 10.5). This indicates that more parasitic faradaic reactions – oxygen reduction and hydrogen reduction reaction – occurred in the presence of AC.

These two studies were a proof of concept and demonstrated that PBAs could be used as active material in slurry electrodes. Although the authors in both studies stated that the PBA might perform better than activated carbon in higher cell voltages, the desalination rates observed in both systems were quite similar. Furthermore, the studies compared the same mass percentage in the electrode, i.e., ~5% AC ~5% PBA wt%. It is worth mentioning that in some preliminary experiments ran in our laboratory, even without a viscosimeter to determine the shear stress of the suspension, a PBA + carbon black mixture is much more viscous than a mixture of active carbon and carbon black. Thus, it is likely that the electrode with carbon black and PBA will require more pumping energy.

Besides, it is well known that the increase of active carbon concentration in the suspension facilitates the charge percolation and consequently reduces the system's resistance. In general, the studies in the literature use at least 7 wt.% of activated carbon in the suspension. The PBA was compared with an AC flow electrode with only 5 wt. % in those studies. Hence, the best condition for a system with activated carbon was not tested. We believe that the maximum amount of AC was 5% wt in the studies, as it is likely that the authors could not produce a PBA + CB suspension with more than 5 wt% of electroactive material due to the viscosity.

In summary, PBAs may perform better than activated carbon due to their higher capacity, increasing the desalination rate. However, two main issues remain regarding the use of PBA as electroactive material. First, it is necessary to make a suspension with more active material. One straightforward option is using active carbon as an additive, as AC generally produces less viscous suspensions. Second, the electrical conductivity of PBA is lower than the AC one. Thus, it is necessary to improve the charge transfer of PBA in suspensions to allow the use of all insertion capacity. As described in the following section, the application of redox mediators could be a method to improve the charge transfer in flow-electrodes with non-carbon particles.

3.4.3 Redox targeting reactions and Prussian Blue Analogs

Due to the poor charger transfer between PBAs and current collectors in flow electrode systems, it is necessary to modify the flow electrode to improve its conductivity. However, preliminary studies of our group observed that carbon additives are typically insufficient to improve the PBA applicability. Thus, we seek another strategy reported in the literature called redox-targeting reactions. As demonstrated in various studies, the redox-targeting reactions enable swift charge exchanges between the redox mediators and the electroactive solid (Chen et al., 2019; X. Wang et al., 2021; Zhou et al., 2020, 2017).

In this strategy, a redox mediator (RM) – for instance, a soluble redox couple such as $Fe(CN)_6^{3-}/Fe(CN)_6^{4-}$ or Fe^{2+}/Fe^{3+} – are the species that oxidize or reduce at the current collectors. According to the Nernst equation, the potential of a redox mediator species changes depending on the concentration of the oxidized or reduced species. If the redox mediator species have a redox potential similar to the potential of PBAs, the redox couple can be used to reduce and oxidize the PBA, depending on the electrode compartment (Vivo-Vilches et al., 2021; Zhou et al., 2017).

Upon charge and discharge, the equilibrium potential of a redox mediator (E_{RM}) depends on the activities of soluble species, as shown in Eq. (3.1):

$$E_{RM} = E_{RM}^o + \frac{RT}{F} ln\frac{a_{RM+}}{a_{RM}} \qquad (3.1)$$

Regarding the PBAs, their equilibrium potential depends only on the activity of sodium ions present in the solution, Eq. (3.2):

$$E_{PBA} = E_{PBA}^o + \frac{RT}{F} lna_{Na+} \qquad (3.2)$$

If the standard potential E_{RM} and E_{PBA} are similar, the potential difference between the redox mediator and PBA can be expressed according to Eq. (3.3):

$$\Delta E = \frac{RT}{F} ln\frac{a_{RM+}}{a_{RM} \cdot a_{Na+}} \qquad (3.3)$$

As shown in Eq. (3.3), the driving force for the reaction between PBA and the redox mediator depends on Na^+ and redox couple activities. The FCDI operation with redox mediators and PBA can be described with two associated events occurring inside each cell compartment.

In the cell, the current collector reacts with the redox mediator, and the electrochemical reaction of RM/RM$^+$ is represented in Eq. (3.4):

$$RM \rightleftharpoons RM^+ + e^-$$

<div align="right">(3.4)</div>

Then, the oxidized redox mediator (RM$^+$) reacts with the PBA particles – represented with a simplified chemical formula – in suspension in the flow-electrodes, as shown in Eq. (3.5).

$$NaNi_{1.5}[Fe(CN)_6] + RM^+ \rightleftharpoons Ni_{1.5}[Fe(CN)_6] + RM + Na^+$$

<div align="right">(3.5)</div>
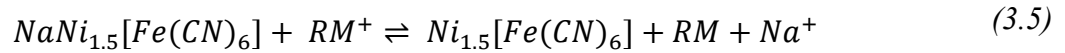
At the anodic compartment, more RM$^+$ is formed by RM oxidation – Eq. (3.4)–, which results in a positive ΔE in Eq. (3.3). Thus, RM$^+$ will react with PBA – Eq. (3.5) –, and sodium ions are deintercalated from the PBA structure. Conversely, the RM$^+$ reduces to RM at the cathodic compartment so that ΔE in Eq. (3.3). Then, PBA particles are reduced by RM – Eq. (3.5) backward –, and sodium ions intercalate in the PBA structure. The method described is a novel strategy, and it may allow the use of PBAs as active materials, which can, in turn, improve the desalination efficiency of FCDI.

4 Enhanced desalination performance with flow electrodes based on nickel hexacyanoferrate and redox mediator

Highlights

- Redox mediator improves the charge transfer in flow electrodes with faradaic material
- Higher desalination rate with NiHCF + redox mediator slurry than activated carbon
- Redox mediator concentration influences the desalination rate
- UV/vis and FT-IR demonstrate the redox-mediated reaction mechanism

Graphical abstract
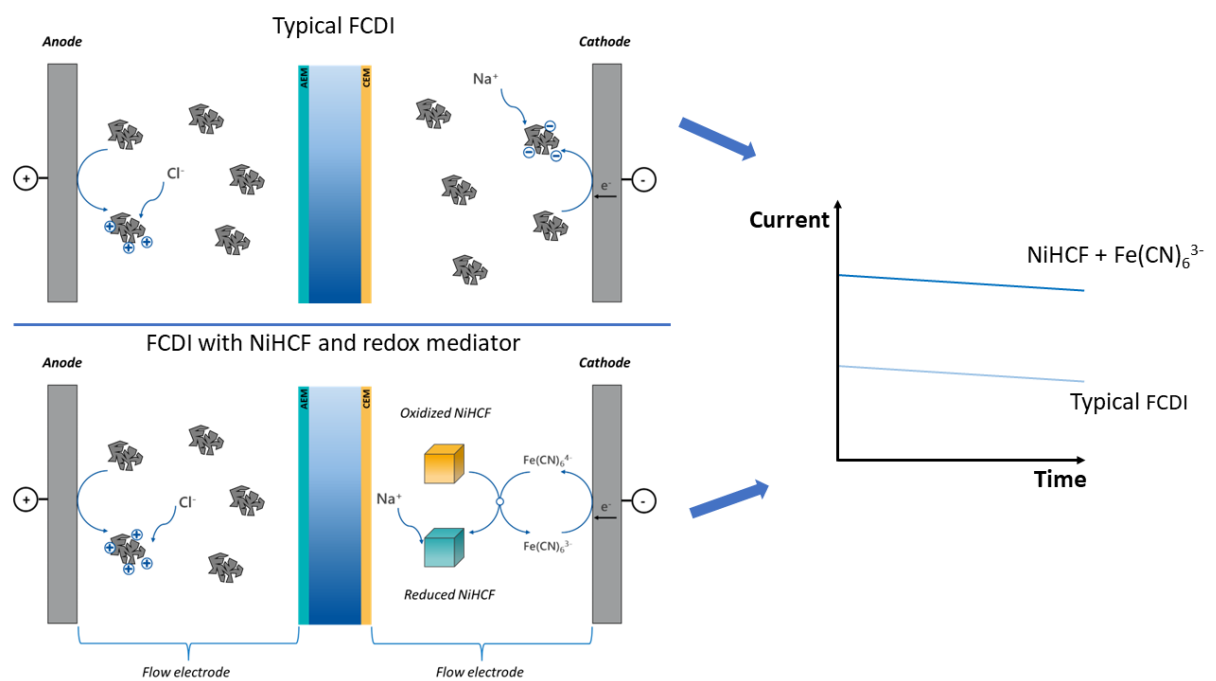
Abstract

Flow-electrode Capacitive Deionization (FCDI) is an electrochemical-driven technology for desalination typically combining ion-exchange membranes and carbon-based flow electrodes. The use of faradaic materials in FCDI has been hindered by their relatively poor performance ascribed to a deficient charge transfer. The application of soluble redox couples ($Fe(CN)_6^{3-}$/ $Fe(CN)_6^{4-}$) as redox mediators to facilitate the charge transfer to a Prussian blue analog nickel hexacyanoferrate (NiHCF) slurry is shown by the first time in FCDI. This slurry was used in the cathodic current collector, where $Fe(CN)_6^{3-}$ ions are reduced and then carry the electrons to NiHCF, which, then intercalates sodium ions. It was shown that flow electrodes with NiHCF and a redox meaditor provide a twofold increase in the current relatively to typical flow electrodes with activated carbon (AC). Compared to the system where the redox mediator is also added to the AC flow electrode, the combination of NiHCF with a redox mediator resulted in higher and more stable currents during desalination. UV/vis and FTIR show the redox mediator concentration in the flow electrode and the chemical reduction of NiHCF particles over time, confirming the reaction mechanism. The results demonstrate that the addition of a redox mediator is an excellent strategy to enhance the charge transfer in flow electrodes based on faradaic materials. This finding opens new possibilities for the application of other intercalation materials in FCDI.

4.1   Introduction

Developing sustainable technologies for water treatment and recovering valuable chemicals from water and wastewater is a major technological challenge. Four billion people experience severe water scarcity during some part of the year (Mekonnen and Hoekstra, 2016). Also, it is increasingly necessary to produce drinking water from sources often requiring treatment before consumption, such as groundwater and seawater. Furthermore, the level of contaminants in wastewater is controlled by legislation, which has become more restrictive, whereas recovery of metals is becoming more relevant in a circular economy. In this context, flow-electrode capacitive deionization (FCDI) has emerged as a new technique (Jeon et al., 2013) capable of treating brackish water, seawater (Jeon et al., 2014), and brine (Rommerskirchen et al., 2020a, 2020b), as well as removing specific ions from water (Linnartz et al., 2017; Saif et al., 2023).

The FCDI cell operates by applying an electrical potential between the anodic and cathodic current collectors, which then charge a suspension of electroactive particles, usually carbon-based materials such as activated carbon. The solid particles are electrically charged through direct contact with the current collectors or interparticle charge percolation networks to facilitate electron transport away from the current collectors (Rommerskirchen et al., 2019). Thus, ions are electro-adsorbed onto the surface of charged active materials (capacitive process). However, the capacitive materials do not present good selectivity for ion adsorption.

Hence, it is relevant to investigate new materials for FCDI so that the flow electrode can be optimized regarding its selectivity, slurry viscosity, and electrochemical performance. In this way, flow electrodes with intercalation materials allow the application of several new active solids in FCDI. Those materials are widely used in battery applications, and their working principle relies on reversible faradaic reactions and intercalation of ions in the crystal lattice of the materials. One advantage of intercalation materials is their higher selectivity regarding ion removal relatively to activated carbons (Li et al., 2020; Sayed et al., 2021; K. Singh et al., 2020; Kaustub Singh et al., 2020). For instance, desalination batteries have been investigated for the selective removal of lithium from seawater (Zhao et al., 2020) and selective removal of monovalent cations over divalent ions (Kaustub Singh et al., 2020).

For FCDI, the application of intercalation materials is scarce, and only a few studies can be found in the literature. To the authors' knowledge, only two intercalation materials were studied in FCDI cells, both Prussian Blue Analogs (PBAs): Copper Hexacyanoferrate (CuHCF) (Chang et al., 2019) and Nickel Hexacyanoferrate (NiHCF) (Xu et al., 2021). The cell configuration used in those studies was the Isolated Closed-Cycle (ICC), and the slurry with PBA circulated

in the cathodic compartment in the desalination cycle. The desalination rate of those PBAs slurries was slightly superior to the pure activated carbon slurry at cell voltages higher than 2.4 V. This is unpractical for FCDI applications due to water oxidation and reduction reactions and oxidation of activated carbon. Furthermore, the weight percentage of active materials in the slurry was only 5 %, which may result in poor charge percolation for AC. Commonly, in the FCDI literature, the mass fraction of solids ranges from 7.5 to 15 wt.% (Folaranmi et al., 2022; Lim et al., 2020; Ma et al., 2020; Tran et al., 2022; Zhang et al., 2021). Also, carbon black was used as an additive along with PBAs (Chang et al., 2019; Xu et al., 2021), but it likely increases the viscosity of the slurry.

The poor performance of PBAs as flow electrodes is likely due to their intrinsic lower electronic conductivity compared to activated carbon, resulting in poor charge transfer between the current collector and the PBAs, and poor charge percolation between the PBA particles. To overcome this issue, we propose the application of soluble redox couples as charge carriers in the flow electrodes, facilitating the charge transfer from the current collector to the active material. Thus, the poor charge transfer between the particles and the current collector would not be a barrier to applying those materials in flow electrodes. This strategy was investigated for several battery devices to boost the energy storage capacity and the performance of those systems (X. Wang et al., 2021; Zhou et al., 2020, 2017). However, to the authors' knowledge, redox mediators and faradaic materials have not been investigated as flow electrodes in FCDI.

The concept of Redox-Targeting Systems was first proposed in 2006 (Wang et al., 2006), where the possibility of using a redox couple in the electrolyte to charge and discharge a solid battery material was demonstrated. The working principle is that a soluble redox couple acts as a redox mediator, transporting the electrons from the current collector to the active material. A redox mediator ($RM1_{ox}$) with a lower reduction potential than the solid material reduces at the current collector forming ($RM1_{red}$), which in turn reduces the solid. The regeneration step is carried out by a second redox mediator ($RM2_{red}$) with a higher reduction potential than the solid. The $RM2_{red}$ is oxidized to $RM2_{ox,}$ oxidizing the solid.

This mechanism is exemplified in and Eq. (4.1) and Eq. (4.2), where S represents an electroactive solid.

$$RM1_{ox} + e^- \rightleftharpoons RM1_{red} \tag{4.1}$$

$$RM1_{red} + S_{ox} \rightleftharpoons RM1_{ox} + S_{red} \tag{4.2}$$
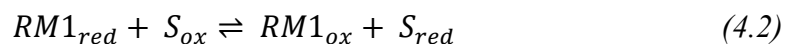
We investigated NiHCF as an active material and ferricyanide – $[Fe(CN)_6]^{3-}$ – as a redox mediator in the cathodic flow electrode. It is demonstrated that $[Fe(CN)_6]^{3-}$ reduces to ferrocyanide – $[Fe(CN)_6]^{4-}$ – in the current collector and then reacts with the NiHCF particles. We compared the desalination rate with typical activated carbon slurries and demonstrated that higher desalination rates are achieved with the NiHCF + $[Fe(CN)_6]^{3-}$ flow electrode. This work is a proof of concept demonstrating that using a redox mediator along with any intercalation material – here, nickel hexacyanoferrate – is an excellent strategy to improve the charge transfer in flow electrodes and the FCDI desalination rate.

4.2   Experimental

4.2.1   FCDI cell setup

The FCDI experiments were performed using the cell design described in a previous work (Linnartz et al., 2017). The cell consisted of two acrylic end plates; two epoxy-impregnated graphite current collectors (Müller & Rössner GmbH & Co. KG) with 3 mm in width and 2 mm in-depth carved flow channels; one cation and one anion exchange membrane: Fumasep FKB-PK-130 and Fumasep FAB-PK-130, respectively (Fumatech BWT GmbH). A 0.5 mm mesh spacer (Fumatech BWT GmbH, ED-40) was used as a water channel between the membranes, and the effective surface area between the membranes and the spacer was 22.4 cm^{-2}. A peristaltic pump (Ismatec Reglo ICC, Cole-Palmer) was used to supply water to the FCDI cell, and a pump (MasterFlex Easyload II Dual Channel) was used to pump the flow electrodes. A power supply (Keysight Agilent E3644A) was used to control the applied voltage in the FCDI cell. The conductivity of the product solution was monitored with conductivity probes (Knick SE 615/1-MS, Knick Elektronische Messgeräte GmbH & Co. KG), and the chloride and sodium content was determined by high-performance liquid chromatography (Agilent 1200, HPLC). The crossover of $[Fe(CN)_6]^{3-}$ to the water stream was analyzed by ICP-OES analysis of the iron concentration in the product water (PlasmaQuant PQ9000 Elite, Analytik Jena).

The FCDI cell was set up in the isolated closed cycle (ICC). In this way, the flow electrode has two reservoirs, one circulating inside the anodic current collector and the other inside the cathodic current collector, as shown in the scheme in Figure 4.1.
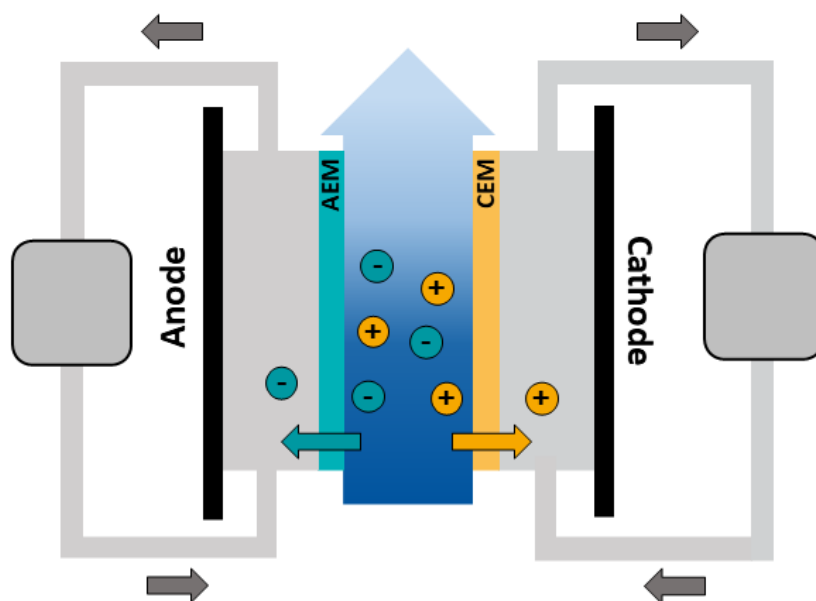
Figure 4.1 – Scheme of the FCDI cell used for the experiments. The flow electrodes are set up in the isolated closed-cycle configuration. The feedwater is in a single-pass mode, so the cell was continuously supplied with a new electrolyte.

4.2.2 Synthesis and characterization of NiHCF

NiHCF particles were synthesized using the co-precipitation method commonly described in the literature (Porada et al., 2017; Zakaria and Chikyow, 2017). Briefly, for the synthesis of NiHCF, 1 L of 0.1 M $K_3[Fe(CN)_6]^{3-}$ and 1 L of 0.05 M $NiSO_4$ were added into a beaker containing 1 L of deionized water at 25°C acidified with HCl to reach pH 1. The solutions were pumped into the beaker at 20 mL min^{-1} and continuously stirred. After adding the solution, the mixture was mixed for one more hour and then let to settle at room temperature for 12 h The precipitates were washed with dialysis membrane tubes in deionized water several times until the conductivity reached at least 30 µS cm^{-1}. The precipitates were then centrifugated and freeze-dried for 48 h.

The NiHCF powder was later characterized by thermogravimetric analysis on a TA Instruments SDT600 system to determine the amount of adsorbed and crystal water in the material. The tests were run at a heating rate of 10 °C min^{-1} under N_2 atmosphere at a flux of 50 mL min^{-1}, and the temperature ranged from 25 to 800 °C. Scanning electron microscopy (SEM) was used to analyze the morphology and size of the particles in a Hitachi SU5000, at

the accelerating voltage of 5 kV. The crystal structure was assessed by powder X-ray diffraction in an X-ray diffractometer (PANalytical, Empyrean) with Cu Kα radiation ($\lambda = 1.54$ Å), in the range of 10 - 80 2Θ, and step size of 0.02° min^{-1}. The functional groups were characterized by infrared spectroscopy by a photometer (Perkin Elmer Spectrum 3), in the attenuated total reflection mode (ATR). The infrared spectra were collected in the range of 400 – 4000 cm^{-1}, with a resolution of 4 cm^{-1}.

4.2.3 Electrochemical characterization

The electrochemical characterizations were performed with a potentiostat (Bio-Logic BP-300). The working electrode was prepared by coating a mixture of NiHCF mixed with carbon black (Alfa Aesar) and polyvinylidene fluoride (PVDF - Solef 1012 - Solvay) dissolved in N-methyl-pyrrolidone (NMP Merck, proportion 2:1) in a ratio of 7:1:1 onto a carbon cloth. Cyclic voltammetry was carried out in 2 g L^{-1} NaCl electrolytes. The potential windows ranged from -0.1 – 1.2 (V. vs. Ag/AgCl}), and scan rates between 0.1 – 1 mV s^{-1} were applied. Galvanostatic charge-discharge (GCD) tests determined the capacity and stability of NiHCF during charge and discharge cycles with a current of approximately a C/10-rate (the current to discharge the NiHCF equivalent mass in 10 h). The system can be considered in equilibrium for this low electrochemical reaction rate, and the potentials measured are equivalent to the thermodynamic potential.

4.2.4 The capacity of NiHCF in flow electrode

The FCDI cell was used to determine the capacity of NiHCF as a flow electrode in an asymmetric configuration, as the composition of the cathode and anode reservoir differs. The salt solutions used as feed water consisted of 2 g L^{-1} of NaCl (Carl Roth chemicals, 99 %) and MiliQ water (Millipore Synergy UV System). On the anodic side, the flow electrode consisted of activated carbon (Carbopal SP11) with a mass of 300 g, and a solid concentration of 15 wt. % – 45 g of AC – in suspension in 2 g L^{-1} NaCl. The activated carbon was characterized in a previous study (Rommerskirchen et al., 2019), and it was found to have a BET surface area of 950 m^2 g^{-1}, and particle size d90 and d50 equal to 64 and 16 μm, respectively. Three different compositions were investigated in the flow electrode at the cathode side. First, 5 g (10 wt.%) of NiHCF in suspension in a 2 g L^{-1} of NaCl electrolyte and total flow electrode mass of 50 g. Second, a total mass of 45 g of a solution of 0.1 M of K$_3$[Fe(CN)$_6$] was used as a flow electrode. Finally, a slurry with 5 g of NiHCF and 45 g of a electrolyte with 0.1 M of K$_3$[Fe(CN)$_6$] and 2 g L^{-1} of NaCl was investigated to determine the NiHCF capacity. The applied voltage was

1.2 V, and the feed water flow rate was 5 ml min^{-1} in a single pass, while the slurries flow rate was 200 ml min^{-1}. When the current response of the system dropped to near 0 mA, it was considered that the capacity of the cathodic flow electrode was reached.

4.2.5 Desalination experiments

For the desalination experiments, the feed water and anodic flow electrode were the same as stated above. However, the cathodic slurry had 15 wt. % of solid as active material. A higher mass was used in the anode so the saturation of the cathode would be reached first, and the anodic slurry influenced the experiments less. The effect of several cathode flow-electrode compositions was compared in experiments with a constant applied voltage of 1.2 V. The typical AC slurry was used as a baseline to compare the results with typical FCDI systems. A flow electrode with 42.5 mL of a solution consisting of 0.1 M of $K_3[Fe(CN)_6]$ was analyzed to compare the effect of the RM_{ox} without any particles. The experiments were realized in triplicates, and the composition of cathodic flow electrodes and the parameters chosen for the desalination experiments are shown in Table 4.1.

Table 4.1 – Overview of cathodic flow-electrode compositions and FCDI system parameter settings for desalination experiments.

Composition	Flow Electrode				Feed water	
	[FeCN]	Solid	[NaCl]	Flow rate	NaCL	Flow rate
	M	%	g L^{-1}	mL min^{-1}	g L^{-1}	mL min^{-1}
AC	0	15	2	200	2	5
NiHCF	0	15	2	200	2	5
[FeCN]	0.1	0	2	200	2	5
AC + [FeCN]	0.1	15	2	200	2	5
NiHCF + [FeCN]	0.1	15	2	200	2	5

Later, the influence of initial RM concentration on the NiHCF desalination performance was investigated following the same anode composition and operational parameters described in Table 4.1. However, $[Fe(CN)]_6^{-3}$ was evaluated in concentrations of 0.05 M, 0.1 M, and 0.2 M.

4.2.6 Analysis of desalination performance

The performance of the desalination experiments was analyzed using the applied cell voltage, the electrical current, the flow rate of feed water, and the salt concentration of product

water. The average salt removal rate (ASRR, μmol cm^{-2} min^{-1}) was calculated according to Eq. (4.3).

$$ASRR = \frac{(C_0 - C_t) \cdot V_s}{t \cdot A_{eff}} \qquad (4.3)$$

Where C_O is the concentration of Na$^+$ in the feedwater and C_t is the salt concentration of the product water (mol L^{-1}) at a given time t. V_S is the total volume of treated water during time t, and A_{eff} is the membrane area in contact with the flow electrode. The charge efficiency (CE) is the ratio of charge transported by ions to the total electrical charge introduced into the system, as shown in Eq. (4.4).

$$CE = \frac{z \cdot F \cdot (C_0 - C_t) \cdot V_s}{\int idt} \qquad (4.4)$$

Where F is the Faraday constant (96485 C mol^{-1}), z is the equivalent number of electrons per mol of ions removed, M_{salt} is the molar mass of Na$^+$, and dt is time. The volumetric energy consumption (E_{vol}, kWh m^{-3}) for desalination can be calculated as follows in Eq. (4.5).

$$E_{vol} = \frac{i \cdot V \cdot t}{V_s} \qquad (4.5)$$

Where V is cell voltage, which was 1.2 V for all experiments. The energy consumption per mol of removed salt (E_{mol}, kJ mol^{-1}) was calculated by Eq. (4.6).

$$E_{mol} = \frac{\int iV \, dt}{(C_0 - C_t) \cdot V_s} \qquad (4.6)$$

4.2.7 Validation of the redox-targeting reactions

The desalination reaction was investigated using with a flow electrode consisting of 15 wt.% NiHCF + 0.1 M K$_3$[Fe(CN)]$_6$. Samples with 1 mL were taken from the cathodic flow-electrode reservoir after 30, 60, 90, 120, 150, 180, and 210 min of the experiment. These samples were centrifuged, and the solution was diluted by a factor of 250 and analyzed by

UV/vis spectroscopy by a Hitachi U-5100 photo spectrometer, in the wavelength ranging from 250 to 500 nm. The solid was washed with deionized water, frozen with liquid nitrogen, and then freeze-dried. Then, the dried powder was analyzed by infrared spectroscopy as previously described.

4.3 Results and Discussion

4.3.1 Characterization of synthesized NiHCF

The morphology of NiHCF particles was investigated by SEM and is shown in Figure 4.2.
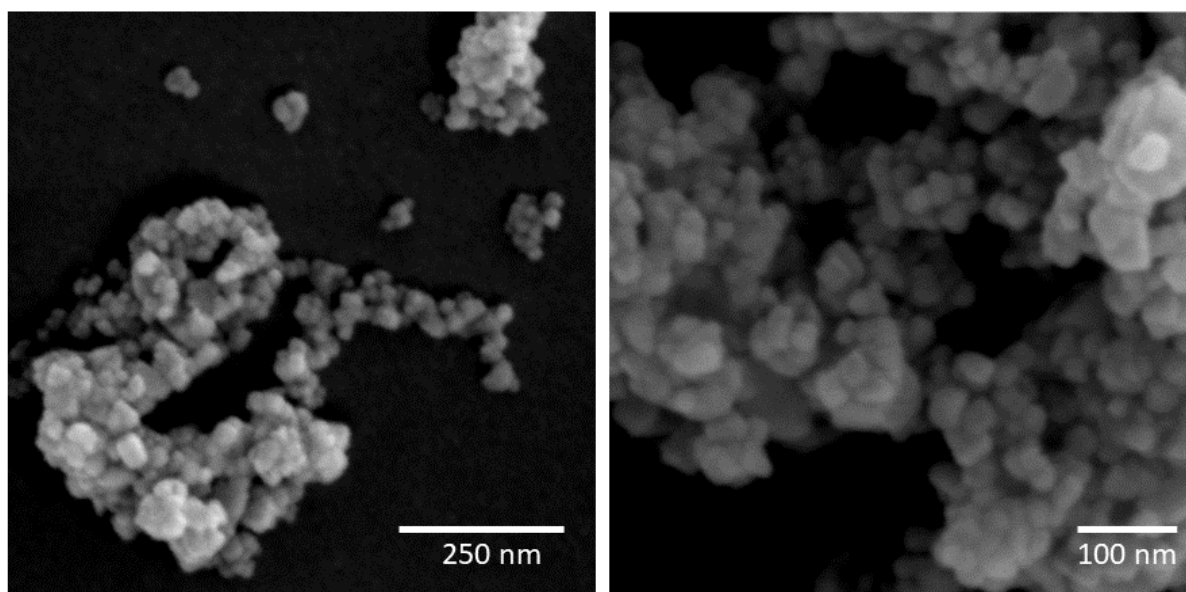
Figure 4.2 – Typical scanning electron microscopy images of NiHCF particles.

The SEM images show that the particle size is around 30 nm, and they have a near cubic shape, as expected for PBAs particles. The small size of particles is relevant for the RT reactions, as more surface area is available for the reaction between the redox mediator and the NiHCF. The typical structural characterization of NiHCF by XRD, FT-IR, and thermogravimetry is shown in Figure A.1, in the Appendix A.

4.3.2 Electrochemical characterization of NiHCF

The synthesized NiHCF particles were characterized by their electrochemical performance, and the results were compared with typical values reported in the battery literature. The galvanostatic charge-discharge curves (GCD) and cyclic voltammetry are presented in Figure 4.3.
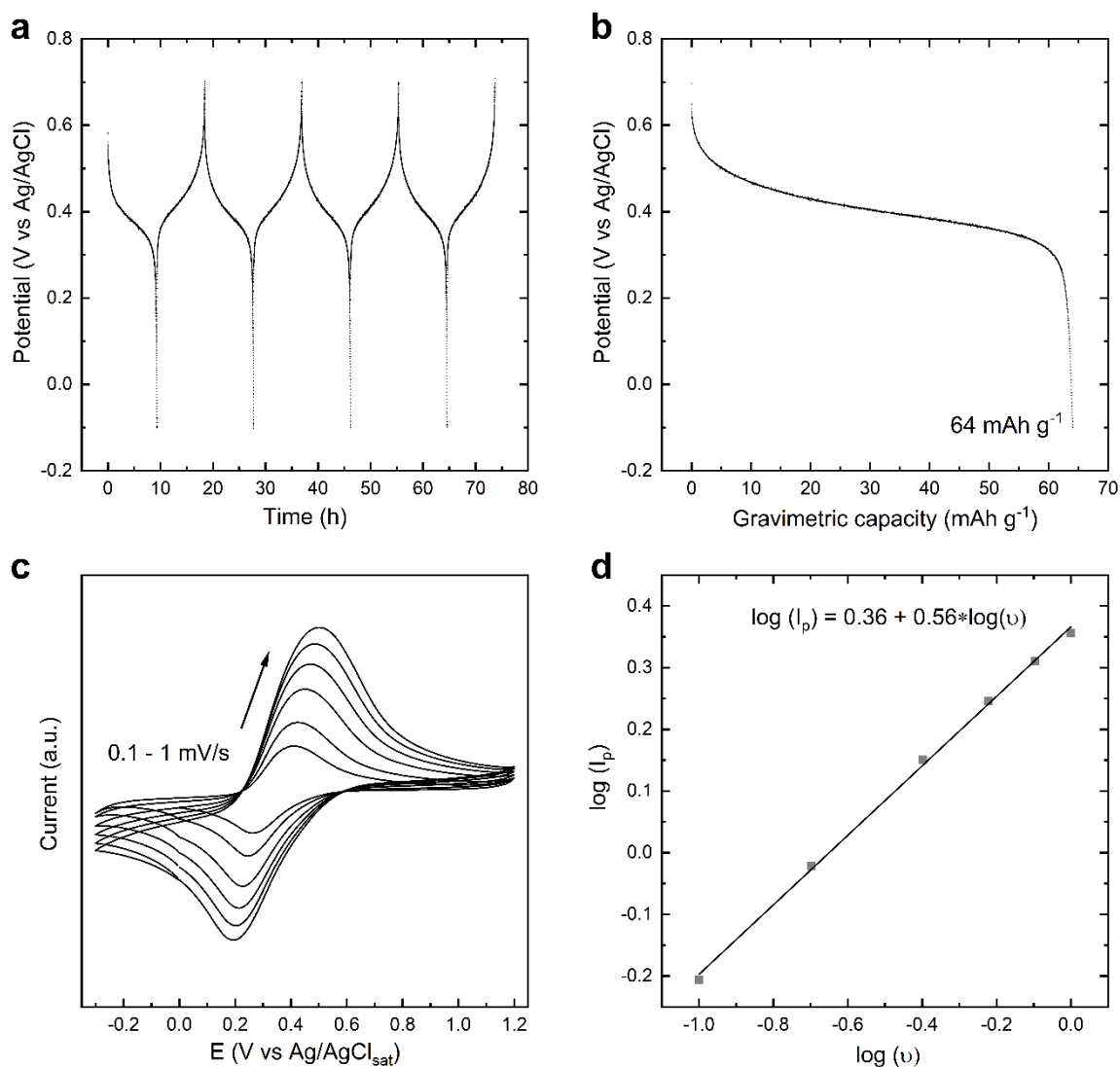
Figure 4.3 – Electrochemical characterization of NiHCF particles: galvanostatic charge-discharge (GCD) curves show the stability of the material over several cycles in an electrolyte of 1 M NaCl and pH around 7 (a); The gravimetric capacity calculated from GCD curves (b); Cyclic voltammetry curves for several scan-rates (c); Logarithm of the power law of peak current height vs. scan rate.

Several cycles of GCD curves are shown in Figure 4.3a, where the NiHCF potential over time is presented. The curves show that after several cycles, the time necessary for a charge-discharge cycle remains constant for an electrolyte of 1 M NaCl and pH around 7, and no change in the electrolyte color was observed. The repeated cycles demonstrated that the material is not degraded over the cycling, proving its stability in aqueous media. Figure 4.3b shows one discharge cycle of NiHCF and its corresponding electrochemical potential change ranging from

the more oxidized state – 0 capacity – to the fully reduced state – a 64 mAh g^{-1}. This value of gravimetric capacity agrees with the theoretical value expected (67 mAh g^{-1}) for NiHCF considering as an approximated formula Ni$_3$[Fe(CN)$_6$]$_2$.11H$_2$O, and also with other values previously reported (Chong et al., 2020).

Cyclic voltammetry was performed to characterize the electrochemical potentials under which the material oxidizes and reduces, and it is shown in Figure 4.3c. The cyclic voltammetry was performed with solid electrodes prepared by coating a dispersion of electroactive material onto a carbon cloth. The electrical current is presented in arbitrary units, as the current depends on the total mass of material coated onto the carbon cloth. The conventional current and voltage signals are used in the plots; positive current for oxidation and negative current for reduction. All potentials are reported in Ag/AgCl in saturated KCl solution at 25 °C.

The peaks observed in voltammograms are due to the redox reactions occurring in the NiHCF. The exact attribution of those peaks is often complex, and other associated techniques, such as spectroscopy, must be used for the correct interpretation. In solid-state electrochemistry, this association can be even more challenging as the same redox couple – for instance, Fe^{3+}/Fe^{2+} in the structure of PBA – can present different peaks due to the chemical environment in the structure, such as vacancies, chemical ligands, and high and low spin configuration (Agrisuelas et al., 2012). The oxidation peak at around 0.55 V (vs. Ag/AgCl) is attributed to the oxidation of Fe^{2+} to Fe^{3+}, and the reduction peak at around 0.2 V (vs. Ag/AgCl) to the reverse reaction (Shen et al., 2020). The peak positions remain almost constant as the scan rate increases, indicating that the process is reversible. As expected, there is no peak related to the redox reactions of nickel, as this reaction occurs in potentials lower than -0.2 V (vs. Ag/AgCl). After the cyclic voltammetry experiments, the electrolyte remained transparent, and no degradation was observed, as reported in other studies (Porada et al., 2017; Shen et al., 2020; Shi et al., 2021; K. Singh et al., 2020).

The scan rate in the cyclic voltammetry influences the thickness of the diffusion layer on the electrode surface, and the peak current is given by Randles-Sevcik equation. Thus, a plot of the peak current I$_p$ vs. v$^{1/2}$ (where v is the scan rate) will be linear if the process is controlled by diffusion. However, if the reaction involves the adsorption onto the electrode surface, the I$_p$ is proportional to the scan rate. Usually, the reaction has a contribution from both processes, and the peak current can be plotted by the empirical Eq. (4.7):

$$I_p = a \cdot v^b \qquad\qquad (4.7)$$

Where v is the scan rate, a is a proportional constant, and b is a parameter that indicates the diffusion or adsorption control. This equation can be linearized as shown in Eq. (4.8):

$$\log(I_p) = \log(a) + b \cdot \log(v) \qquad (4.8)$$

Figure 4.3d shows the plot of $\log(I_p)$ vs. $\log(v)$. For a fully diffusion-controlled process, the angular coefficient b equals 0.5; for a capacitive process, b equals 1. As shown in linear fit, calculate b equals 0.56, indicating that the electrochemical reaction is controlled by diffusion in the cyclic voltammetry.

With the potential of GCD curves and the cyclic voltammetry, we can choose an appropriate RM_{ox} for the desalination experiments. The redox potential of the redox couple RM_{ox}/RM_{red} must be lower than the redox potential of NiHCF indicated in the GCD curves and cyclic voltammetry. In this way, the redox couple $[Fe(CN)_6]^{-3}/[Fe(CN)_6]^{-4}$ was chosen as an RM as its redox potential (0.159 V (vs. Ag/AgCl)) is below the values measured for NiHCF (0.6 - 0.3 V (vs. Ag/AgCl)) depending on the state of charge, as shown in Figure 4.3a,b).

4.3.3 Characterization of NiHCF as flow electrodes

The desalination experiments to determine the capacity of NiHCF as a slurry are shown in Figure 4.4a. A cell voltage of 1.2 V was applied in those experiments. When the current response of the system dropped to near 0 mA, it was considered that the capacity of the cathode flow electrode was reached. For the experiments with NiHCF slurries without a redox mediator, the current response in the FCDI was approximately 12 mA, likely due to the poor charge transfer between the current collector and NiHCF particles, as shown in Figure 4.4a. Hence, the experiments would take several hours until the capacity of NiHCF particles was fully reached. To reach faster the capacity of NiHCF slurries electrodes, $[Fe(CN)_6]^{3-}$ was added as a redox mediator to react with NiHCF and increase the desalination current. Then, it was necessary to determine the capacity of an electrolyte with 45 mL and 0.1 M of $[Fe(CN)_6]^{3-}$.
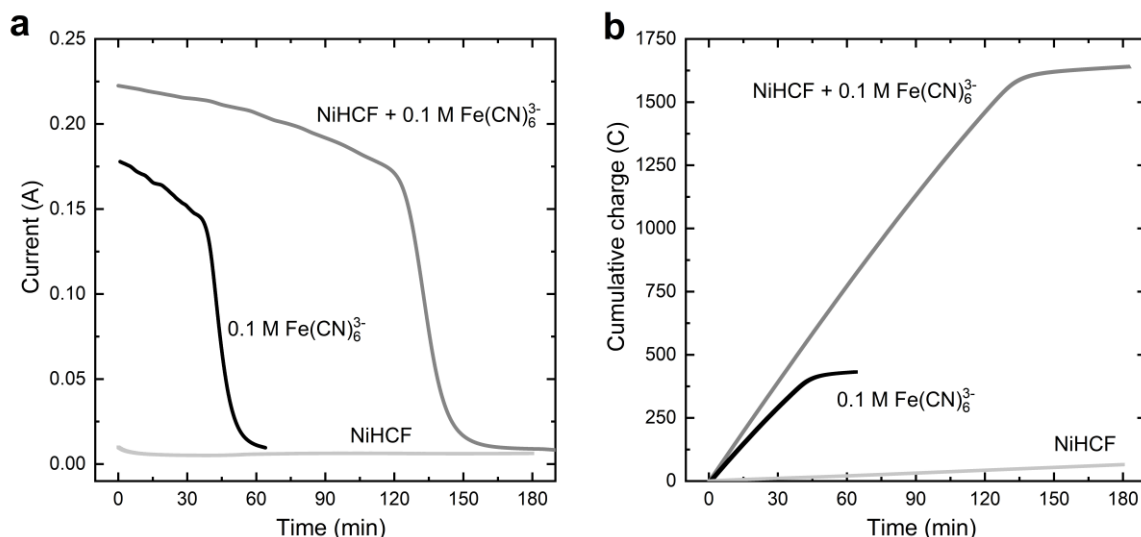
Figure 4.4 – Current vs. time curves for different flow-electrode compositions used as the cathode in the FCDI cell (a); Total charge transferred until the saturation of the cathodic flow electrodes (b).

The integration of the current vs. time curve in Figure 4.4a gives the total charge in Coulombs for the saturation of the flow electrode. As the experiments were performed with 45 mL of a solution containing 0.1 M of $[Fe(CN)_6]^{3-}$, a total of 0.0045 mol of $[Fe(CN)_6]^{3-}$ could be reduced in the electrolyte. Considering the transfer of one equivalent electron, the expected capacity is 434 C. The charge measured for the electrolyte is 432 C (Figure 4.4b), which agrees with the theoretical value.

Then, the capacity of the mixture of 5 g of NiHCF + 45 mL of 0.1 M $[Fe(CN)_6]^{3-}$ was determined as shown in Figure 4.4a, and the value obtained by integration was 1609 C (Figure 4.4b). Subtracting the capacity of this mixture by the capacity measured for only the electrolyte 45 mL solution of $[Fe(CN)_6]^{3-}$, gives the capacity of 5 g of NiHCF, which equals 1117 C, or 327 mAh. Compared with the typical solid electrode experiments, it corresponds to a gravimetry capacity of 65 mAh g^{-1}. This result demonstrates that the gravimetric capacity of NiHCF in the flow electrode is the same as in a solid electrode. Hence, it can be concluded that even though the reaction between the redox mediator ($[Fe(CN)_6]^{3-}$) occurs at the surface of the NiHCF particles, not only the surface but also the bulk of those particles are being reduced in the flow electrode. This means that the total capacity of the material is used, which is a benefit for the process as the electrode may take longer to be saturated.

4.4 Desalination experiments

4.4.1 Effect of redox mediator on the desalination rate

As shown in Table 4.1, several flow-electrode compositions were investigated in the cathode side of the FCDI cell. As the experiments had a constant voltage of 1.2 V, a higher electrical current means a higher desalination rate, i.e., better performance. The current vs. time curves can be seen in Figure 4.5a. The corresponding normalized conductivity of the water product is shown in Figure A.2. The respective average salt removal rate (ASRR) is shown in Figure 4.5b. For simplicity, the ASRR is not shown for the $[Fe(CN)_6]^{3-}$ and NiHCF flow electrodes alone, as the values are low due to the low desalination current.
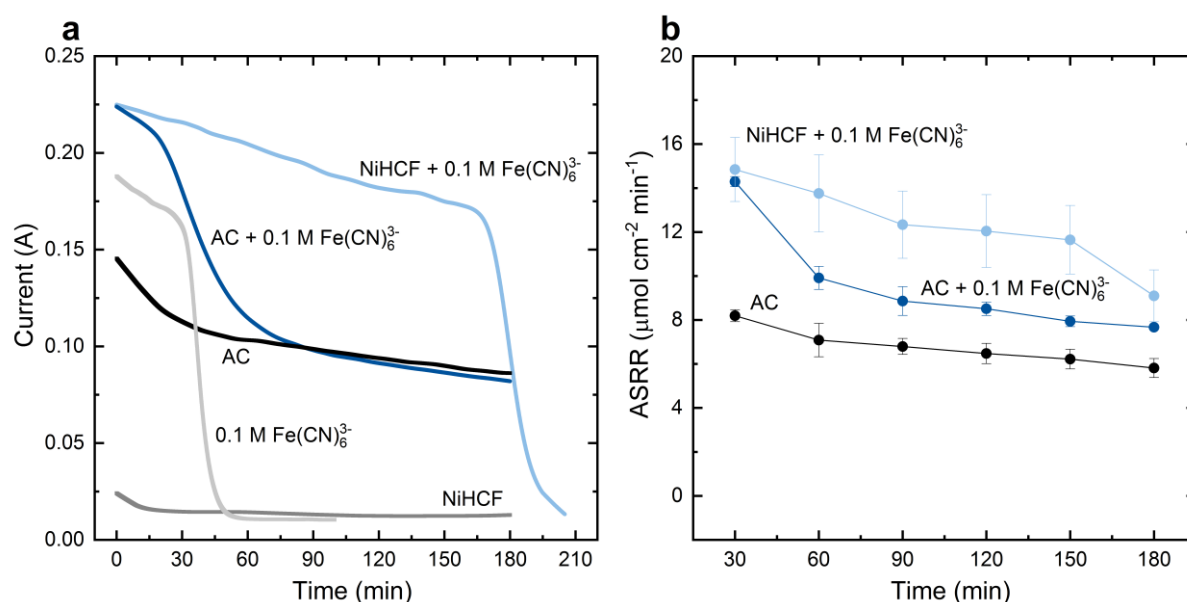
Figure 4.5 – FCDI cell current with different slurries as flow electrode in the cathode reservoir (a). Desalination rate over time for different flow electrodes (b).

The typical flow electrode with AC in both the anodic and cathodic compartments was used as a control system. The flow electrode with only AC presented an initial current of approximately 150 mA, which later fell to 100 mA and slowly decreased over time. The ASRR ranged from 8.2 $\mu mol\ cm^{-2}\ min^{-1}$ at 30 min to 5.8 $\mu mol\ cm^{-2}\ min^{-1}$ at 180 min. In the ICC setup used in those experiments, the activated carbon is not continually regenerated and becomes saturated with Na^+ in the cathode and Cl^- in the anode. Thus, the current should decrease over time at a constant applied voltage. It is relevant to mention that according to the experimental design this decrease in current is caused mainly by the cathode, as the anode has a significant

excess of activated carbon. The change in the current curve slope observed around 20 min may be due to the change in the energy for the electroadsorption of Na^+ and Cl^- ions in the AC. First, Na^+ and Cl^- are likely adsorbed on more favorable sites forming a monolayer and then on the increasingly difficult ones.

The flow electrode with only NiHCF presented the worst performance, as the current remained below 25 mA. The reason is likely due to a high charge transfer resistance between the graphite current collector and the NiHCF particles, as NiHCF is a semiconductor and less conductive than activated carbon. Furthermore, it is commonly discussed in the flow-electrode literature that a charge percolation between the active particles may increase the system's performance (Akuzum et al., 2020; Rommerskirchen et al., 2019). Then, it can also be assumed that the flow electrode with NiHCF has a lower charge percolation than activated carbon.

The flow electrode with only RM – 0.1 M $[Fe(CN)_6]^{3-}$ and no solid – presented an initial current of around 180 mA. This current steadily decreases until 40 min, sharply reducing to less than 10 mA. The reason for that behavior is that $[Fe(CN)_6]^{3-}$ is reduced to $[Fe(CN)_6]^{4-}$, so the concentration of $[Fe(CN)_6]^{3-}$ decreases, and after some minutes, the mass transport of the species may control the kinetics of the electrochemical reactions, increasing the cell resistance. Later, all RM_{ox} is reduced, and the desalination process stops.

The flow electrode with RM and AC presented an initial current of around 225 mA. This current is higher than the current with only $[Fe(CN)_6]^{3-}$ and only AC, suggesting a synergistic effect when the RM is added to the AC slurry. It can be observed that the current steadily reduces until approximately 20 min and then sharply decreases. Considering the total charge transferred in this experiment, and assuming that all this charge was transferred to the $[Fe(CN)_6]^{3-}$, at 35 min, 432 C were transferred to the system, and all the RM_{ox} was reduced. Then, the reaction can only proceed with the transfer of electrons to the AC, and the system behaves as an AC-only flow electrode. In this way, the current drops to around 100 mA, the same as in the only AC flow electrode. The current shift reflected in the ASRR, which is higher (14.3 $\mu mol.cm^{-2} min^{-1}$) at 30 min and decreases to 7.7 $\mu mol.cm^{-2} min^{-1}$ at 180 min.

The flow electrode with redox mediator and NiHCF presents an initial current of around 225 mA, similar to AC + RM. However, the current does not drop sharply after 40 min and slowly decreases over 180 min to around 170 mA. Consequently, the desalination rate was more stable over the experiment and ranged from 14.8 $\mu mol.cm^{-2} min^{-1}$ to 9.1 $\mu mol.cm^{-2} min^{-1}$, from 30 to 180 min. The RM_{red} ($[Fe(CN)_6]^{4-}$) produced at the cathode has a lower redox potential than NiHCF particles. Thus, NiHCF acts as a oxidizing agent for $[Fe(CN)_6]^{4-}$, and

$[Fe(CN)_6]^{3-}$ is produced again. In this way, it is expected that the concentration of $[Fe(CN)_6]^{3-}$ remains constant as long as the NiHCF is not fully reduced. This redox-targeting reaction process was proven to happen in the flow electrode, as shown later in this study. Considering that all charge was used to reduce the NiHCF particles, and using the capacity measured in the NiHCF slurries, after approximately 141 min, the NiHCF is fully reduced. Consequently, the RM_{ox} cannot be restored, its concentration decreases, and the current drops near 0 mA as no species can be reduced at the cathode. The performance of this flow electrode was better than AC + RM, as for the same cell voltage, the current was higher during the whole desalination process. This result supports the hypothesis formulated in this work that the RM can improve the system with faradaic materials.

4.4.2 Effect of redox mediator concentration

The effect of the concentration of RM_{ox} on the desalination rate was investigated for concentrations of 0.05, 0.1, and 0.2 M. The FCDI cell current over time curves for an applied voltage of 1.2 V are shown in Figure 4.6a, and the corresponding normalized conductivity of the product water is shown in Figure A.4. Figure 4.6b shows the ASRR of each flow electrode.
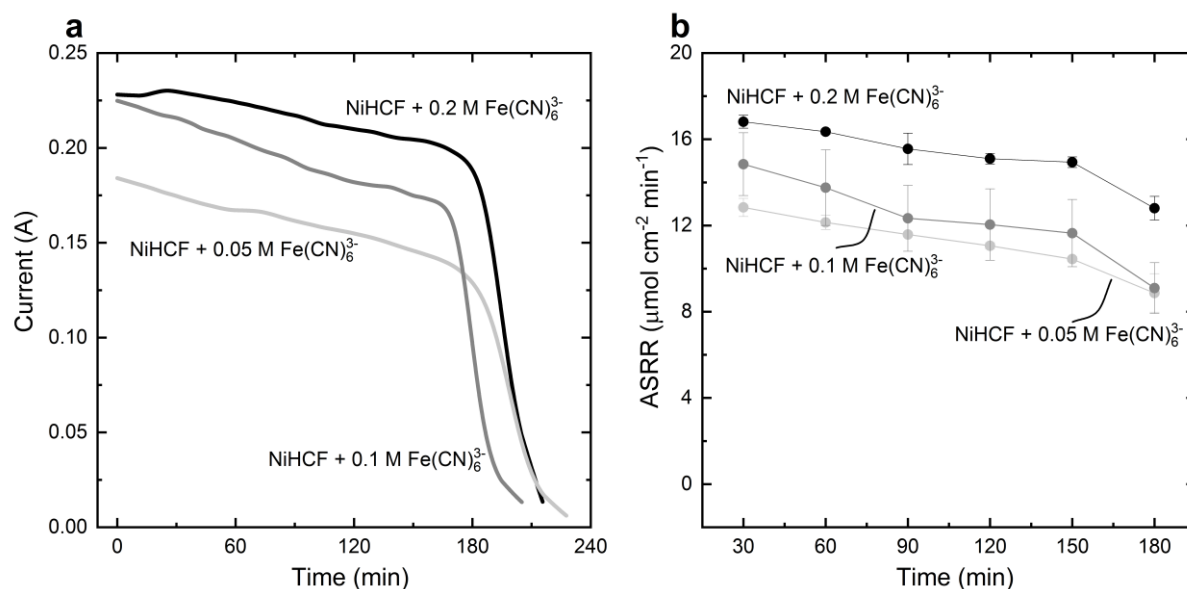
Figure 4.6 – Current response of FCDI cell for different flow electrodes with NiHCF and different concentrations of RM_{ox} (a). Desalination rate over time for different flow electrodes (b).

The flow electrode with 0.05 M $[Fe(CN)_6]^{3-}$ resulted in the worst desalination performance of all experiments. Initially, the FCDI presented a current around 187 mA, which drops lower

than 150 mA after 180 min. Around 225 min, the capacity of the cathodic flow electrode is reached, and the FCDI current drops to nearly 0 mA.

The flow electrode with NiHCF + 0.2 M $[Fe(CN)_6]^{3-}$ shows the highest current, which slowly varies from 225 to 212 mA after 180 min of the experiment. The expected total charge to reduce the RM and NiHCF is 2565 C. Then, after integrating the current vs. time curve, it is projected that around 155 min all the NiHCF is reduced, and the concentration of redox mediator drops resulting in a sharp decrease in current. The initial currents were similar for the experiments with 0.2 M and with 0.1 M $[Fe(CN)_6]^{3-}$ but decreased faster for the latter. Figure 4.6b shows that for 0.2 M, the ASRR ranged from 16.8 to 12.8 $\mu mol\ cm^{-2}\ min^{-1}$, and for 0.1 M the ASRR ranged from 14.8 to 9.1 $\mu mol\ cm^{-2}\ min^{-1}$. Consequently, a higher RM concentration leads to a lower salt concentration in the product water (Figure A4). For all experiments, current efficiency was close to unity, showing the RM concentration has no detrimental effect on ion removal. Furthermore, the iron concentration in the product water was investigated by ICP-OES. For the experiments with 0.2 M of $[Fe(CN)_6]^{3-}$, the concentration was below the detection limit of the equipment (0.01 $mg\ L^{-1}$).

The current of all three experiments dropped roughly simultaneously despite the redox mediator concentration. However, as the current responses in the experiments were different, this resulted in different reaction rates in the system. Then, the complete reduction of NiHCF and $[Fe(CN)_6]^{3-}$ occurred at different times. If the desalination experiments were run with a constant current, higher redox mediator concentration would result in longer experiments, as more RM would be available for reduction. Also, for experiments with constant current, a lower cell voltage is expected for higher RM concentrations, which means lower energy consumption. Alternatively, a higher current can be applied in the system with more redox mediators until it reaches 1.2 V. Consequently, the feed water flow rate can also be increased, so the productivity $(L\ m^{-2}\ h^{-1})$ of desalinated water is enhanced.

The reason for the better performance with a higher RM concentration is beyond the scope of this investigation. The change in concentration of RM acting as the charge carrier may change the overpotential of the reduction reaction of $[Fe(CN)_6]^{3-}$ at the current collector, increasing the current in the system. Furthermore, considering the Nernst equation, the higher the concentration of RM in the system, the lower the redox potential of the electrolyte (Figure A.6). This may increase the driving force between the RT reaction between RM_{red} and NiHCF, accelerating the electron transfer in the system. Yet, the concentration can influence the process if the RT reaction or the reduction of RM at the current collector is diffusion limited. Further

increase in RM concentration may cause some loss in a desalination system. For instance, if the cathode compartment has a much higher salt concentration than the water channel, water crossover to the flow electrode may happen due to osmosis, reducing the process efficiency.

4.4.3 Validation of redox mediator reaction with NiHCF

A spectroscopy investigation was conducted to demonstrate the mechanism of RT reaction in the cathodic flow electrode containing $[Fe(CN)_6]^{3-}$ and NiHCF. In the FT-IR spectra, the peaks at wavenumbers of 2163 and 2093 cm^{-1} are related respectively with the presence of Fe^{III} and Fe^{II} bonded to the CN group in the NiHCF lattice. Hence, those peaks indicate the state of oxidation of the NiHCF particles qualitatively (Shen et al., 2020). UV/vis spectroscopy was used to qualitatively analyze the concentration of the $[Fe(CN)_6]^{3-}$ over time. The peak at a wavelength of 420 nm is related to the concentration of $[Fe(CN)_6]^{3-}$, as the species $[Fe(CN)_6]^{4-}$ does not absorb light at this wavelength. Figure 4.7a and b show part of the measured UV/vis and FTIR spectra. The full spectra are shown in Appendix A (Figure A.7).
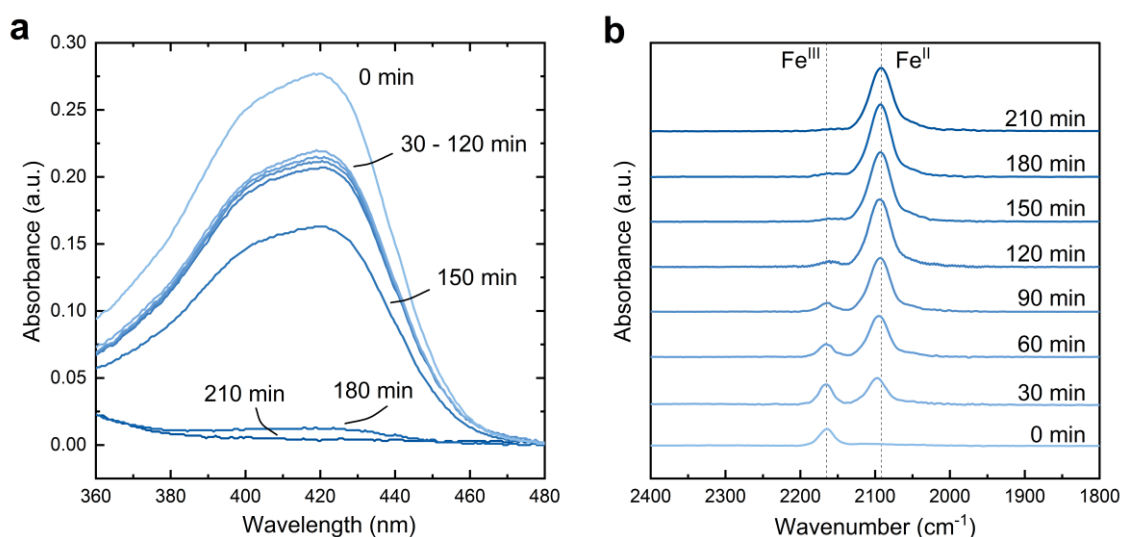
Figure 4.7 – Spectroscopy analysis of the electrolyte and NiHCF particles from the flow-electrode reservoir at different desalination time intervals: UV/vis spectra of the electrolyte show the decrease of $[Fe(CN)_6]^{3-}$ concentration (a) and FT-IR spectra show the reduction of the NiHCF (b) with increasing time.

As shown in Figure 4.7a and b, before the start of the experiment – 0 min – the UV/vis and FT-IR spectra correspond to the maximum concentration of $[Fe(CN)_6]^{3-}$ and the pristine NiHCF respectively. For the NiHCF, only the band at 2163 cm^{-1} is present, indicating that NiHCF is

likely fully oxidized. After 30 min of desalination experiment, the peak intensity at 420 nm (UV/vis spectra) decreases, which indicates the reduction of $[Fe(CN)_6]^{3-}$ to $[Fe(CN)_6]^{4-}$ in the cathode, as shown in Eq. (4.9). Regarding the FT-IR spectra at 30 min, a new peak at 2093 cm^{-1} related to the presence of Fe^{II} appeared, compared to the pristine sample. That indicates part of NiHCF was reduced after 30 min of the experiment. For 60, 90, and 120 min samples, the peak at 420 nm of UV/vis spectra remains with almost the same intensity as for 30 min, and so the $[Fe(CN)_6]^{3-}$ concentration is similar from 30 to 120 min. The FT-IR shows that the peak at 2093 cm^{-1} increased over time in those samples, demonstrating that the NiHCF is being reduced during the experiment. The RT reaction mechanism shown in Eq. (4.10)(4.10 can explain the behavior of both spectra. First, the $[Fe(CN)_6]^{3-}$ is reduced according to Eq. (4.9). Then, as the redox couple $[Fe(CN)_6]^{3-}/[Fe(CN)_6]^{4-}$ has lower redox potential compared to NiHCF, the $[Fe(CN)_6]^{4-}$ species act as a reducing agent, and electrons are transferred to NiHCF. The reduced NiHCF intercalates Na^+ in the electrolyte, and $[Fe(CN)_6]^{4-}$ is oxidized back to $[Fe(CN)_6]^{3-}$, as shown in Eq.(4.10), and represented in Figure 4.8. In this way, the concentration of $[Fe(CN)_6]^{3-}$ remains almost constant between 30 and 120 minutes of the experiment. This process might continue until the capacity of NiHCF is over, and the particles can no longer be reduced. Hence, the $[Fe(CN)_6]^{3-}$ is consumed, and its concentration drops until all the reactant is reduced.

$$[Fe(CN)_6]^{3-} + e^- \rightleftharpoons [Fe(CN)_6]^{4-} \qquad (4.9)$$

$$[Fe(CN)_6]^{4-} + Na^+ + Ni_{1.5}[Fe^{III}(CN)_6] \rightleftharpoons [Fe(CN)_6]^{3-} + NaNi_{1.5}[Fe^{II}(CN)_6] \quad (4.10)$$
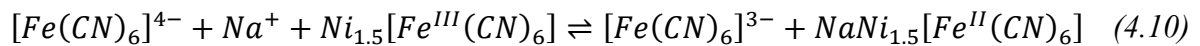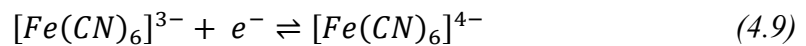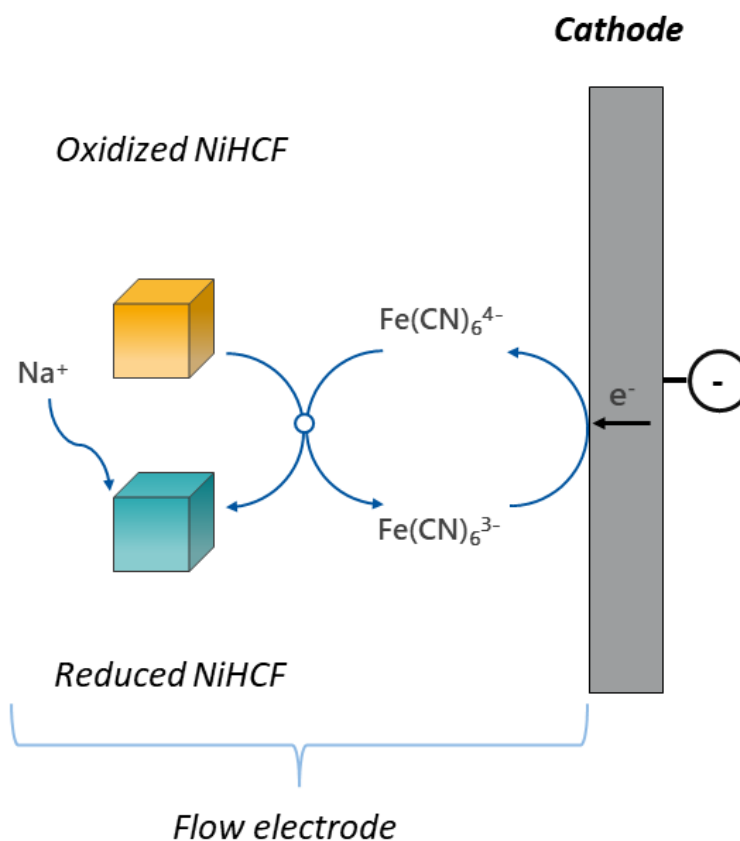
Figure 4.8 – Working principle of a redox-mediated process in the cathodic flow electrode. One electron is transferred to the flow electrode through the reduction of $[Fe(CN)_6]^{3-}$ to $[Fe(CN)_6]^{4-}$. Then, the $[Fe(CN)_6]^{4-}$ reduces the NiHCF, producing again the $[Fe(CN)_6]^{3-}$. Upon reduction, the NiHCF intercalates Na^+ present in the electrolyte. The concentration of $[Fe(CN)_6]^{3-}$ remains almost constant until all the NiHCF is reduced.

Integrating the current vs. time curve gives the charge transferred for the slurry during the desalination. Assuming that all charge transferred was used to reduce NiHCF – which is not true as the UV/vis showed that the concentration is of $[Fe(CN)_6]^{3-}$ decreases from 0 to 30 min –, and considering the capacity of NiHCF is 64 mAh g^{-1}, at around 153 min all NiHCF will be reduced. Since NiHCF particles and $[Fe(CN)_6]^{3-}$ were removed by sampling, the NiHCF was fully reduced a few minutes before 153 min. In this way, it is expected that around 150 min, the concentration of $[Fe(CN)_6]^{3-}$ will decrease, as the RT reaction shown in Eq. (4.10) can no longer take place. At 150 min, the $[Fe(CN)_6]^{3-}$ concentration is not constant anymore as the peak intensity is reduced. In Figure 4.7b, the peak corresponding to Fe^{III} almost vanishes, and the peak related to Fe^{II} increased more compared to Fe^{III} at 150 min. For 180 and 210 min, the FT-IR shows that the NiHCF peaks remain unchanged, and only the peak at 2093 cm^{-1} is visible.

As discussed, this indicates that all the solid was reduced, and consequently, the concentration of $[Fe(CN)_6]^{3-}$ decreases until all the species are consumed. As shown in Figure A.8 in the supplementary material, the current response in the FCDI cell drops until the desalination stops, as no reaction takes place at the cathode. Then, it demonstrates that $[Fe(CN)_6]^{3-}$ is reacting in the cathodic current collector, producing $[Fe(CN)_6]^{4-}$, which then gives the electrons to the NiHCF particle until the particles are fully reduced.

4.5   Conclusion

This work demonstrates that the selection of an adequate redox mediator allows the application of faradaic materials in flow-electrode capacitive deionization cells. The performance of flow electrodes with $[Fe(CN)_6]^{3-}$ as a redox mediator and NiHCF as active particles were compared with typical activated carbon slurries, in the presence and absence of a redox mediator. The flow electrode with 0.2 M of $[Fe(CN)_6]^{3-}$ showed a current response varying from 225 mA to 210 mA, which represents more than 100 % increase in the cell current compared to the system with activated carbon slurry only (approximately 150 mA to 100 mA).

It was also found that the redox mediator concentration is decisive for the desalination rate. Higher and more stable currents were obtained using higher redox mediator concentrations – from 0.05 M to 0.2 M. No crossover of redox mediator and in turn no contamination of product water with iron was observed for the concentrations investigated here. The results of FTIR and UV/vis spectroscopy demonstrate the role of $[Fe(CN)_6]^{3-}$ as a redox mediator for the redox-targeting reaction between $[Fe(CN)_6]^{4-}$ and NiHCF. It is shown that redox mediators double the system's desalination performance with a faradaic material. This study also demonstrated that FCDI cells with flow electrodes based on faradaic materials and redox couples perform better than activated carbon-only slurries. This opens new strategies to enhance the charge transfer in flow electrodes based on faradaic materials, allowing other intercalation materials to be applied in FCDI.

5 Flow electrode capacitive deionization with iron-based redox electrolyte

Highlights

- Low-cost iron-based redox couples outperformed typical activated carbon FCDI
- The concentration of iron chloride influences the salt removal rate
- 0.2 M of iron chloride double the desalination compared to activated carbon
- Iron chloride in flow electrode decreases the pH of diluate and concentrate streams
- Iron citrate increases desalination by 23%, and the water product has a pH around 7

Graphical abstract
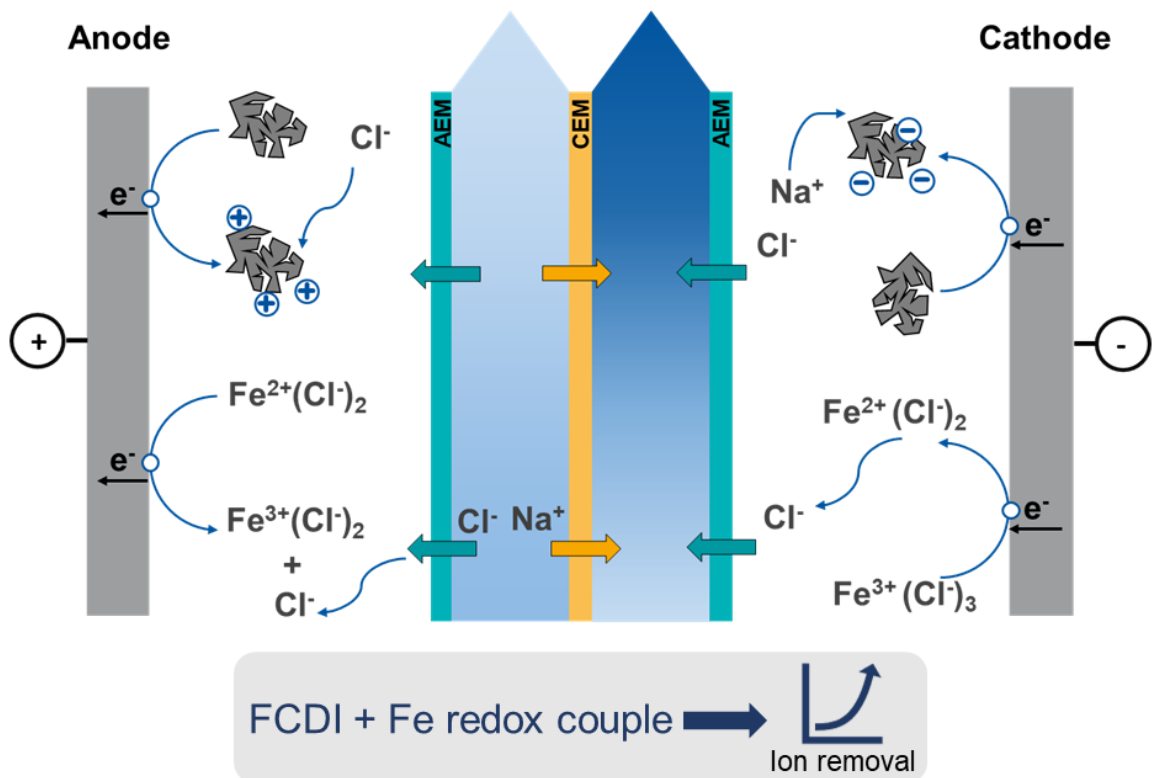
Abstract

Flow electrode capacitive deionization (FCDI) is a promising electrochemical separation method based on flow electrodes with carbon-based materials. The use of redox couples as additives, such as vanadium, ferricyanide, and organic molecules, has been proven to increase the desalination rate of FCDI. However, those additives should fulfill the following requirements: have low cost, do not undergo any reaction within the electrolytes, and have low toxicity. Herein, we investigate using two iron redox couples based on their low cost and lower risk for human health. Hence, iron chloride and iron citrate were used along with activated carbon (AC) in the flow electrodes. We show that both species enhance by a factor of 100% and 23% of the salt removal rate of FCDI cells compared to typical AC slurries. In our system, the salt removal rate for the AC is 7.8 μmol cm^{-2} min^{-1} and increases up to 15.6 μmol cm^{-2} min^{-1} in the iron chloride system, while iron citrate flow electrodes improved the desalination rate to 9.6 μmol cm^{-2} min^{-1}. It is also demonstrated that the concentration of iron chloride in the flow electrode influences the iron crossover to the water streams and their pH, which becomes acid for the iron chloride flow electrode. However, the iron citrate-based slurry presents negligible iron concentration and a circumneutral pH suitable for potable water. The results of this work show that iron-based redox couples are interesting additives for FCDI slurries and that the composition of the flow electrode should be tuned depending on the intended ion removal application.

5.1 Introduction

Water resource management is a significant concern in a context where scarcity is predicted to grow over time. Therefore, water treatment for potable water production, water recycling in industrial processes, or recovering valuable ions is relevant. In this context, electrochemical processes have attracted interest recently due to the possibility of treatment of different feedwater compositions and their energy efficiency.

Among those techniques, electrodialysis (ED), capacitive deionization (CDI), flow-electrode capacitive deionization (FCDI), and redox-flow desalination (RFD) are the most investigated processes. However, CDI is limited to treating low salt concentration streams due to the limitation of salt adsorption capacitive at the electrodes. Electrodialysis is a mature technology, and it is considered to be more efficient in salt concentrations lower than 3 g L^{-1} of salt.

RFD and FCDI are based on flow electrodes but with distinguished compositions and working principles. While RFD is based on the redox flow batteries architecture, it operates with flow electrodes based on soluble redox couples that are oxidized and reduced in the electrodes. On the other hand, in FCDI, the flow electrodes consist of a slurry, where the active materials are commonly based on carbon materials, such as activated carbon (AC), carbon black (CB), graphene, and carbon nanotubes (CNTs). The current collector charges the materials, which in turn electro-adsorb ions from the electrolyte. As the electrons are transported via the physical contact of the particles on the current collector or via the charge transfer between the slurry particles, the resistance of the flow electrode in FCDI is high. Some studies tried to improve the flow electrode by increasing the solid content or mixing different carbon materials. However, those strategies increase the chance of clogging, the pumping energy, and the cost of flow electrodes.

Recently, a new strategy to improve conductivity in the flow electrode involved mixing the carbon particles with redox couples. Several inorganic redox couples such as $[Fe(CN)_6]^{3-}$/$[Fe(CN)_6]^{4-}$ (Kim et al., 2022; S. Kim et al., 2023; Luo et al., 2022), V^{2+}/V^{3+} (Z. Wang et al., 2021), I^-/I_3^- (Luo et al., 2021), and organic redox couples such as sodium anthraquinone - 2 - sulfonate (AQS), 4 - hydroxy - 2,2,6,6 - tetramethylpiperi - dine 1 - oxyl (TEMPO), and hydroquinone (H_2Q/Q) (Luo et al., 2022). Among those redox couples, $[Fe(CN)]_6^{3-}$/$[Fe(CN)]_6^{4-}$ is the most applied reactant due to its fast electrochemical kinetics and accessibility. However, this redox couple reacts with several transition metals, such as iron, copper, nickel, manganese, and zinc, and co-precipitate, forming solid particles known as Prussian Blue Analogs. These

precipitates will likely foul the membrane, hindering their application in real applications. The species V^{2+}/V^{3+} and I^-/I_3^- can be toxic in water environments, and vanadium salts are also expensive chemicals. Furthermore, organic redox couples are usually expensive, have limited water solubility, and also offer environmental risks. Iron-based flow electrodes can be an interesting alternative to those reactants, as iron is a ubiquitous element with several non-costly salts. Iron can also be complexed with organic molecules in a variety of complexes, allowing different compounds to be investigated. Studies have reported the use of iron diethylenetriamine pentaacetate DPTA (Xie et al., 2023) and iron citrate (Fe-Cit) (Mohandass et al., 2022) for RFB, and iron malonate (Han et al., 2023) with and without CNTs in the flow electrode. Those studies suggest a low energy consumption and high productivity of water purification.

Here, we propose the application of iron chloride (Fe-Cl) and Fe-Cit as flow electrodes in a typical FCDI cell. The desalination performance of those redox couples with and without AC is evaluated. The aim is to determine if those redox couples can improve the salt removal in FCDI cells and determine the concentration's effect on the performance. It is shown that even the lowest concentration of Fe-Cl in this study (0.05 M) has a better desalination rate than typical FCDI slurries with 15 wt.% of AC. Depending on the concentration, the salt removal rate can increase with the additives two-fold, indicating the possibility of enhancing FCDI productivity with iron-based salts. Based on the results, it is demonstrated that both redox couples are interesting alternatives for flow electrodes, and the choice of the appropriate composition of the flow electrode should be tailored to the specific application.

5.2   Experimental

5.2.1   Materials

The feedwater was prepared with NaCl (Carl Roth chemicals, 99.5%). Activated carbon (Carbopal SP11), iron (III) chloride hexahydrated (Carl Roth chemicals, 99.0%), iron (II) chloride tetrahydrated (Carl Roth chemicals, 99.0%), and sodium citrate tribasic (Sigma-Aldrich, 99.0%) were used for the preparation of the flow electrodes.

5.2.2   FCDI cell configuration

The FCDI experiments were performed with the same cell design described in a previous work (Linnartz et al., 2017). The FCDI cell was set up in the so-called single-module (SM) configuration. In this way, the flow electrode has one reservoir, and the slurry recirculated through the current collectors, as shown in the scheme in Figure 5.1. The cell consisted of two

acrylic end plates and two epoxy-impregnated graphite current collectors (Müller & Rössner GmbH & Co. KG) with 3 mm in width and 2 mm in-depth carved flow channels. Two 0.5 mm mesh spacers (Fumatech BWT GmbH, ED-40) were used as a water channel between the membranes, one spacer being the diluate channel and the other being the concentrate one.

Cation and anion exchange membrane: Fumasep FKB-PK-130 and Fumasep FAB-PK-130, respectively (Fumatech BWT GmbH), were applied in the system. The cell used three membranes, and the configuration depended on the charge iron complexes evaluated. To avoid the diffusion of the redox couples from the flow electrode to the water channels when the iron complex had a positive charge (Fe-Cl flow electrode), an anion-cation-anion exchange membrane (ACA) configuration was used. Conversely, when the iron complex had a negative charge (Fe-Cit), the cell was assembled in a cation-anion-cation exchange membrane (CAC).

A peristaltic pump (Ismatec Reglo ICC, Cole-Palmer) was used to supply water to the FCDI cell, and a pump (MasterFlex Easyload II Dual Channel) was used to pump the flow electrodes. A power supply (Keysight Agilent E3644A) was used to control the applied voltage in the FCDI cell. The conductivity of the product solution was monitored with conductivity probes (Knick SE 615/1-MS, Knick Elektronische Messgeräte GmbH & Co. KG), and the chloride and sodium content of the diluate and concentrate was determined by high-performance liquid chromatography (Agilent 1200, HPLC).
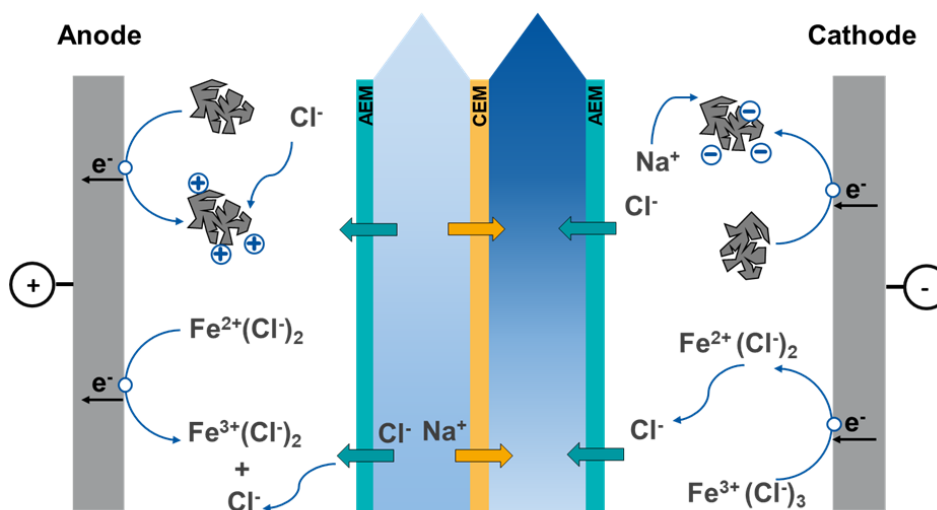
Figure 5.1 – Scheme of the FCDI cell used for the experiments. The flow electrodes are set up in the single-module configuration. The feedwater is in a single-pass mode, so the cell was continuously supplied with a new electrolyte.

5.2.3 Synthesis of iron-based electrolytes

This study investigated two iron complexes: iron chloride (Fe-Cl) and iron citrate (Fe-Cit). The iron chloride flow electrodes were prepared by mixing equimolar quantities of iron chloride (III) and iron chloride (II) and dissolving the salts in deionized water. The final pH was approximately 1.7. The total iron concentration (Fe$_T$) was 0.05, 0.1, 0.2, and 0.4 M, and NaCl was added to the electrolyte, so the flow electrode has the same concentration of NaCl (5 g L^{-1}) as the feedwater channels. The iron citrate solution consisted of an iron/citrate ratio of 1:3, with a total iron concentration of 0.2 M. For the synthesis of iron citrate (Fe-Cit), equimolar quantities of iron(III) chloride and iron(II) chloride were dissolved in deionized water along with NaCl (the equivalent of 5 g L^{-1}). In another beaker, sodium citrate was dissolved in deionized water and then mixed with the iron chloride solution. There was no adjustment of the electrolyte pH for the iron chloride and iron citrate experiments. In all experiments, the total electrode volume was 100 mL. In the experiments with activated carbon, it was added to make a 15 wt.% of solids slurry.

The crossover of iron to the water streams was analyzed by ICP-OES (PlasmaQuant PQ9000 Elite, Analytik Jena), and the citrate crossover was investigated by measuring the total organic carbon with a Total Organic Carbon Analyzer (Shimadzu Europa GmbH, Duisburg, Germany).

5.2.4 Desalination experiments

The experiments were carried out with 5 g L^{-1} of NaCl in the feed water. The flow rate of diluate and concentrate was 5 mL min^{-1}, meaning the water recovery (WR), given by Eq. (5.1)(5.1, was 50% for all tests (where Q_d and Q_c are the diluate and concentrate flow rates).

$$WR = \frac{Q_d}{Q_d + Q_c} \qquad (5.1)$$

We first investigated the FCDI cell in experiments with AC-only, Fe-Cl-only, and a mixture of Fe-Cl and AC. The composition of the flow electrodes and the parameters chosen for the desalination experiments are summarized and shown in Table 5.1.

Table 5.1 – Overview of the flow electrode compositions and FCDI system parameter settings for desalination experiments with iron chloride and activated carbon.

Composition	Flow electrode								
AC (wt.%)	0	0	0	0	15	15	15	15	15
Fe_{Total} (mol L^{-1})	0.05	0.1	0.2	0.4	0.05	0.1	0.2	0.4	0.05

In the experiments with Fe-Cit, the same parameters described for Fe-Cl were applied. However, the flow electrodes were investigated with only 0.2 M of Fe_T, with and without AC.

5.2.5 Analysis of desalination performance

The performance of the desalination experiments was analyzed using the same metrics presented in the previous chapter. The average salt removal rate (ASRR, µmol cm^{-2} min^{-1}) was calculated according to Eq. (4.3), the charge efficiency (CE), shown in Eq. (4.4), volumetric energy consumption (E_{vol}, kWh m^{-3}) for desalination can be calculated as follows in Eq. (4.5), the energy consumption per mol of removed salt (E_{mol}) was calculated by Eq. (4.6).

5.3 Results and discussion

5.3.1 Comparison of desalination with iron chloride and AC-only flow electrodes

This section compares flow electrodes with several concentrations of Fe-Cl and a typical FCDI AC flow electrode. The experiments were run at a constant voltage of 1.2 V to avoid the reduction and oxidation of water. For the flow electrode with only AC, the system typically works as FCDI cells, where the AC particles touch the current collector and become charged. Then, the AC adsorbs the ions with opposite charges in the flow electrodes, and ions cross the membrane to balance the charge. For the system consisting of $FeCl_3/FeCl_2$ redox couple, the $FeCl_2^+$ and $FeCl^+$ (the predominant Fe^{3+} and Fe^{2+} species) are oxidized and reduced, according to Eq. (5.2) and Eq. (5.3), respectively.

Anodic reaction:

$$FeCl^+ + Cl^- + \rightleftharpoons FeCl_2^+ + e^-$$
(5.2)

Cathodic reaction:

$$FeCl_2^+ + e^- \rightleftharpoons FeCl^+ + Cl^-$$
(5.3)
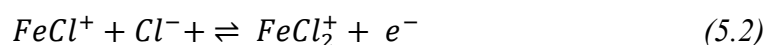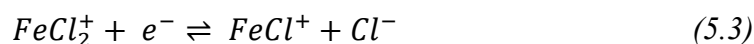
In this way, the reduction reaction creates an excess of negative charge at the cathodic side, and Cl⁻ must cross the anion exchange membrane (AEM) from the flow electrode to the concentrate channel, as shown in Figure 5.1. Conversely, the oxidation reaction creates a positive charge excess on the anodic side, and Cl⁻ crosses the AEM from the diluate channel to the flow electrode. The results of desalination currents of flow electrodes with several Fe-Cl concentrations and a typical FCDI AC slurry are shown in Figure 5.2a.
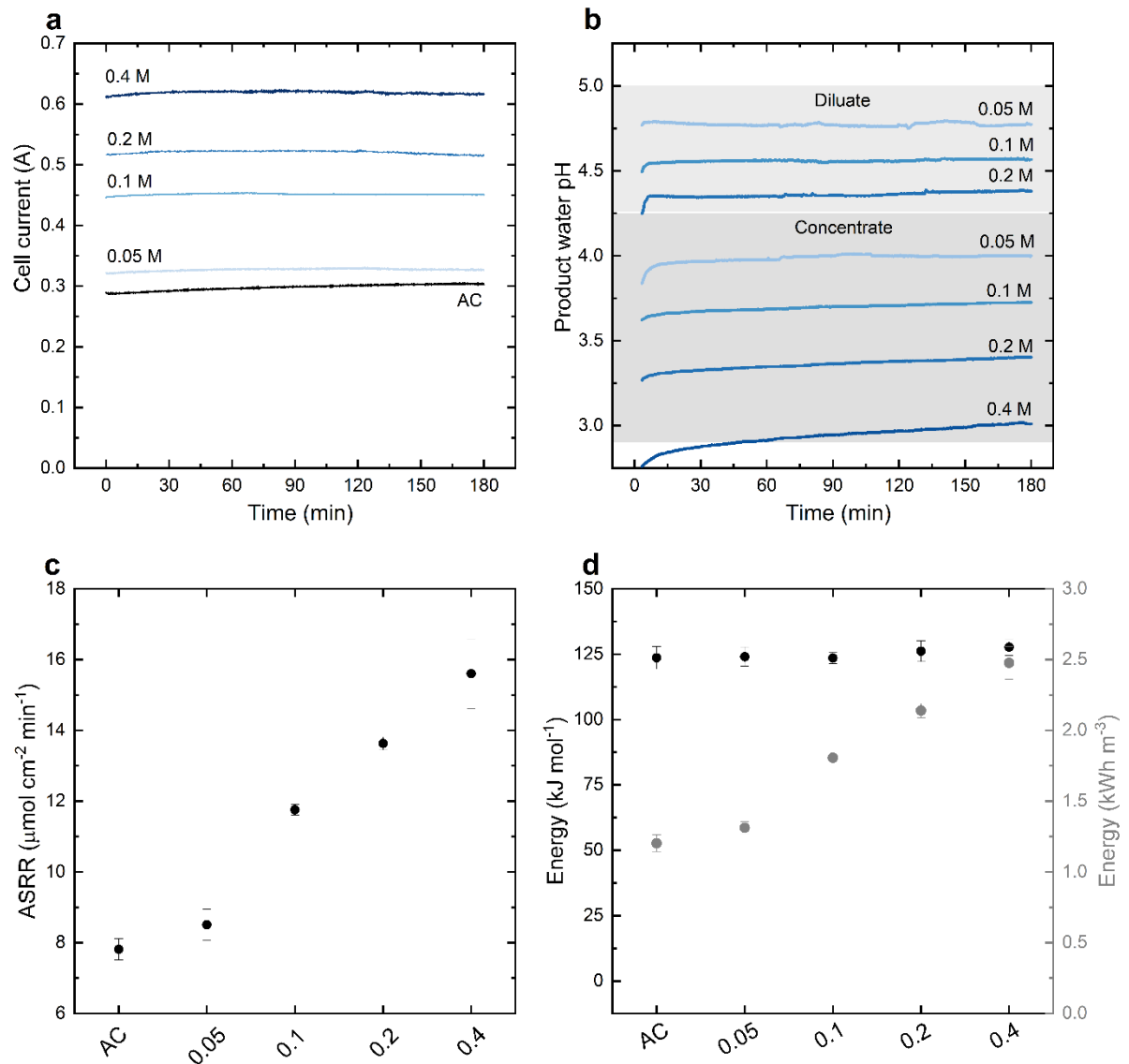
Figure 5.2 – Comparison of desalination performance of several Fe-Cl and typical AC FCDI flow electrodes. The electrical current during desalination (a); the pH of the water produced in the diluate and concentrate channels (b); the salt removal rate (c); and the energy consumption per mole of NaCl removed from the diluate and volumetric energy per volume treated in the diluate channel (d).

In Figure 5.2a, the start of the experiment (0 min) was considered after 3 min of the power supply was turned on. In this way, the current peak that appeared at the experiments' start was removed, making the plots clearer. The current response for the flow electrode with AC was around 298 mA, and remained almost constant over 180 min of the experiment. Regarding the Fe-Cl flow electrodes, the current in the cell was higher for all iron concentrations than the AC flow electrode. For the 0.05, 0.10, 0.20, and 0.40 M of Fe_T, the average current for the experiments was 327, 451, 534, and 619 mA, respectively. Thus, for 0.05, 0.10, 0.20, and 0.40 M, the improvement relative to AC flow electrode was around 10, 51, 79 and 108 %.

The enhanced current for the Fe-Cl system is due to the facile charge transfer in the flow electrode, as the cell works like so-called redox flow desalination systems (S. Kim et al., 2023) or redox-mediated electrodialysis (Kim et al., 2022). The Fe-Cl species oxidized at the anode are later reduced at the cathode and vice-versa, as the Fe-Cl species are recirculated in the current collectors, as shown in Eq. (5.2) and Eq. (5.3). The Nernst equation gives the anodic and cathodic electrochemical potential of the half-cell reactions, as represented in Eq. (5.4) and Eq. (5.5), respectively.

$$E_a \rightleftharpoons 0.77\ V - 0.059V \cdot log\frac{[FeCl_2^+]}{[FeCl^+]} \tag{5.4}$$

$$E_c \rightleftharpoons 0.77\ V - 0.059V \cdot log\frac{[FeCl^+]}{[FeCl_2^+]} \tag{5.5}$$

The difference between the anode potential, E_a, and the cathode potential, E_c gives the overall thermodynamical potential for the reaction. Since the standard potential E^O of the anodic and cathodic reactions is the same, these terms cancel each other. Additionally, under the assumption that the activities of $FeCl_2^+$ and $FeCl^+$ are equal (considering the activities as the ion concentration and the concentration change of the species in the current collector is negligible), the terms within the logarithm in both equations are equal and cancel each other. Consequently, the overall thermodynamical potential for the operation of the cell should be zero.

In this way, the potential drop in the cell mainly arises from three sources of resistance: the overpotentials of the Faradaic reactions; the resistance within the spacers (mainly in the diluate channel due to its lower salt concentration); the resistance of the membranes. In the case of cells with AC flow electrodes, the resistance in the spacers and membranes is equivalent to the Fe-

Cl system. Consequently, the resistance of the flow electrodes is the main difference between the systems. The lower current for the AC flow electrodes suggests that the electron transfer resistance between the current collector and the AC particles is less favorable than in the Faradaic system.

Due to the lower resistance for electron transfer and the higher currents in the cell, the average salt removal rate (ASRR) also increases. As shown in Figure 5.2c, the ASRR for the AC-only flow electrode, 7.8 μmol cm^{-2} min^{-1}, is enhanced to 13.6 μmol cm^{-2} min^{-1} and 15.6 μmol cm^{-2} min^{-1}, for the 0.2 M and 0.4 M of Fe-Cl. The energy consumption per mol of NaCl is approximately 125 kJ mol^{-1} and remains stable for the AC-only and Fe-Cl flow electrodes. The energy consumption per volume of treated water leaving the diluate channel increases for the flow electrodes with Fe-Cl, as the electrical current in those experiments was higher. However, it should be considered that the experiments with higher current also have higher ASRR, thus resulting in a lower salt concentration in the diluate water. Suppose the experiments were run with a constant current. In that case, it would be expected that the system with Fe-Cl would result in lower cell voltages for higher Fe-Cl concentrations and, consequently, lower energy consumption per volume of treated water.

5.3.2 Comparison of desalination with AC + iron chloride vs. AC-only flow electrodes

Following the improved desalination rate achieved by Fe-Cl flow electrodes, the synergetic effect of the AC and Fe-Cl mixture was investigated. In Figure 5.3, we compare the desalination performance across various flow electrode compositions. The cell current of the experiments with several Fe-Cl concentrations in the electrolyte is shown in Figure 5.3a.
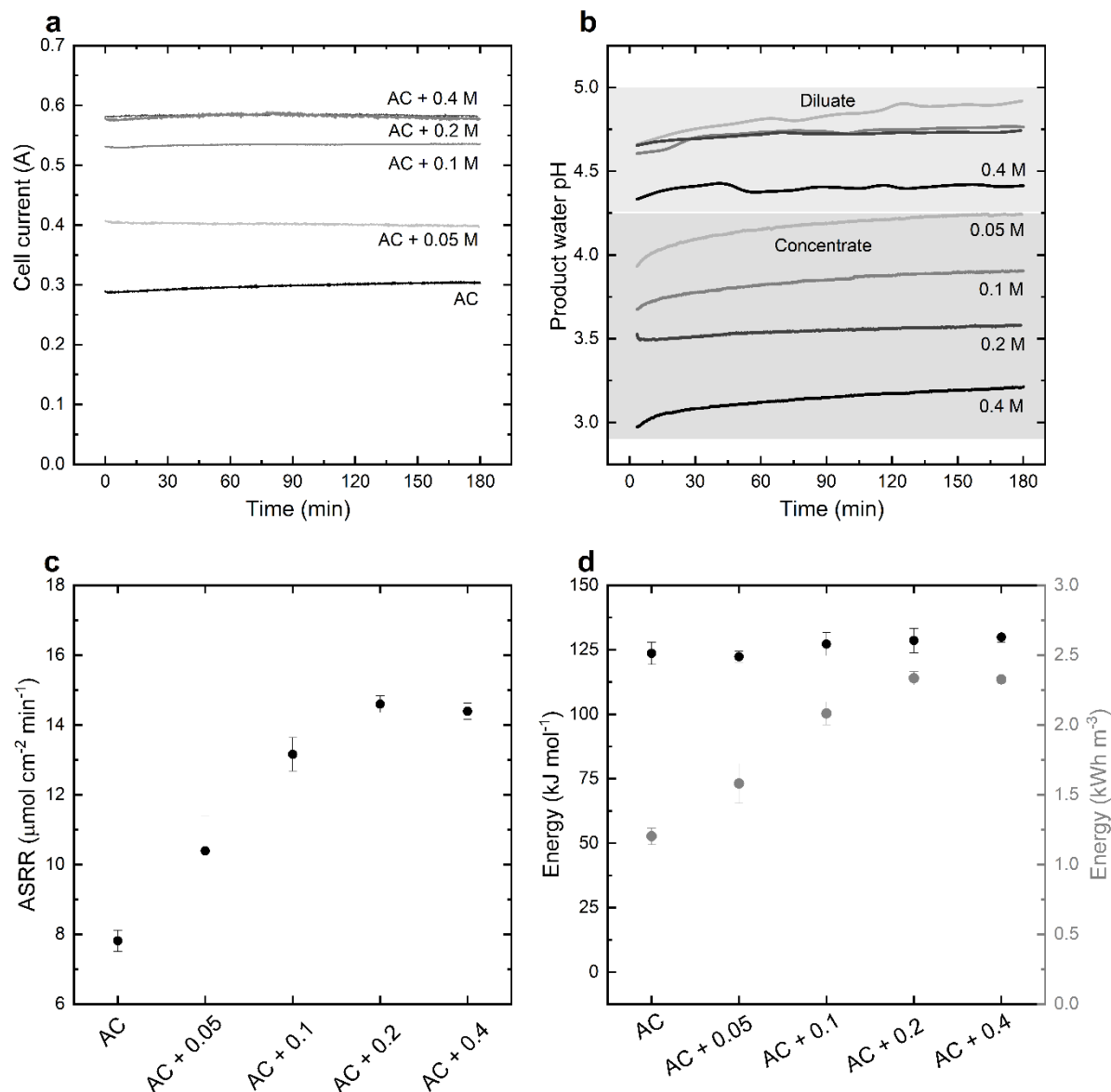
Figure 5.3 – Comparison of desalination performance with flow electrodes with AC and AC + different concentrations of Fe-Cl. Comparison of the electrical current during desalination (a). The pH of the water produced in diluate and concentrate channels (b). The salt removal rate (c). The energy consumption per mole of NaCl removed from the diluate and volumetric energy per volume treated in the diluate channel (d).

In Figure 5.3a, it is shown that the mixed flow electrodes result in higher currents compared to the AC-only slurry. The average currents were approximately 441, 537, 584, and 584 mA, which means that the currents are higher in the AC + Fe-Cl than the same Fe concentration in the Fe-Cl system (except for 0.4 M of Fe_T). Furthermore, the increase in current becomes smaller as the iron concentration increases. For instance, increasing the iron concentration from 0.05 M to 0.1 M increased the current by around 96 mA, while increasing the concentration

from 0.1 to 0.2 mA increased the current only by 47 mA. For the conditions of the experiments investigated, increasing the Fe-Cl to 0.4 M in the presence of AC had no benefit. The smaller increment in current occurs due to a few factors. First, as the salt removal increases with the increase in Fe-Cl concentration, the diluate channel has 0.75 g L^{-1} of NaCl for the 0.2 M, while it has around 2.75 g L^{-1} of NaCl concentration in the experiment with 0.05 M. Thus, the resistance in the diluate channel is higher for 0.2 M. Second, the higher iron concentration in the flow electrode poses resistance to removing ions from the diluate channel. Finally, the iron concentration can affect the electrochemical kinetics of the Fe-Cl redox reaction, and the exchange current density and mass transfer of Fe-Cl species can change. However, this electrochemical investigation is out of the scope of this study.

The increase in current consequently increased the ASRR of AC + Fe-Cl flow electrodes, as shown in Figure 5.3c. The highest ASRR value was obtained for the AC + 0.2 M Fe-Cl flow electrode, reaching 14.6 μmol cm^{-2} min^{-1}. This value is around 7% higher than the flow electrode with the same Fe$_T$ concentration and no AC, which had an ASRR of 13.6 μmol cm^{-2} min^{-1}. Although the AC + 0.4 M resulted in the same current, a slight decrease in the ASRR was observed – 14.4 μmol cm^{-2} min^{-1} – which is slightly lower than the AC + 0.2 M experiments. A slight decrease in the current efficiency is the reason for this reduction, as the flow electrode compartment has more salt than the diluate and concentrate channels, and back diffusion can occur.

The energy consumption per mol was approximately the same for all experiments, around 125 kJ mol^{-1}. A slight increase can be observed in higher iron concentrations (Figure 5.2d), as observed in the Fe-Cl flow electrodes. As previously discussed, the salt concentration of the water product is different. Hence, comparing the volumetric energy of different flow electrodes is not reasonable. For the highest desalination rate with AC + 0.2 M, the volumetric energy was 2.4 kWh m^{-3}, for a productivity of 134 L h^{-1} m^{-2} and a change in concentration in the diluate channel from 5 g L^{-1} to around 0.75 g L^{-1}.

The parameters investigated in this study show that the mixture of AC and Fe-Cl has a synergetic effect and improves the desalination compared to the typical FCDI flow electrode. This effect was previously observed in studies with Vanadium (Z. Wang et al., 2021), FeCN (Luo et al., 2022), and organic redox couples such as TEMPO and Hydroquinone (Luo et al., 2022). The experimental conditions of the present study and the other studies are very different regarding the salt concentrations, operational mode of the water channels (batch versus continuous), and the redox couple concentration. In this study, we investigate redox couple

concentrations higher than the previous studies, as also done with Fe-CN only by Mohandass et al. (Mohandass et al., 2022) and Kim et. al (Y. Kim et al., 2023). In Luo et al. (Luo et al., 2022), for the flow electrode with 15 wt.% of AC and 0.01 M of FeCN, the increase in the ASRR was around 25 %. We demonstrate here that increasing the concentration of Fe-Cl, up to 0.2 M, affects the system positively, as the ASRR almost doubles.

It is important to note that the energy consumption associated with the operation of the pumps was not considered in the overall energy requirements for desalination. A trade-off assessment is necessary when considering the inclusion of AC in the system. On the one hand, the addition of AC offers advantages regarding the energy in the cell. On the other hand, the flow electrode with AC entails higher material costs and demands increased energy for the slurry pumping process. Addressing these concerns necessitates a dedicated study to comprehensively evaluate factors such as changes in viscosity, cost implications, and energy expenditure.

5.3.3   Analysis of water produced

The water product must meet specific salt concentration and pH criteria according to the application of water deionization, i.e., potable water production, ion recovery, or salt metathesis. For instance, for potable water production, the recommended pH should range between 6.5 and 8.5, according to the World Health Organization (WHO) (World Health Organisation, 2007). The iron chloride species $FeCl_3/FeCl_2$ are both Lewis acids, as they can receive a pair of electrons. According to the Pourbaix diagram of the Fe-H_2O system and Fe-Cl-H_2O system (Figure B.1 and Figure B.2), there is a pH limit where the iron soluble species are stable without precipitating iron oxide, usually in the form of ferrihydrite (Cornell and Schwertmann, 2003). This pH limit is increased by the presence of Cl^- as a ligand, but according to our preliminary experiments and other studies in the literature (Hawthorne et al., 2014), at pH above 2.2, the Fe^{3+} precipitates. In this way, the pH of the flow electrode with Fe-Cl was not increased in our experiments, and the flow electrode had an acidic pH of approximately 1.7. As the concentration of ions is higher in the flow electrode than in the diluate and concentrate channels, it is necessary to measure the product water's pH and determine whether the iron species are crossing the membranes.

The pH of the flow electrode with AC-only results in the diluate channel water of approximately pH 10 and the concentrate channel pH of around 7, as shown in Figure B.3.

Figure 5.2b and Figure 5.3b show the pH of diluate and concentrate channels for the experiments with Fe-Cl and AC + Fe-Cl, respectively.

For all the experiments, it is clear from Figure 5.2b and Figure 5.3b that the concentrate stream always has lower pH than the diluate. In the concentrate, a trend can be observed where the higher the iron concentration in the flow electrode, the lower the pH of the product water. Hence, it is likely that H^+ ions cross the membrane to the water channels due to the low pH in the flow electrode. After 180 min, the pH of the concentrate in the experiments with Fe-Cl flow electrode was around 4.0, 3.75, 3.4, and 3.0, for the concentration of 0.05, 0.1, 0.2, and 0.4 M of Fe, respectively. For the same concentration of Fe_T on AC + Fe-Cl system, the pH of concentrate channels after 180 min was 4.5, 3.8, 3.6, and 3.2. Thus, it can be concluded that the presence of AC in the flow electrode slightly attenuates the change in pH in the concentrate channel. This effect could be due to the adsorption of iron chloride species onto the AC particles, slightly reducing the iron chloride concentration in the bulk solution. Also, as shown in Figure B.3, the pH of the concentrate channel in AC-only flow electrodes tends to be circumneutral and can also influence the concentrate pH.

Regarding the diluate channel, in the experiments with Fe-Cl-only (except for 0.4 M), there is also a trend where the higher iron concentration results in lower pH in the diluate channel, as shown in Figure 5.2b. For the experiments with AC + Fe-Cl (Figure 5.3b), the pH for the Fe_T concentration of 0.1 and 0.2 M is similar but lower than the pH for 0.05 M. Furthermore, the flow electrode with 0.4 M of iron has the lowest pH. Apart from some deviation, those results show a relevant influence of the iron concentration of the flow electrode on the water product pH. In a study using Fe-CN as a flow electrode, the reported pH of the diluate channel ranged from 6 to 8 (H. Kim et al., 2023). Other studies with V^{2+}/V^{3+} (Z. Wang et al., 2021) and iron malonate (Han et al., 2023) did not report the pH of flow electrodes and water streams. Vanadium salts are soluble at low pH, and iron malonate was reported to have a fairly acidic pH (Hawthorne et al., 2014). Here, our results suggest that the pH should continually be monitored when working with redox couples as additives for FCDI slurries or in electrolytes for RFD.

Besides the pH, it is also relevant to determine whether the redox couple contaminates the water. Samples of the product water in both diluate and concentrate channels were analyzed by ICP-OES to determine the Fe content. The results of the chemical analysis are presented in Table 5.2.

Table 5.2 – Iron concentration in µmol L^{-1} and mg L^{-1} in the diluate and concentrate streams for different flow electrode compositions. The detection limit of iron is 0.01 mg L^{-1}.

Flow electrode	Iron concentration			
[Fe]	Diluate	Concentrate	Diluate	Concentrate
mol/L	mol/L		mg/L	
0.05	-	3.6E-07	<0.01	0.020
0.1	2.5E-07	3.4E-07	0.014	0.019
0.2	4.1E-07	6.5E-07	0.023	0.036
0.4	4.1E-06	5.6E-06	0.231	0.311
AC + 0.05	-	-	<0.01	<0.01
AC + 0.1	4.7E-07	5.8E-07	0.026	0.032
AC + 0.2	7.2E-07	1.1E-06	0.040	0.062
AC + 0.4	4.9E-06	6.5E-06	0.272	0.363

As shown in Table 5.2, for the experiments with Fe_T of 0.05 M, the iron concentration in the product water is below the detection limit of the equipment for the experiments with AC + Fe-Cl. A low iron concentration of 0.02 mg L^{-1} (0.36 µmol L^{-1}) was found in the concentrate with no AC in the slurry. Iron was always detected in the water streams for the experiments with higher than 0.05 M Fe-Cl in the flow electrode. The Fe content in the product water appears to depend on the Fe concentrations in the flow electrode, as the iron concentration in the water increased with the concentration of Fe-Cl in the flow electrode. The iron concentration in the water stream increases relatively slowly for the flow electrodes up to 0.2 M of Fe_T. At 0.4 M, the iron concentration sharply increases in the water streams. Previously, studies did not observe the redox couple contamination (Luo et al., 2022; Z. Wang et al., 2021), but the highest additive concentration investigated was below 0.05 M, which is the lowest concentration studied here. For another study with flow electrodes with 0.4 M of Fe-CN in an RFD cell, iron was found in the water stream in concentrations of 23 µmol L^{-1} in the concentrate and 0.7 µmol L^{-1} in the diluate.

As the salt concentration in the flow electrode is higher than in the water channels, especially the iron concentration, the ions migrate through the membranes to balance the concentration. It is also evident that the concentrate channel has a higher iron concentration than the diluate channels. The reason for the higher concentration in the concentrate can be the flux of ions. For instance, Cl$^-$ ions cross the AEM from the cathode flow electrode to the concentrate channel. On the other hand, in the diluate channel, the Cl$^-$ crosses the AEM from

the diluate to the anode compartment. The ion exchange membranes are not 100% selective (Luo et al., 2018), and consequently, co-ions can cross the membranes. Thus, it is likely that some Fe-Cl species, despite their positive charge, cross the AEM along with the Cl⁻ to the concentrate stream.

As iron crosses the flow electrode and goes to the water channels, it is expected that the flow electrodes will be depleted in iron after some time. The time needed to decrease the initial iron concentration to 90% ($t_{0.9}$) and 50% ($t_{0.5}$) is estimated for 100 mL of electrolyte in the flow electrode used in the experiments. The iron loss in the experiments is assumed to remain constant, and no Fe-Cl was adsorbed in the AC. Table 5.3 presents the time for $t_{0.9}$ and $t_{0.5}$ in days.

Table 5.3 – Calculated iron loss based on the iron concentration of diluate and concentrated streams and the feed water flow rate.

Time (Day)	Flow electrode							
	0.05	0.1	0.2	0.4	AC + 0.05	AC + 0.1	AC + 0.2	AC + 0.4
$t_{0.9}$	194	234	262	57	-	133	152	49
$t_{0.5}$	970	1172	1312	287	-	663	760	245

For the flow electrode with AC + 0.05 M no iron was detected (Table 5.2). According to Table 5.3, the flow electrodes with concentrations of up to 0.2 M have a $t_{0.9}$ of at least 133 days. The flow electrodes with 0.4 M have fewer days until they lose 10% of iron despite their higher concentration. As shown in Table 5.2, the iron loss rate was much higher for 0.4 M than for the other concentrations. Due to the lower iron crossover, the flow electrodes with 0.05 and 0.1 M last longer until they lose 10% of their initial concentration. It is relevant to mention that those numbers may change in other experimental conditions. For instance, if the NaCl concentration is increased in the feed water, the diffusion of Fe-Cl species to the water channels may be lowered. However, based on the results presented here, it seems reasonable to assume that iron loss is not the primary concern regarding the life-spam of the flow electrode. FCDI and similar technologies are mainly lab-scale, with a few reported scale-up studies. Thus, the minimum requirement for how long a flow electrode should last to be economically feasible (which also depends on its composition) is yet to be determined. Apart from the iron loss, we also foresee that water crossover (due to osmotic effects) from the feed stream to the flow electrode may play an essential role in the process. Nonetheless, we could not observe water cross for those sets of experiments lasting 180 min, and more extended duration tests (e.g., a few days) should be performed in the future.

5.3.4   Desalination with Fe-Cit

As demonstrated by our previous results, the acid flow electrode changes the pH of the water channels. Hence, we investigate how to increase the pH of the flow electrodes with Fe-Cl to control the pH of flow channels. However, the solubility of the Fe^{3+} in the Fe-Cl system is restricted by around pH 2.2, according to our experiments. As previously shown in redox flow batteries, the pH of iron-based organic complexes electrolytes can be increased to a greater extent while avoiding precipitation (Hawthorne et al., 2014). Hence, citrate was chosen as a complexant, as iron citrate and citrate are not hazardous in low concentrations in water. Also, citrate is used as an additive in several foods, does not pose a risk to human health, and is not an expensive chemical, keeping the objective to use a non-expensive additive in FCDI flow electrodes.

The highest desalination rate with a Fe-Cl system without iron contamination, within the WHO standards for potable water, was obtained with 0.2 M of Fe_T in the flow electrode. Thus, the same concentration of Fe_T was tested in the desalination experiments, and the flow-electrode electrolyte consisted of iron and citrate in the concentration of 0.2 M and 0.6 M, respectively. The experiments were run with and without AC, and the pH of the flow electrode was 5.4, with no pH adjustment prior to the tests. The membrane configuration of the cell was changed compared to the Fe-Cl-based flow electrode. The expected Fe-Cit complexes and the citrate ion are negatively charged (Silva et al., 2009). Thus, two cation exchange membranes (adjacent to the flow electrodes) and one anion exchange membrane between the concentrate and diluate spacers were used. For the system with the Fe-Cit salt only, the reaction at the anode and cathode are represented, respectively, in Eq. (5.6) and Eq. (5.7).

Anodic reaction:

$$Fe^{II} - Cit \; \rightleftharpoons \; Fe^{III} - Cit + \; e^- \qquad\qquad (5.6)$$

Cathodic reaction:

$$Fe^{III} - Cit + \; e^- \; \rightleftharpoons \; Fe^{II} - Cit \qquad\qquad (5.7)$$
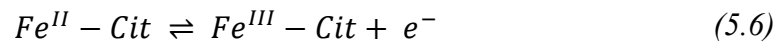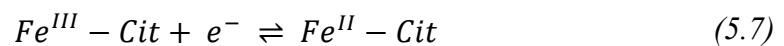
The desalination performance of Fe-Cit-based flow electrodes is presented in Figure 5.4. The cell current for 0.2 M of Fe-Cit and the 0.2 M of Fe-Cl are compared in Figure 5.4a with and without AC.
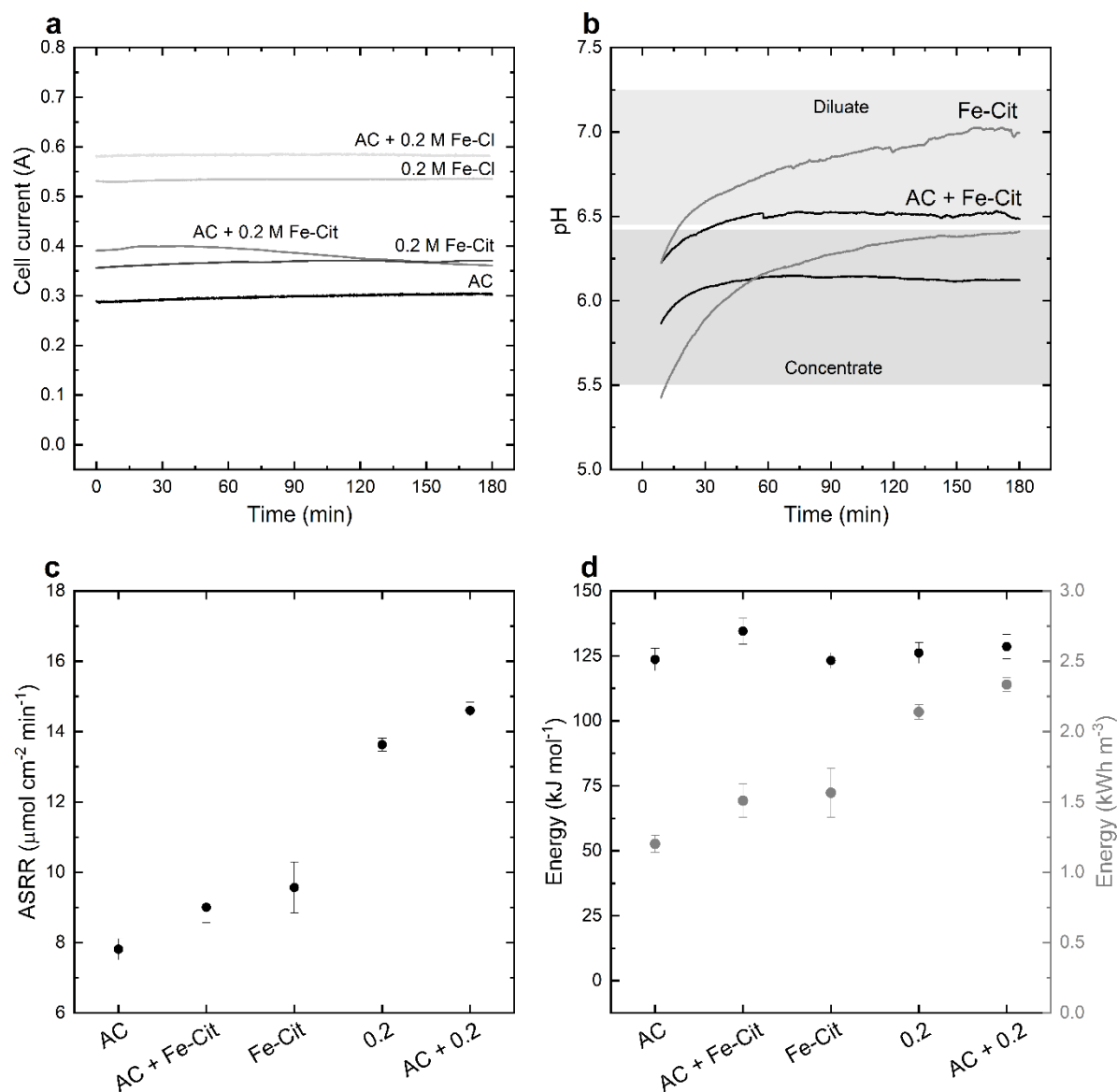
Figure 5.4 – Desalination performance of flow electrodes with AC and AC + Fe-Cit slurries. The electrical current during desalination (A). The pH of the water produced in diluate and concentrate channels (B). The salt removal rate (C). The energy consumption per mole of NaCl removed from the diluate and volumetric energy per volume treated in the diluate channel (D).

It is shown in Figure 5.4a that the current for the flow electrode with citrate was lower than the current with Fe-Cl. The current was around 54% higher for the Fe-Cl system compared to Fe-Cit, without AC in the flow electrode. The Fe-Cit species are bigger than Fe-Cl ones, and the diffusion coefficient is lower for the Fe-Cit. The diffusion coefficient in water for 0.1 M of $FeCl_3$ was found to be 4.8×10^{-6} cm^{-2} s^{-1} (Hawthorne et al., 2014), and 5.7×10^{-6} cm^{-2} s^{-1} for $FeCl_2$ (Hawthorne et al., 2014). For the same concentration, the Fe-Cit species (Fe^{III} species) have a lower diffusion coefficient, 1.1×10^{-6} cm^{-2} s^{-1}. Furthermore, the exchange current density

(io) reported for Fe-Cl and Fe-Cit species on a glassy carbon working electrode are 2.3 and 0.9 mA cm^{-2} (Hawthorne et al., 2014), respectively. As previously discussed for the Fe-Cl-based flow electrodes, it is necessary to investigate the controlling step in the faradaic reactions of those Fe-based species in the future. In this study, as the flow rate of the flow electrode was 200 mL min^{-1}, and the concentration of iron species did not significantly change inside the current collector, the diffusion of species likely had a lower effect on the electrochemical kinetics here. Thus, the exchange current had a larger influence on the electrochemical kinetics.

The currents of AC + Fe-Cit and Fe-Cit flow electrodes after 180 min of the experiment were around 350 mA, which is more than the AC-only flow electrodes. For the AC + Fe-Cit, the current started around 400 mA but then decreased over time and remained close to the current of Fe-Cit system. After 120 min of the experiment, the presence of AC in the flow electrode had no advantage compared to Fe-Cit regarding the desalination current. However, comparing the ASRR of Fe-Cit flow electrode, 9.6 μmol cm^{-2} min^{-1}, and the ASRR for AC + Fe-Cit, 9.0 μmol cm^{-2} min^{-1}, it was shown that the desalination rate was higher for Fe-Cit. Also, the energy per mol of salt removed was slightly higher for AC + Fe-Cit than Fe-Cit. Then, the mixture of AC and Fe-Cit does not seem to be an advantage, considering the desalination rate and the energy consumption. AC + Fe-Cit consumed around 135 kJ mol^{-1}, while only Fe-Cit consumed 123 kJ mol^{-1}. The possible reason for no improvement in the desalination rate in the presence of AC in the Fe-Cit flow electrode is possibly due to citrate or iron citrate adsorption. Previous studies have investigated AC flow electrodes with organic redox couples, such as sodium anthraquinone-2-sulfonate (AQS), 4-hydroxy-2,2,6,6-tetramethylpiperidine 1-oxyl (TEMPO), hydroquinone (HQ) (Luo et al., 2022). Those organic species alone presented very similar desalination rates compared to their mixture with AC. Those organic compounds were found to have a strong affinity for the AC surface. The adsorption of species onto the surface of the AC reduces the concentration of the redox couples in the electrolyte, and it can increase the energy necessary to charge the electron transfer from the current collector to the AC.

5.3.5 Analysis of water produced by the Fe-Cit-based flow electrodes

The pH of the diluate and concentrate channels are shown in Figure 5.4b. In both flow electrodes with Fe-Cit, the pH was increased relative to the Fe-Cl-based flow electrodes. In the presence of AC, however, the increase was slightly smaller, and after 180 min of the experiments, the diluate and concentrate had approximately pH 6.5 and 6.1, respectively. On the other hand, the diluate and concentrate streams with no AC had pH 7 and 6.4, respectively.

In another study with Fe-Cit and a redox flow battery setup (Mohandass et al., 2022), the pH of the flow electrode was adjusted to 7. However, the pH of the diluate and concentrate channels was not reported. Here, the higher pH of the Fe-Cit system relative to the Fe-Cl is due to the natural pH of the flow electrode, which is around 1.7 in Fe-Cl and 5.4 in the Fe-Cit system. Hence, it is relevant to control the pH of the flow electrode and find soluble redox couples in circumneutral pH if the intended application is the production of potable water or a low pH of the product water is undesirable.

Concerning the crossover of ions in the citrate system, in this case, not only is the iron relevant, but also the citrate is of interest. The citrate anions were in stoichiometric excess compared to the iron, so some free citrate could cross the membrane. Iron citrate is expected to be found in anionic form at the experimental conditions, and the iron citrate is larger than iron chloride, so a lower crossover of iron crossover was expected. The concentration of iron and Total Organic Carbon (TOC) are shown in Table 5.4.

Table 5.4 – Fe and total organic carbon concentration in the diluate and concentrate channels for flow electrode based on Fe-Cit electrolyte.

Flow electrode	Iron concentration		Total Organic Carbon	
	Diluate	Concentrate	Diluate	Concentrate
	mg/L		mg/L	
Fe-Cit	<0.01	<0.01	0.474	0.494
AC + Fe-Cit	<0.01	<0.01	0.269	0.349

Table 5.4 shows that for both flow electrodes based on Fe-Cit, the iron concentration in the water streams was below the detection limit of the equipment. That indicates that for the same concentration Fe-Cl (0.2 M), there is less iron crossing the membrane in the citrate system. The reason is the size of the iron citrate species, which has two citrate ions coordinated with an iron center. The literature reported iron contamination of 0.7 and 0.2 μmol L^{-1}, for a 0.4 M of Fe$_T$ and 1.2 M of citrate (Mohandass et al., 2022). Regarding the citrate, the TOC analysis indicated the presence of organic carbon in the water. The crossover was lower for the flow electrode with AC, as likely AC adsorbs some citrate. As iron was not found in the water channels, it is reasonable to assume that free citrate ions that are not bonded to the iron are permeating the membrane. Again, the concentrate water stream shows a higher concentration of crossover ions than the diluate, which aligns with the results shown elsewhere (Mohandass et al., 2022). However, in the present study, the highest contamination in the concentrate channel was

0.494 mg L^{-1} (equivalent to 6.9 µmol L^{-1} of citrate), while 2.56 mg L^{-1} (36 µmol L^{-1} of citrate) was found in the study of Mohandass et al. (Mohandass et al., 2022). However, this study has a flow electrode 0.4 M of Fe$_T$ and 1.2 M of citrate. Considering the experimental conditions of this work, the iron citrate complex is an interesting alternative to AC slurries regarding the desalination rate. However, the loss of citrate ions must be considered, and likely, over long-run experiments, the flow electrode composition must be monitored and controlled.

5.4   Conclusion

This work investigated a typical FCDI cell's desalination performance by introducing iron-based additives: iron chloride and iron citrate. The system was compared with flow electrodes with typical activated carbon, only the redox couples, and the mixture of activated carbon and redox couples additives.

It was demonstrated that both Fe-Cl and Fe-Cit activated carbon-based flow electrodes enhance the desalination performance compared to a 15 wt.% AC flow electrode. In the Fe-Cl system, even the lowest concentration of 0.05 M shows higher cell current and increased salt removal rate by 10% compared to activated carbon only. The Fe-Cl was shown to increase the desalination rate up to a concentration of 0.4 M, reaching a salt removal rate of 15.6 µmol cm^{-2} min^{-1}, compared to 7.8 µmol cm^{-2} min^{-1} for the flow electrode with only AC. This represents a 100% increase in the desalination rate. In the flow electrode based on activated and Fe-Cl, 0.2 M has the highest salt removal rate of 13.6 µmol cm^{-2} min^{-1}, which is an increase of 74% compared to AC slurry.

The Fe-Cl was found to reduce the pH of the product water, and the higher the concentration, the lower the pH. The concentrate channel has lower pH than the diluate channel, ranging from 4.25 to 3.25. Furthermore, iron was found to cross the membranes, and the contamination became more relevant at 0.4 M of Fe-Cl. The optimum iron concentration for the iron chloride was 0.2 M, where the desalination rate was high, and the iron levels were still low in the water channels.

The iron citrate was compared to the iron chloride at 0.2 M of Fe$_T$. It was demonstrated that the citrate-based flow electrodes perform better than the AC-only flow electrode. The salt removal rate for the citrate system is lower than Fe-Cl. However, the product water's pH is circumneutral, making this system a better option for potable water consumption. No iron was detected in the water streams, and citrate ions were found in the product water ranging from 1.4

to 2.6 µmol L^{-1}. Finally, the mixture of iron citrate with the AC does not seem to benefit the desalination current and salt removal rate.

Based on our results, it is shown that iron-based redox couples present an interesting low-cost alternative for additives for FCDI flow electrodes. The appropriate additive and its concentration should be chosen considering the application of ion removal. In future research, other additives that reduce the cross-over of the iron and the complexant but still have good electrochemical kinetics are of interest.

6   Considerações finais

Os dois estudos apresentaram novas possibilidades para a melhora do desempenho das células de deionização capacitiva por eletrodo de fluxo (FCDI) por meio da incorporação de pares redox baseados em ferro como aditivos. O primeiro estudo determinou a eficácia do uso de $[Fe(CN)_6]^{3-}$ como mediador redox em conjunto com NiHCF como partículas ativas. Essa combinação aumentou significativamente a corrente da célula, mostrando uma melhoria notável de mais de 100% em comparação com as suspensões de carvão ativado tipicamente utilizadas no FCDI. Além disso, foi mostrado que a concentração do mediador redox tem um papel fundamental na taxa de dessalinização, sendo que concentrações mais altas resultam em correntes mais estáveis e sem contaminação da água tratada.

O segundo estudo explorou o impacto dos aditivos à base de ferro, especificamente o cloreto de ferro (Fe-Cl) e o citrato de ferro (Fe-Cit), no desempenho do FCDI. O Fe-Cl apresentou uma melhora na taxa de dessalinização, levando a um aumento de 100% na remoção de sal na concentração ótima de 0,2 M. No entanto, observou-se que o Fe-Cl reduziu o pH da água do produzida e apresentou problemas de contaminação em concentrações mais altas. Por outro lado, o Fe-Cit demonstrou melhor desempenho de dessalinização em comparação com eletrodos de fluxo somente de carvão ativado, mantendo um pH neutro na água produzida e atenuando a contaminação por ferro. No entanto, foi detectada contaminação por citrato, e a melhoria na dessalinização foi de 23%, o que é inferior aos eletrodos de fluxo de Fe-Cl.

Ambos os estudos ressaltam o potencial dos mediadores redox e dos aditivos à base de ferro como meios econômicos de aprimorar o desempenho das células FCDI. Os resultados mostram que é possível obter taxas de dessalinização mais altas em comparação com os eletrodos de fluxo de carvão ativado. A contaminação da água produzida é indesejável, pois, em primeiro lugar, a água tem um íon de não interesse e, em segundo lugar, a concentração do eletrodo de fluxo é afetada pela perda de íons e pela mudança de pH. Dessa forma, o controle da passagem dos aditivos é fundamental para a implementação futura de pares redox em sistemas de dessalinização eletroquímica.

Embora os pares redox tenham sido diferentes em ambos os estudos, o fato de que nenhum cruzamento de ferro foi detectado no primeiro estudo (usando uma configuração ICC) e tendo apenas o eletrodo de fluxo catódico com par redox sugere que a contaminação do fluxo de água pode ocorrer principalmente a partir do canal de concentrado, na configuração SCC usada no

segundo trabalho. Assim, o diluído pode ser contaminado principalmente pela passagem de íons do canal do fluxo concentrado.

Com relação ao efeito sinérgico da mistura das partículas eletroquimicamente ativas e dos pares redox, o aumento de corrente mostrado no primeiro e no segundo estudos foi relativamente pequeno quando as partículas foram adicionadas ao eletrodo de fluxo. Os eletrodos de fluxo com partículas são, em geral, mais viscosos do que os eletrólitos. Além disso, a adição de partículas ao sistema pode aumentar o custo dos materiais do eletrodo de fluxo, a energia de bombeamento e o risco de entupimento. Portanto, é necessário avaliar se as misturas de pares redox com partículas eletroativas são benéficas para o consumo geral de energia e o custo do processo de remoção de íons. Além disso, os experimentos deste estudo usaram uma célula adaptada para FCDI, com a largura e a profundidade dos canais na placa de grafite projetada para comportar um eletrodo de fluxo com partículas de carbono ativo. Se um eletrodo de fluxo sem partículas for aplicado, novos desenhos de células eletroquímicas são possíveis, e um aumento na área de contato do eletrodo de fluxo e do coletor de corrente provavelmente melhorará ainda mais a corrente no sistema.

6.1   Sugestões para trabalhos futuros

Pesquisas futuras devem explorar aditivos alternativos com crossover reduzido e cinética eletroquímica mais rápida para avançar ainda mais no campo da deionização capacitiva. Essas descobertas oferecem caminhos promissores para o desenvolvimento de tecnologias de dessalinização mais eficientes e versáteis.

i.   Determinar um segundo mediador redox para regenerar as partículas de NiHCF ou um sistema com um único mediador redox.

ii.   Estudar os parâmetros que afetam a passagem de ferro do eletrodo para a água, como a salinidade do fluxo de alimentação e os revestimentos da membrana.

iii.   Investigar a contaminação por pares redox em células eletroquímicas com mais pares de espaçadores entre os eletrodos de fluxo.

iv.   Determinar a etapa de controle cinético nos eletrodos de fluxo somente com pares redox.

v.   Investigar outros complexos de ferro e outros pares redox no eletrodo de fluxo.

7 Final considerations

The two studies presented insights into enhancing the performance of flow-electrode capacitive deionization (FCDI) cells through the incorporation of redox couples and iron-based additives. The first study established the efficacy of using $[Fe(CN)_6]^{3-}$ as a redox mediator in conjunction with NiHCF as active particles. This combination significantly increased the cell's current, showing a remarkable improvement of over 100% when compared to typical activated carbon-only slurries. Furthermore, the concentration of the redox mediator played a critical role in determining desalination rates, with higher concentrations leading to more stable currents and no observed crossover issues.

The second study explored the impact of iron-based additives, specifically iron chloride (Fe-Cl) and iron citrate (Fe-Cit), on FCDI performance. Fe-Cl exhibited a remarkable enhancement in desalination rate, leading to a 100% increase in salt removal at its optimal concentration of 0.2 M. However, it was noted that Fe-Cl reduced the product water's pH and had some crossover issues at higher concentrations. On the other hand, Fe-Cit demonstrated improved desalination performance compared to activated carbon-only flow electrodes while maintaining a neutral pH in the product water and mitigating iron contamination. However, citrate contamination was detected, and the improvement in desalination was 23%, which is inferior to the Fe-Cl flow electrodes.

Both studies underscore the potential of redox mediators and iron-based additives as cost-effective means to enhance FCDI cell performance. The results show that higher desalination rates compared to typical AC flow electrodes can be achieved, even with any active particle in the flow electrodes. The contamination of the water streams is undesirable as; first, the water has an undesirable ion, and second, the flow electrode concentration is affected by the loss of ions and change of pH. In this way, controlling the crossover is fundamental to the further implementation of redox couples in electrochemical desalination systems.

Although the redox couples were different in both studies, the fact that no iron crossover was detected in the first study (using an ICC setup) and having only the cathode flow electrode with redox couple suggest that the contamination of the water stream may occur mainly from the concentrate channel, in the SCC configuration used in the second paper. Thus, the diluate may be mainly contaminated by the crossover of ions from the concentrate channel.

Regarding the synergetic effect of mixing the electrochemically active particles and the redox couples, the current increase shown in the first and second studies was relatively small

when particles were added to the flow electrode. Flow electrodes with particles are, in general, more viscous than electrolytes. Also, adding particles into the system potentially increases the cost of the flow electrode materials, the pumping energy, and the risk of clogging. Hence, it is necessary to assess whether the mixtures of redox coupled with particles are beneficial to the overall energy consumption and cost of the ion removal process. Furthermore, the experiments in this study used a cell tailored for FCDI, with the width and depth of channels in the graphite plate designed to comport a flow electrode with active carbon particles. If a flow electrode without particles is applied, new electrochemical cell designs are possible, and an increase in the contact area of the flow electrode and current collector is likely to improve the current in the system even further.

7.1   Suggestions for future investigation

Future research should explore alternative additives with reduced crossover and improved electrochemical kinetics to further advance the field of capacitive deionization. These findings offer promising avenues for developing more efficient and versatile desalination technologies.

vi.   Determine a second redox mediator to regenerate NiHCF particles or a single redox mediator system.

vii.   Study the parameters that affect the iron crossover, such as feedstream salinity and membrane coatings.

viii.   Investigate the contamination by the redox couples in electrochemical cells with more space pairs between the flow electrodes.

ix.   Determine the kinetic controlling step in the flow electrodes with redox couples only.

x.   Investigate other iron complexes and other redox couples in the flow electrode.

8 References

Agrisuelas, J., García-Jareño, J.J., Vicente, F., 2012. Identification of processes associated with different iron sites in the Prussian blue structure by in situ electrochemical, gravimetric, and spectroscopic techniques in the dc and ac regimes. J. Phys. Chem. C 116, 1935–1947. https://doi.org/10.1021/jp207269c

Akuzum, B., Singh, P., Eichfeld, D.A., Agartan, L., Uzun, S., Gogotsi, Y., Kumbur, E.C., 2020. Percolation Characteristics of Conductive Additives for Capacitive Flowable (Semi-Solid) Electrodes. ACS Appl. Mater. Interfaces 12, 5866–5875. https://doi.org/10.1021/acsami.9b19739

Campos, J.W., Beidaghi, M., Hatzell, K.B., Dennison, C.R., Musci, B., Presser, V., Kumbur, E.C., Gogotsi, Y., 2013. Investigation of carbon materials for use as a flowable electrode in electrochemical flow capacitors. Electrochim. Acta 98, 123–130. https://doi.org/10.1016/j.electacta.2013.03.037

Carmona-Orbezo, A., Dryfe, R.A.W., 2021. Understanding the performance of flow-electrodes for capacitive deionization through hydrodynamic voltammetry. Chem. Eng. J. 406, 126826. https://doi.org/10.1016/j.cej.2020.126826

Chang, J., Duan, F., Cao, H., Tang, K., Su, C., Li, Y., 2019. Superiority of a novel flow-electrode capacitive deionization (FCDI) based on a battery material at high applied voltage. Desalination 468, 114080. https://doi.org/10.1016/j.desal.2019.114080

Chen, F., Wang, J., Feng, C., Ma, J., David Waite, T., 2020. Low energy consumption and mechanism study of redox flow desalination. Chem. Eng. J. 401, 126111. https://doi.org/10.1016/j.cej.2020.126111

Chen, R., Huang, Y., Xie, M., Wang, Z., Ye, Y., Li, L., Wu, F., 2016. Chemical Inhibition Method to Synthesize Highly Crystalline Prussian Blue Analogs for Sodium-Ion Battery Cathodes. ACS Appl. Mater. Interfaces 8, 31669–31676. https://doi.org/10.1021/acsami.6b10884

Chen, R., Sheehan, T., Ng, J.L., Brucks, M., Su, X., 2020. Capacitive deionization and electrosorption for heavy metal removal. Environ. Sci. Water Res. Technol. 6, 258–282. https://doi.org/10.1039/c9ew00945k

Chen, Y., Zhou, M., Xia, Y., Wang, X., Liu, Y., Yao, Y., Zhang, H., Li, Y., Lu, S., Qin, W., Wu, X., Wang, Q., 2019. A Stable and High-Capacity Redox Targeting-Based Electrolyte for Aqueous Flow Batteries. Joule 3, 2255–2267.

https://doi.org/10.1016/j.joule.2019.06.007

Chong, S., Yang, J., Sun, L., Guo, S., Liu, Y., Liu, H.K., 2020. Potassium Nickel Iron Hexacyanoferrate as Ultra-Long-Life Cathode Material for Potassium-Ion Batteries with High Energy Density. ACS Nano 14, 9807–9818. https://doi.org/10.1021/acsnano.0c02047

Cornell, R.M., Schwertmann, U., 2003. The Iron Oxides. Wiley. https://doi.org/10.1002/3527602097

Dahiya, S., Mishra, B.K., 2020. Enhancing understandability and performance of flow electrode capacitive deionisation by optimizing configurational and operational parameters: A review on recent progress. Sep. Purif. Technol. 240, 116660. https://doi.org/10.1016/j.seppur.2020.116660

Dennison, C.R., Beidaghi, M., Hatzell, K.B., Campos, J.W., Gogotsi, Y., Kumbur, E.C., 2014. Effects of flow cell design on charge percolation and storage in the carbon slurry electrodes of electrochemical flow capacitors. J. Power Sources 247, 489–496. https://doi.org/10.1016/j.jpowsour.2013.08.101

Duduta, M., Ho, B., Wood, V.C., Limthongkul, P., Brunini, V.E., Carter, W.C., Chiang, Y.M., 2011. Semi-solid lithium rechargeable flow battery. Adv. Energy Mater. 1, 511–516. https://doi.org/10.1002/aenm.201100152

Fan, C.S., Liou, S.Y.H., Hou, C.H., 2017. Capacitive deionization of arsenic-contaminated groundwater in a single-pass mode. Chemosphere 184, 924–931. https://doi.org/10.1016/j.chemosphere.2017.06.068

Fan, C.S., Tseng, S.C., Li, K.C., Hou, C.H., 2016. Electro-removal of arsenic(III) and arsenic(V) from aqueous solutions by capacitive deionization. J. Hazard. Mater. 312, 208–215. https://doi.org/10.1016/j.jhazmat.2016.03.055

Fang, K., Gong, H., He, W., Peng, F., He, C., Wang, K., 2018. Recovering ammonia from municipal wastewater by flow-electrode capacitive deionization. Chem. Eng. J. 348, 301–309. https://doi.org/10.1016/j.cej.2018.04.128

Folaranmi, G., Tauk, M., Bechelany, M., Sistat, P., Cretin, M., Zaviska, F., 2022. Investigation of fine activated carbon as a viable flow electrode in capacitive deionization. Desalination 525, 115500. https://doi.org/10.1016/j.desal.2021.115500

Gaikwad, M.S., Balomajumder, C., 2018. Removal of Cr(VI) and fluoride by membrane capacitive deionization with nanoporous and microporous Limonia acidissima (wood apple) shell activated carbon electrode. Sep. Purif. Technol. 195, 305–313.

https://doi.org/10.1016/j.seppur.2017.12.006

Gaikwad, M.S., Balomajumder, C., 2017a. Simultaneous electrosorptive removal of chromium(VI) and fluoride ions by capacitive deionization (CDI): Multicomponent isotherm modeling and kinetic study. Sep. Purif. Technol. 186, 272–281. https://doi.org/10.1016/j.seppur.2017.06.017

Gaikwad, M.S., Balomajumder, C., 2017b. Tea waste biomass activated carbon electrode for simultaneous removal of Cr(VI) and fluoride by capacitive deionization. Chemosphere 184, 1141–1149. https://doi.org/10.1016/j.chemosphere.2017.06.074

Gontijo, V.L., Teixeira, L.A. V., Majuste, D., Ciminelli, V.S.T., 2022. A review of thermodynamic data for lanthanum, iron, and thorium applied to rare earth extraction. Hydrometallurgy 213, 105951. https://doi.org/10.1016/j.hydromet.2022.105951

Ha, Y., Jung, H. Bin, Lim, H., Jo, P.S., Yoon, H., Yoo, C.-Y., Pham, T.K., Ahn, W., Cho, Y., 2019. Continuous Lithium Extraction from Aqueous Solution Using Flow-Electrode Capacitive Deionization. Energies 12, 2913. https://doi.org/10.3390/en12152913

Ha, Y., Lee, H., Yoon, H., Shin, D., Ahn, W., Cho, N., Han, U., Hong, J., Anh Thu Tran, N., Yoo, C.-Y., Suk Kang, H., Cho, Y., 2020. Enhanced Salt Removal Performance of Flow Electrode Capacitive Deionization with High Cell Operational Potential. Sep. Purif. Technol. 254, 117500. https://doi.org/10.1016/j.seppur.2020.117500

Han, M., Tang, L., Xiao, Y., Li, M., Chen, H., Songsiriritthigul, P., Oo, T.Z., Zaw, M., Lwin, N.W., Aung, S.H., Karthick, R., Chen, F., 2023. Enhanced continuous desalination performance with iron-complexed malonate redox couples. Environ. Sci. Water Res. Technol. 9, 2368–2377. https://doi.org/10.1039/D3EW00400G

Hatzell, K.B., Beidaghi, M., Campos, J.W., Dennison, C.R., Kumbur, E.C., Gogotsi, Y., 2013. A high performance pseudocapacitive suspension electrode for the electrochemical flow capacitor. Electrochim. Acta 111, 888–897. https://doi.org/10.1016/j.electacta.2013.08.095

Hawks, S.A., Ramachandran, A., Porada, S., Campbell, P.G., Suss, M.E., Biesheuvel, P.M., Santiago, J.G., Stadermann, M., 2019. Performance metrics for the objective assessment of capacitive deionization systems. Water Res. 152, 126–137. https://doi.org/10.1016/j.watres.2018.10.074

Hawthorne, K.L., Wainright, J.S., Savinell, R.F., 2014. Studies of Iron-Ligand Complexes for an All-Iron Flow Battery Application. J. Electrochem. Soc. 161, A1662–A1671. https://doi.org/10.1149/2.0761410jes

He, C., Ma, J., Zhang, C., Song, J., Waite, T.D., 2018. Short-Circuited Closed-Cycle Operation of Flow-Electrode CDI for Brackish Water Softening. Environ. Sci. Technol. 52, 9350–9360. https://doi.org/10.1021/acs.est.8b02807

Huang, S.Y., Fan, C.S., Hou, C.H., 2014. Electro-enhanced removal of copper ions from aqueous solutions by capacitive deionization. J. Hazard. Mater. 278, 8–15. https://doi.org/10.1016/j.jhazmat.2014.05.074

Jeon, S., Park, H., Yeo, J., Yang, S., Cho, C.H., Han, M.H., Kim, D.K., 2013. Desalination via a new membrane capacitive deionization process utilizing flow-electrodes. Energy Environ. Sci. 6, 1471. https://doi.org/10.1039/c3ee24443a

Jeon, S., Yeo, J., Yang, S., Choi, J., Kim, D.K., 2014. Ion storage and energy recovery of a flow-electrode capacitive deionization process. J. Mater. Chem. A 2, 6378. https://doi.org/10.1039/c4ta00377b

Jones, E., Qadir, M., van Vliet, M.T.H., Smakhtin, V., Kang, S. mu, 2019. The state of desalination and brine production: A global outlook. Sci. Total Environ. 657, 1343–1356. https://doi.org/10.1016/j.scitotenv.2018.12.076

Kim, H., Kim, S., Kim, N., Su, X., Kim, C., 2023. Multi-electrode scale-up strategy and parametric investigation of redox-flow desalination systems. Desalination 549, 116350. https://doi.org/10.1016/j.desal.2022.116350

Kim, N., Jeon, J., Elbert, J., Kim, C., Su, X., 2022. Redox-mediated electrochemical desalination for waste valorization in dairy production. Chem. Eng. J. 428, 131082. https://doi.org/10.1016/j.cej.2021.131082

Kim, S., Nitzsche, M.P., Rufer, S.B., Lake, J.R., Varanasi, K.K., Hatton, T.A., 2023. Asymmetric chloride-mediated electrochemical process for CO_2 removal from oceanwater. Energy Environ. Sci. 3–8. https://doi.org/10.1039/d2ee03804h

Kim, Y., Jeon, S., Ahn, D., Kim, H., Kim, C., Lee, Y., 2023. Parametric investigation of ferri/ferrocyanide redox flow for performance optimization of redox flow desalination. Desalination 550, 116406. https://doi.org/10.1016/j.desal.2023.116406

Kim, Y.J., Choi, J.H., 2010. Improvement of desalination efficiency in capacitive deionization using a carbon electrode coated with an ion-exchange polymer. Water Res. 44, 990–996. https://doi.org/10.1016/j.watres.2009.10.017

Lee, J.B., Park, K.K., Eum, H.M., Lee, C.W., 2006. Desalination of a thermal power plant wastewater by membrane capacitive deionization. Desalination 196, 125–134. https://doi.org/10.1016/j.desal.2006.01.011

Li, Q., Zheng, Y., Xiao, D., Or, T., Gao, R., Li, Z., Feng, M., Shui, L., Zhou, G., Wang, X., Chen, Z., 2020. Faradaic Electrodes Open a New Era for Capacitive Deionization. Adv. Sci. 7. https://doi.org/10.1002/advs.202002213

Liang, P., Sun, X., Bian, Y., Zhang, H., Yang, X., Jiang, Y., Liu, P., Huang, X., 2017. Optimized desalination performance of high voltage flow-electrode capacitive deionization by adding carbon black in flow-electrode. Desalination 420, 63–69. https://doi.org/10.1016/j.desal.2017.05.023

Lim, H., Ha, Y., Jung, H. Bin, Jo, P.S., Yoon, H., Quyen, D., Cho, N., Yoo, C.-Y., Cho, Y., 2020. Energy storage and generation through desalination using flow-electrodes capacitive deionization. J. Ind. Eng. Chem. 81, 317–322. https://doi.org/10.1016/j.jiec.2019.09.020

Linnartz, C.J., Rommerskirchen, A., Wessling, M., Gendel, Y., 2017. Flow-Electrode Capacitive Deionization for Double Displacement Reactions. ACS Sustain. Chem. Eng. 5, 3906–3912. https://doi.org/10.1021/acssuschemeng.6b03086

Liu, L., Qiu, G., Suib, S.L., Liu, F., Zheng, L., Tan, W., Qin, L., 2017. Enhancement of Zn2+ and Ni2+ removal performance using a deionization pseudocapacitor with nanostructured birnessite and its carbon nanotube composite electrodes. Chem. Eng. J. 328, 464–473. https://doi.org/10.1016/j.cej.2017.07.066

Luo, K., Chen, M., Xing, W., Duan, M., Du, J., Zeng, G., Tang, W., 2021. Significantly enhanced desalination performance of flow-electrode capacitive deionization via cathodic iodide redox couple and its great potential in treatment of iodide-containing saline wastewater. Chem. Eng. J. 421, 129905. https://doi.org/10.1016/j.cej.2021.129905

Luo, K., Niu, Q., Zhu, Y., Song, B., Zeng, G., Tang, W., Ye, S., Zhang, J., Duan, M., Xing, W., 2020. Desalination behavior and performance of flow-electrode capacitive deionization under various operational modes. Chem. Eng. J. 389, 124051. https://doi.org/10.1016/j.cej.2020.124051

Luo, L., He, Q., Yi, D., Zu, D., Ma, J., Chen, Y., 2022. Indirect charging of carbon by aqueous redox mediators contributes to the enhanced desalination performance in flow-electrode CDI. Water Res. 220, 118688. https://doi.org/10.1016/j.watres.2022.118688

Luo, T., Abdu, S., Wessling, M., 2018. Selectivity of ion exchange membranes: A review. J. Memb. Sci. 555, 429–454. https://doi.org/10.1016/j.memsci.2018.03.051

Ma, J., He, C., He, D., Zhang, C., Waite, T.D., 2018. Analysis of capacitive and electrodialytic contributions to water desalination by flow-electrode CDI. Water Res. 144, 296–303. https://doi.org/10.1016/j.watres.2018.07.049

Ma, Jinxing, Ma, Junjun, Zhang, C., Song, J., Dong, W., Waite, T.D., 2020. Flow-electrode capacitive deionization (FCDI) scale-up using a membrane stack configuration. Water Res. 168, 115186. https://doi.org/10.1016/j.watres.2019.115186

Martínez-Garcia, R., Knobel, M., Reguera, E., 2006. Thermal-Induced Changes in Molecular Magnets Based on Prussian Blue Analogues. J. Phys. Chem. B 110, 7296–7303. https://doi.org/10.1021/jp0555551

Mekonnen, M.M., Hoekstra, A.Y., 2016. Sustainability: Four billion people facing severe water scarcity. Sci. Adv. 2, 1–7. https://doi.org/10.1126/sciadv.1500323

Mink, J., Stirling, A., Ojwang, D.O., Svensson, G., Mihály, J., Németh, C., Drees, M., Hajba, L., 2019. Vibrational properties and bonding analysis of copper hexacyanoferrate complexes in solid state. Appl. Spectrosc. Rev. 54, 369–424. https://doi.org/10.1080/05704928.2018.1459659

Mohandass, G., Chen, W., Krishnan, S., Kim, T., 2022. Asymmetric and Symmetric Redox Flow Batteries for Energy-Efficient, High-Recovery Water Desalination. Environ. Sci. Technol. 56, 4477–4488. https://doi.org/10.1021/acs.est.1c08609

Nam, D.H., Lumley, M.A., Choi, K.S., 2021. Electrochemical Redox Cells Capable of Desalination and Energy Storage: Addressing Challenges of the Water-Energy Nexus. ACS Energy Lett. 6, 1034–1044. https://doi.org/10.1021/acsenergylett.0c02399

Nativ, P., Badash, Y., Gendel, Y., 2017. New insights into the mechanism of flow-electrode capacitive deionization. Electrochem. commun. 76, 24–28. https://doi.org/10.1016/j.elecom.2017.01.008

Nativ, P., Lahav, O., Gendel, Y., 2018. Separation of divalent and monovalent ions using flow-electrode capacitive deionization with nanofiltration membranes. Desalination 425, 123–129. https://doi.org/10.1016/j.desal.2017.10.026

Ojwang, D.O., Grins, J., Wardecki, D., Valvo, M., Renman, V., Häggström, L., Ericsson, T., Gustafsson, T., Mahmoud, A., Hermann, R.P., Svensson, G., 2016. Structure Characterization and Properties of K-Containing Copper Hexacyanoferrate. Inorg. Chem. 55, 5924–5934. https://doi.org/10.1021/acs.inorgchem.6b00227

Pan, S.Y., Haddad, A.Z., Kumar, A., Wang, S.W., 2020. Brackish water desalination using reverse osmosis and capacitive deionization at the water-energy nexus. Water Res. 183, 116064. https://doi.org/10.1016/j.watres.2020.116064

Paolella, A., Faure, C., Timoshevskii, V., Marras, S., Bertoni, G., Guerfi, A., Vijh, A., Armand, M., Zaghib, K., 2017. A review on hexacyanoferrate-based materials for energy storage

and smart windows: Challenges and perspectives. J. Mater. Chem. A 5, 18919–18932. https://doi.org/10.1039/c7ta05121b

Patel, S.K., Biesheuvel, P.M., Elimelech, M., 2021. Energy Consumption of Brackish Water Desalination: Identifying the Sweet Spots for Electrodialysis and Reverse Osmosis. ACS ES&T Eng. https://doi.org/10.1021/acsestengg.0c00192

Petek, T.J., Hoyt, N.C., Savinell, R.F., Wainright, J.S., 2016. Characterizing slurry electrodes using electrochemical impedance spectroscopy. J. Electrochem. Soc. 163, A5001–A5009. https://doi.org/10.1149/2.0011601jes

Porada, S., Shrivastava, A., Bukowska, P., Biesheuvel, P.M., Smith, K.C., 2017. Nickel Hexacyanoferrate Electrodes for Continuous Cation Intercalation Desalination of Brackish Water. Electrochim. Acta 255, 369–378. https://doi.org/10.1016/j.electacta.2017.09.137

Porada, S., Zhang, L., Dykstra, J.E., 2020. Energy consumption in membrane capacitive deionization and comparison with reverse osmosis. Desalination 488, 114383. https://doi.org/10.1016/j.desal.2020.114383

Porada, S., Zhao, R., Van Der Wal, A., Presser, V., Biesheuvel, P.M., 2013. Review on the science and technology of water desalination by capacitive deionization. Prog. Mater. Sci. 58, 1388–1442. https://doi.org/10.1016/j.pmatsci.2013.03.005

Presser, V., Dennison, C.R., Campos, J., Knehr, K.W., Kumbur, E.C., Gogotsi, Y., 2012. The Electrochemical Flow Capacitor: A New Concept for Rapid Energy Storage and Recovery. Adv. Energy Mater. 2, 895–902. https://doi.org/10.1002/aenm.201100768

Qin, M., Deshmukh, A., Epsztein, R., Patel, S.K., Owoseni, O.M., Walker, W.S., Elimelech, M., 2019. Comparison of energy consumption in desalination by capacitive deionization and reverse osmosis. Desalination 455, 100–114. https://doi.org/10.1016/j.desal.2019.01.003

Ramachandran, A., Oyarzun, D.I., Hawks, S.A., Campbell, P.G., Stadermann, M., Santiago, J.G., 2019. Comments on "Comparison of energy consumption in desalination by capacitive deionization and reverse osmosis." Desalination 461, 30–36. https://doi.org/10.1016/j.desal.2019.03.010

Rommerskirchen, A., Alders, M., Wiesner, F., Linnartz, C.J., Kalde, A., Wessling, M., 2020a. Process model for high salinity flow-electrode capacitive deionization processes with ion-exchange membranes. J. Memb. Sci. 616, 118614. https://doi.org/10.1016/j.memsci.2020.118614

Rommerskirchen, A., Gendel, Y., Wessling, M., 2015. Single module flow-electrode capacitive

deionization for continuous water desalination. Electrochem. commun. 60, 34–37. https://doi.org/10.1016/j.elecom.2015.07.018

Rommerskirchen, A., Kalde, A., Linnartz, C.J., Bongers, L., Linz, G., Wessling, M., 2019. Unraveling charge transport in carbon flow-electrodes: Performance prediction for desalination applications. Carbon N. Y. 145, 507–520. https://doi.org/10.1016/j.carbon.2019.01.053

Rommerskirchen, A., Linnartz, C.J., Egidi, F., Kendir, S., Wessling, M., 2020b. Flow-electrode capacitive deionization enables continuous and energy-efficient brine concentration. Desalination 490, 114453. https://doi.org/10.1016/j.desal.2020.114453

Rommerskirchen, A., Linnartz, C.J., Müller, D., Willenberg, L.K., Wessling, M., 2018. Energy Recovery and Process Design in Continuous Flow–Electrode Capacitive Deionization Processes. ACS Sustain. Chem. Eng. 6, 13007–13015. https://doi.org/10.1021/acssuschemeng.8b02466

Saif, H.M., Crespo, J.G., Pawlowski, S., 2023. Lithium recovery from brines by lithium membrane flow capacitive deionization (Li-MFCDI) – A proof of concept. J. Membr. Sci. Lett. 3, 100059. https://doi.org/10.1016/j.memlet.2023.100059

Sayed, E.T., Al Radi, M., Ahmad, A., Abdelkareem, M.A., Alawadhi, H., Atieh, M.A., Olabi, A.G., 2021. Faradic capacitive deionization (FCDI) for desalination and ion removal from wastewater. Chemosphere 275, 130001. https://doi.org/10.1016/j.chemosphere.2021.130001

Seo, S.-J., Jeon, H., Lee, J.K., Kim, G.-Y., Park, D., Nojima, H., Lee, J., Moon, S.-H., 2010. Investigation on removal of hardness ions by capacitive deionization (CDI) for water softening applications. Water Res. 44, 2267–2275. https://doi.org/10.1016/j.watres.2009.10.020

Shen, L., Jiang, Y., Liu, Y., Ma, J., Sun, T., Zhu, N., 2020. High-stability monoclinic nickel hexacyanoferrate cathode materials for ultrafast aqueous sodium ion battery. Chem. Eng. J. 388, 124228. https://doi.org/10.1016/j.cej.2020.124228

Shi, L., Newcomer, E., Son, M., Pothanamkandathil, V., Gorski, C.A., Galal, A., Logan, B.E., 2021. Metal-Ion Depletion Impacts the Stability and Performance of Battery Electrode Deionization over Multiple Cycles. Environ. Sci. Technol. https://doi.org/10.1021/acs.est.0c08629

Shin, Y.U., Lim, J., Boo, C., Hong, S., 2021. Improving the feasibility and applicability of flow-electrode capacitive deionization (FCDI): Review of process optimization and energy

efficiency. Desalination 502, 114930. https://doi.org/10.1016/j.desal.2021.114930

Silva, A.M.N., Kong, X., Parkin, M.C., Cammack, R., Hider, R.C., 2009. Iron(iii) citrate speciation in aqueous solution. Dalt. Trans. 8616–8625. https://doi.org/10.1039/b910970f

Singh, Kaustub, Qian, Z., Biesheuvel, P.M., Zuilhof, H., Porada, S., de Smet, L.C.P.M., 2020. Nickel hexacyanoferrate electrodes for high mono/divalent ion-selectivity in capacitive deionization. Desalination 481, 114346. https://doi.org/10.1016/j.desal.2020.114346

Singh, K., Zhang, L., Zuilhof, H., de Smet, L.C.P.M., 2020. Water desalination with nickel hexacyanoferrate electrodes in capacitive deionization: Experiment, model and comparison with carbon. Desalination 496, 114647. https://doi.org/10.1016/j.desal.2020.114647

Suss, M.E., Porada, S., Sun, X., Biesheuvel, P.M., Yoon, J., Presser, V., 2015. Water desalination via capacitive deionization: what is it and what can we expect from it? Energy Environ. Sci. 8, 2296–2319. https://doi.org/10.1039/C5EE00519A

Suss, M.E., Presser, V., 2018. Water Desalination with Energy Storage Electrode Materials. Joule 2, 10–15. https://doi.org/10.1016/j.joule.2017.12.010

Tang, K., Yiacoumi, S., Li, Y., Gabitto, J., Tsouris, C., 2020. Optimal Conditions for Efficient Flow-Electrode Capacitive Deionization. Sep. Purif. Technol. 240, 116626. https://doi.org/10.1016/j.seppur.2020.116626

Tang, W., Kovalsky, P., Cao, B., He, D., Waite, T.D., 2016. Fluoride Removal from Brackish Groundwaters by Constant Current Capacitive Deionization (CDI). Environ. Sci. Technol. 50, 10570–10579. https://doi.org/10.1021/acs.est.6b03307

Tran, N.A.T., Khoi, T.M., Phuoc, N.M., Jung, H. Bin, Cho, Y., 2022. A review of recent advances in electrode materials and applications for flow-electrode desalination systems. Desalination 541, 116037. https://doi.org/10.1016/j.desal.2022.116037

Vivo-Vilches, J.F., Nadeina, A., Rahbani, N., Seznec, V., Larcher, D., Baudrin, E., 2021. LiFePO4-ferri/ferrocyanide redox targeting aqueous posolyte: Set-up, efficiency and kinetics. J. Power Sources 488, 229387. https://doi.org/10.1016/j.jpowsour.2020.229387

Wang, B., Han, Y., Wang, X., Bahlawane, N., Pan, H., Yan, M., Jiang, Y., 2018. Prussian Blue Analogs for Rechargeable Batteries. iScience 3, 110–133. https://doi.org/10.1016/j.isci.2018.04.008

Wang, C., Li, T., Yu, G., Deng, S., 2021. Removal of low concentrations of nickel ions in electroplating wastewater using capacitive deionization technology. Chemosphere 284, 131341. https://doi.org/10.1016/j.chemosphere.2021.131341

Wang, Q., Zakeeruddin, S.M., Wang, D., Exnar, I., Grätzel, M., 2006. Redox targeting of insulating electrode materials: A new approach to high-energy-density batteries. Angew. Chemie - Int. Ed. 45, 8197–8200. https://doi.org/10.1002/anie.200602891

Wang, X., Zhou, M., Zhang, F., Zhang, H., Wang, Q., 2021. Redox targeting of energy materials. Curr. Opin. Electrochem. 29, 100743. https://doi.org/10.1016/j.coelec.2021.100743

Wang, Z., Hu, Y., Wei, Q., Li, W., Liu, X., Chen, F., 2021. Enhanced Desalination Performance of a Flow-Electrode Capacitive Deionization System by Adding Vanadium Redox Couples and Carbon Nanotubes. J. Phys. Chem. C. https://doi.org/10.1021/acs.jpcc.0c09058

Wei, Q., Hu, Y., Wang, J., Ru, Q., Hou, X., Zhao, L., Yu, D.Y.W.Y.W., San Hui, K., Yan, D., Hui, K.N., Chen, F., 2020. Low energy consumption flow capacitive deionization with a combination of redox couples and carbon slurry. Carbon N. Y. 170, 487–492. https://doi.org/10.1016/j.carbon.2020.07.044

Wessells, C.D., Huggins, R.A., Cui, Y., 2011. Copper hexacyanoferrate battery electrodes with long cycle life and high power. Nat. Commun. 2, 2–6. https://doi.org/10.1038/ncomms1563

Wessells, C.D., McDowell, M.T., Peddada, S. V., Pasta, M., Huggins, R.A., Cui, Y., 2012. Tunable reaction potentials in open framework nanoparticle battery electrodes for grid-scale energy storage. ACS Nano 6, 1688–1694. https://doi.org/10.1021/nn204666v

World Health Organisation, 2007. pH in drinking-water, pH in drinking-water.

Xie, R., Yue, D., Peng, Z., Wei, X., 2023. Achieving Energy-Saving, Continuous Redox Flow Desalination with Iron Chelate Redoxmers. Energy Mater. Adv. 4, 1–9. https://doi.org/10.34133/energymatadv.0009

Xu, Y., Duan, F., Li, Y., Cao, H., Chang, J., Pang, H., Chen, J., 2021. Enhanced desalination performance in asymmetric flow electrode capacitive deionization with nickel hexacyanoferrate and activated carbon electrodes. Desalination 514, 115172. https://doi.org/10.1016/j.desal.2021.115172

Zakaria, M.B., Chikyow, T., 2017. Recent advances in Prussian blue and Prussian blue analogues: synthesis and thermal treatments. Coord. Chem. Rev. 352, 328–345. https://doi.org/10.1016/j.ccr.2017.09.014

Zhang, C., Ma, J., Waite, T.D., 2019a. Ammonia-Rich Solution Production from Wastewaters Using Chemical-Free Flow-Electrode Capacitive Deionization. ACS Sustain. Chem. Eng.

7, 6480–6485. https://doi.org/10.1021/acssuschemeng.9b00314

Zhang, C., Ma, J., Wu, L., Sun, J., Wang, L., Li, T., Waite, T.D., 2021. Flow Electrode Capacitive Deionization (FCDI): Recent Developments, Environmental Applications, and Future Perspectives. Environ. Sci. Technol. https://doi.org/10.1021/acs.est.0c06552

Zhang, C., Wu, L., Ma, J., Pham, A.N., Wang, M., Waite, T.D., 2019b. Integrated Flow-Electrode Capacitive Deionization and Microfiltration System for Continuous and Energy-Efficient Brackish Water Desalination. Environ. Sci. Technol. https://doi.org/10.1021/acs.est.9b04436

Zhang, J., Tang, L., Tang, W., Zhong, Y., Luo, K., Duan, M., Xing, W., Liang, J., 2020. Removal and recovery of phosphorus from low-strength wastewaters by flow-electrode capacitive deionization. Sep. Purif. Technol. 237, 116322. https://doi.org/10.1016/j.seppur.2019.116322

Zhao, X., Feng, M., Jiao, Y., Zhang, Y., Wang, Y., Sha, Z., 2020. Lithium extraction from brine in an ionic selective desalination battery. Desalination 481, 114360. https://doi.org/10.1016/j.desal.2020.114360

Zhao, Y., Ding, Y., Li, Y., Peng, L., Byon, H.R., Goodenough, J.B., Yu, G., 2015. A chemistry and material perspective on lithium redox flow batteries towards high-density electrical energy storage. Chem. Soc. Rev. 44, 7968–7996. https://doi.org/10.1039/c5cs00289c

Zheng, J., Xia, L., Song, S., 2017. Electrosorption of Pb(II) in water using graphene oxide-bearing nickel foam as the electrodes. RSC Adv. 7, 23543–23549. https://doi.org/10.1039/C7RA02956J

Zhou, M., Chen, Y., Salla, M., Zhang, H., Wang, X., Mothe, S.R., Wang, Q., 2020. Single-Molecule Redox-Targeting Reactions for a pH-Neutral Aqueous Organic Redox Flow Battery. Angew. Chemie - Int. Ed. 59, 14286–14291. https://doi.org/10.1002/anie.202004603

Zhou, M., Huang, Q., Pham Truong, T.N., Ghilane, J., Zhu, Y.G., Jia, C., Yan, R., Fan, L., Randriamahazaka, H., Wang, Q., 2017. Nernstian-Potential-Driven Redox-Targeting Reactions of Battery Materials. Chem 3, 1036–1049. https://doi.org/10.1016/j.chempr.2017.10.003

Appendix A

Structural characterization of NiHCF

The structural characterization of the synthesized NiHCF particles was carried out by X-ray diffractometry, Infrared spectroscopy, and thermogravimetric analysis. The results are shown in Figure A.1.
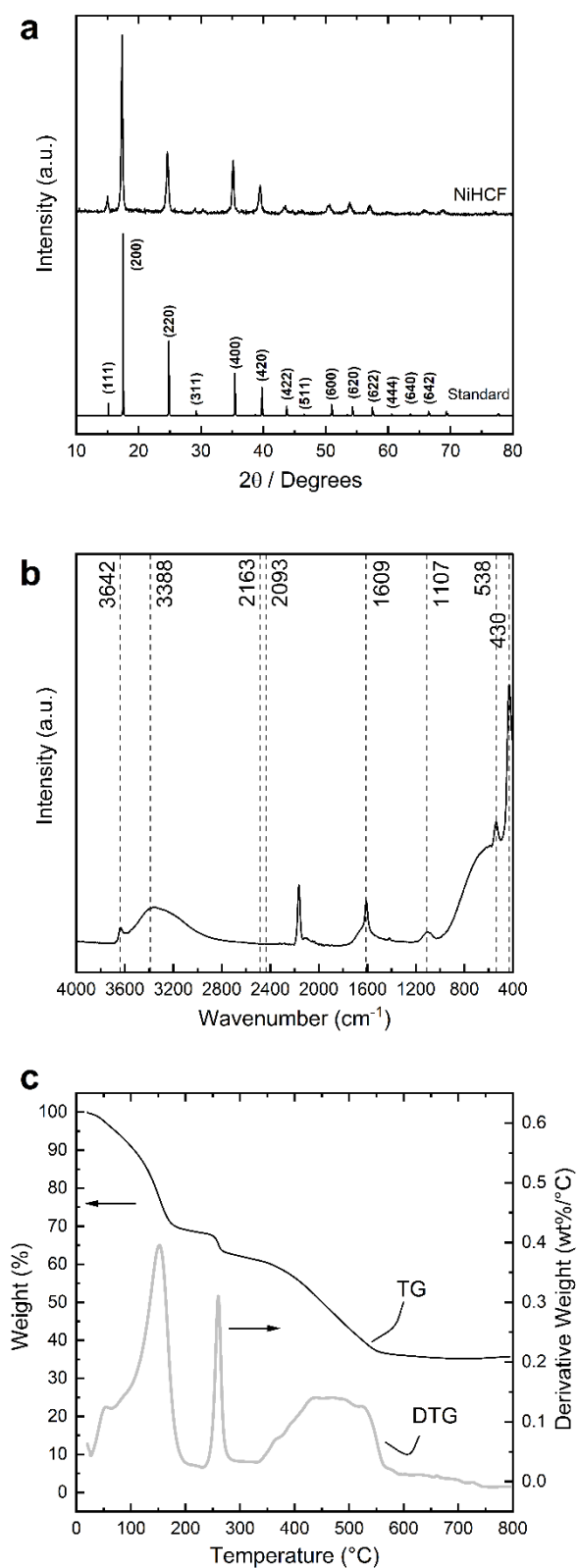
Figure A.1 − *Structural characterization of synthesized NiHCF samples: X-ray diffractograms for the sample and standard (Ojwang et al. 2016) at room temperature (a), vibrational spectra in the infrared region (b), and thermogravimetric analysis curves (c).*

The X-ray diffractogram in Figure A.1a was indexed according to the standard calculated by (Ojwang et al., 2016). The samples show sharp diffraction peaks corresponding to PBAs, demonstrating the synthesis of NiHCF and the high crystallinity of the material. According to Scherrer's equation, Eq. (A.1), the crystallite size of NiHCF particles can be estimated by:

$$L = \frac{K\lambda}{B cos\theta} \qquad (A.1)$$

Where L is the crystallite size, K is a constant depending on the shape factor - here 0.94 - λ is the wavelength of the copper anode (0.154 nm), B is the full width at half maximum of the diffraction peaks, and Θ is the Bragg angle. Then, the estimated crystallite size is 28 nm, which agrees with the particle size shown by SEM.

In Figure A.1b, the infrared spectra of NiHCF are presented. The peaks below 600 cm^{-1} are related to the vibrational modes of the octahedral [Fe(CN)$_6$] unit: ν(CN), δ(FeCN), ν(FeC), and δ(CFeC) (Mink et al., 2019; Ojwang et al., 2016). The band at 3642 cm^{-1} indicates the presence of weakly hydrogen-bonded water molecules, and the band at 3388 cm^{-1} indicates the presence of strongly hydrogen-bonded water molecules in the structure. In addition, the band at 1609 cm^{-1} is a four-component band: at 1678w (weak), 1653vw, sh (very weak and shoulder), 1635w, sh, and 1608s (strong) cm^{-1} and is attributed to coordinated water (Ojwang et al., 2016). For the NiHCF samples, the peaks 2163 and 2093 cm^{-1} are attributed to the vibrational mode of Fe^{III}-CN-Ni^{II}, and Fe^{II}-CN-Ni^{II}, respectively (Mink et al., 2019; Ojwang et al., 2016). In this way, the intensity of those peaks is related to Fe^{III} and Fe^{II}, and the ratio of peak intensities indicates the degree of oxidation of the NiHCF.

Thermogravimetric measurements were performed to determine the water content of PBAs, and are shown in Figure A.1c. The water content in PBAs is due to adsorbed water on the surface of the particles and structural water. This structural water is related to defects in the crystalline structure, commonly caused by fast precipitation, which may lead to more vacancies and interstitial water in the structure, resulting in poor electrochemical performance in battery applications (Chen et al., 2016). Derivative thermogravimetric curves of NiHCF samples show two distinguish peaks at 180 °C and 250 °C, accounting for the loss of adsorbed water and coordinated water, respectively. The weight loss up to 140 °C – around 30% – is due to the loss of adsorbed water on NiHCF. At about 250 °C, the decomposition of the samples starts, and a weight loss of up to 40% is observed, which at this temperature is commonly attributed to

zeolitic and coordinated water losses. Weight loss at temperatures higher than 350 °C is due to CN decomposition (Martínez-Garcia et al., 2006). The loss of coordinated water can be used to estimate the water content in the PBA's structure after chemical analyses of the samples (Martínez-Garcia et al., 2006). The water loss of around 30% measured for the synthesized NiHCF agrees with typical values observed in the literature. Considering that This indicates a reasonable number of defects in the NiHCF structure.

Energy consumption and normalized conductivities of desalination experiments

Figure A.2a shows the current of the FCDI for several cathode flow-electrode compositions. Figure A.2b shows the normalized conductivity of the water product.
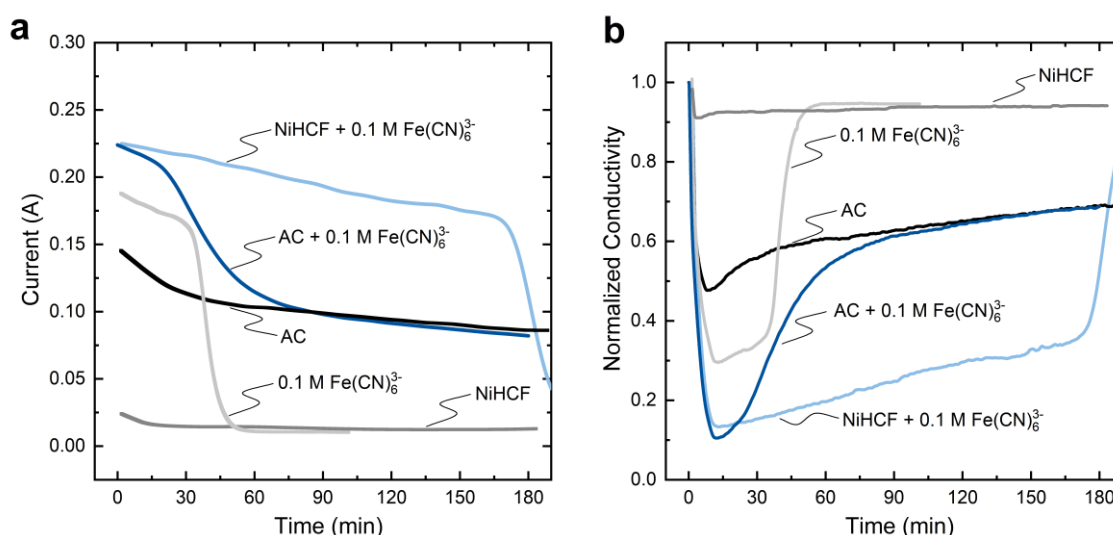

Figure A.2 – Desalination experiment with several compositions in the cathode flow electrode. FCDI cell current with different slurries as flow electrode in the cathode reservoir (a); Normalized conductivity of the water product (b).

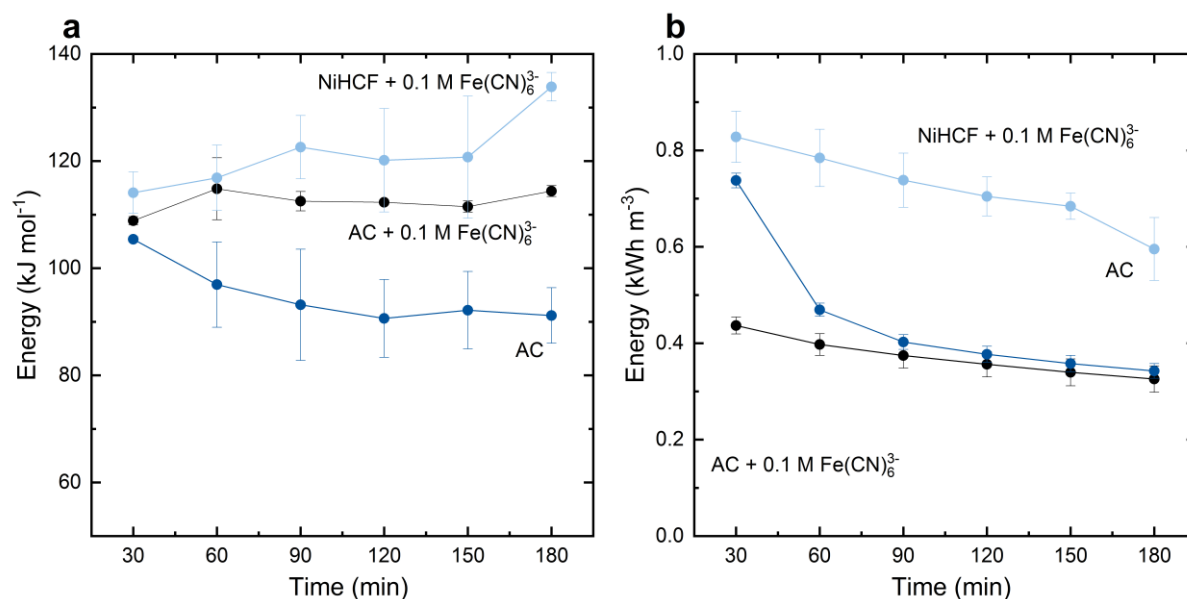Figure A.3 shows the energy consumption for the cathodic flow electrodes with NiHCF + $Fe(CN)_6^{3-}$, AC + $Fe(CN)_6^{3-}$ and AC.

Figure A.3 – Energy consumption for the flow electrode with NiHCF + Fe(CN)$_6^{3-}$, AC + Fe(CN)$_6^{3-}$ and AC. In (a) the energy consumption per mol of removed salt. In (b), the energy consumption per volume of treated water.

Figure A.4a shows the current of the FCDI cell for cathodic flow electrodes with NiHCF and several redox mediator concentrations. Figure A.4b shows the normalized conductivity of the corresponding water product.
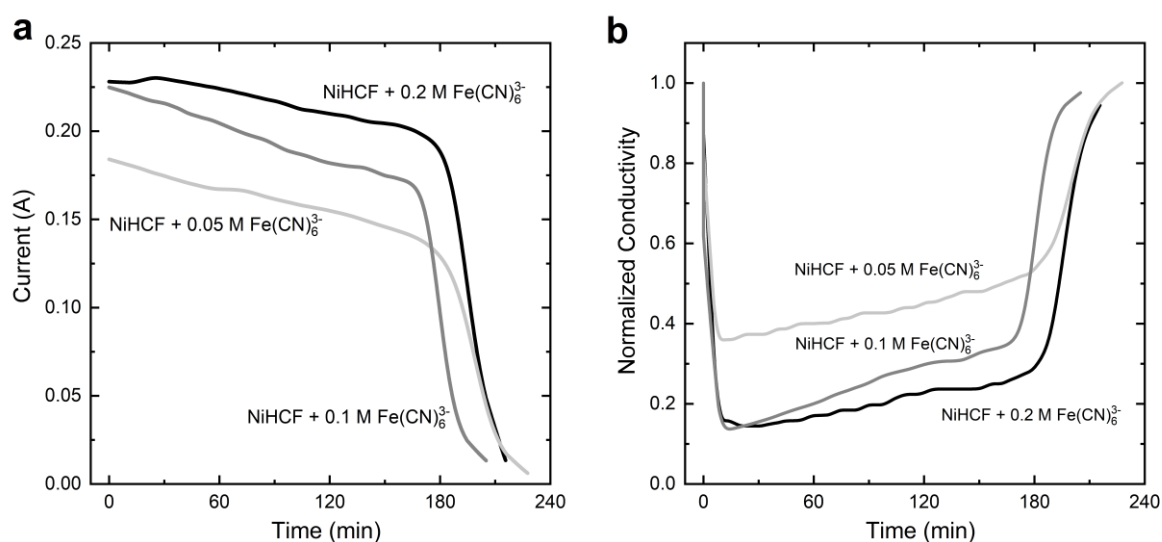

Figure A.4 – Desalination experiment with NiHCF and different concentrations of RM$_{ox}$ in the cathode flow electrode. FCDI cell current vs. time (a); Normalized conductivity of the water product (b).

Figure A.5 shows the energy consumption for the cathodic flow electrodes with NiHCF + 0.05, 0.1 and 0.2 M of $Fe(CN)_6^{3-}$.
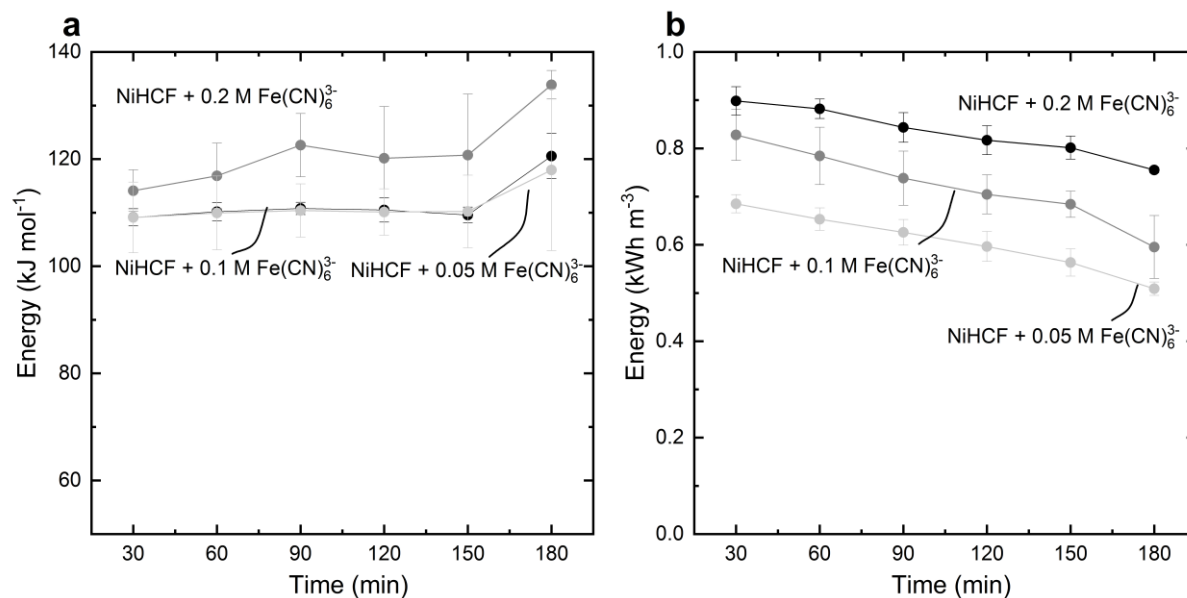

Figure A.5 – Energy consumption for the flow electrode with NiHCF + $Fe(CN)_6^{3-}$, AC + $Fe(CN)_6^{3-}$ and AC. In (a) the energy consumption per mol of removed salt. In (b), the energy consumption per volume of treated water.

Redox potential of NiHCF and electrolytes with RM

Figure A.6 shows the potential of the NiHCF during the discharge process, as shown in Figure 4.3b. The electrode's potential decreases as the material is reduced (higher state of discharge), and Na^+ ions intercalate the material. The curves for Fe(CN) were simulated using the Nernst equation. The standard potential of the reduction reaction of $Fe(CN)_6^{3-}$ to $Fe(CN)_6^{4-}$ used for calculations was 0.358 V (vs. SHE). Figure A.6 demonstrates that the higher the concentration of the redox mediator, the higher the potential difference between the NiHCF particles and the RM.
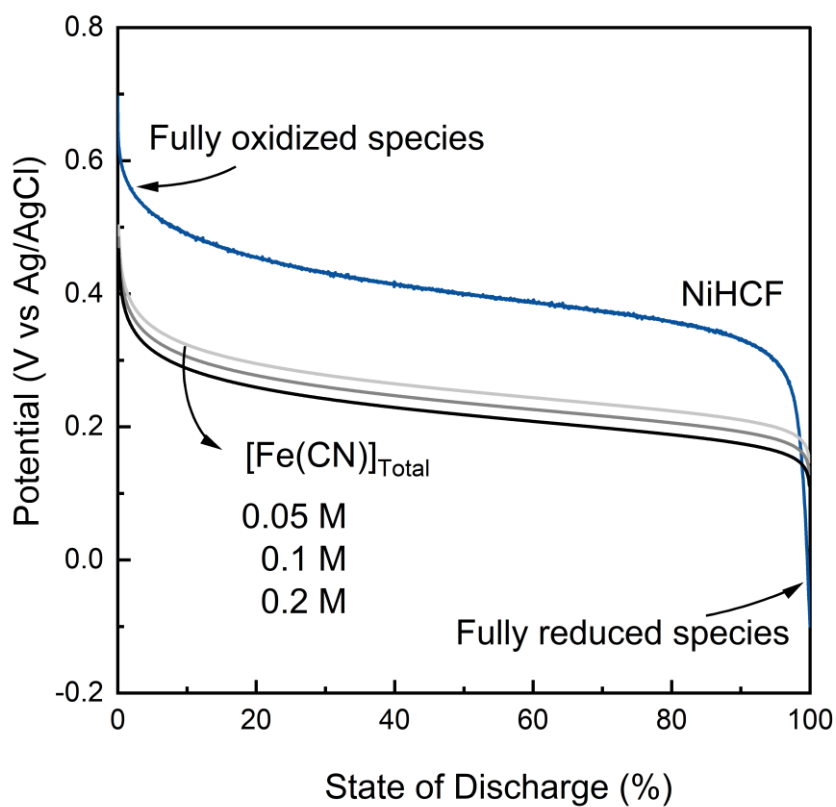
Figure A.6 – Potential of NiHCF sample during its discharge compared to the potential of several iron cyanide electrolytes calculated by the Nernst equation.

UV/vis and FT-IR spectroscopy

Figure A.7a and b show the full spectra obtained for the UV/vis of the electrolyte and the FT-IR of the NiHCF particles collected at several experiment times.
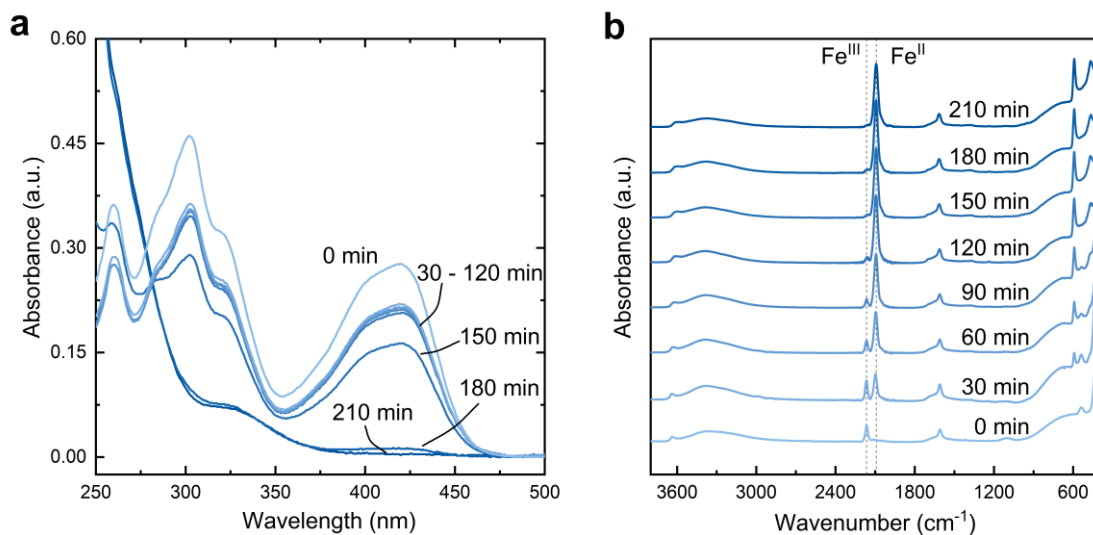
Figure A.7 – Spectra of NiHCF particles and electrolyte collected from the flow electrode reservoir at different desalination time intervals: UV/vis spectra of the electrolyte showing qualitatively the $[Fe(CN)_6]^{3-}$ concentration (a); FT-IR spectra showing the reduction of the NiHCF qualitatively (b).

Figure A.8 shows the current of the FCDI experiment where samples were collected from the flow electrode reservoir during the experiment. As discussed in the main text, around 150 min, the capacity of the NiHCF is theoretically reached.
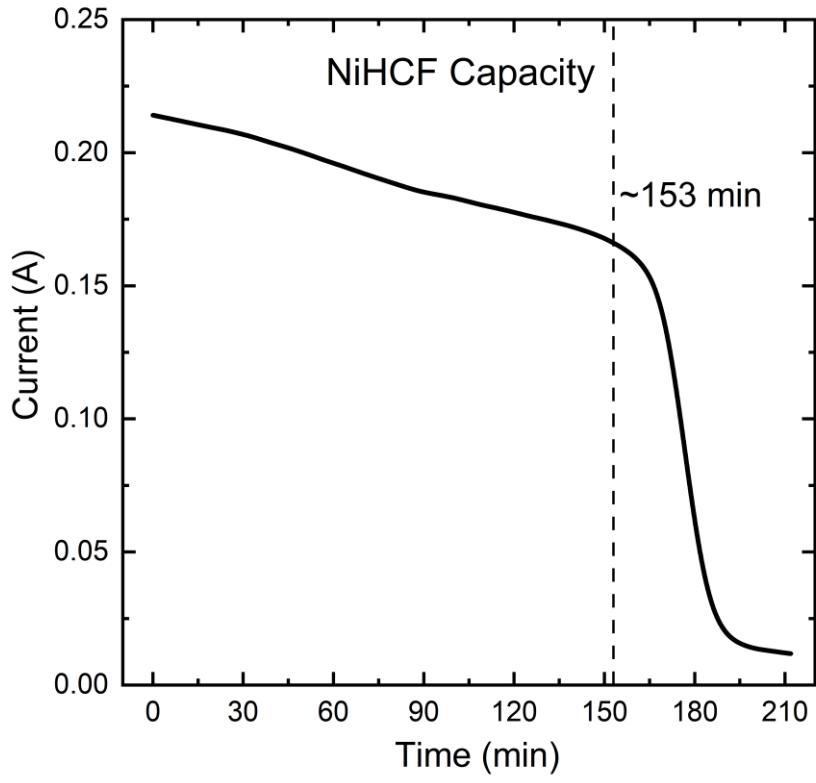
Figure A.8 – Current response of the FCDI cell during desalination experiment.

Appendix B

Eh-pH diagram for the Fe-H₂O and Fe-Cl-H₂O

For the proper operation of the FCDI system, it is required that iron species stay soluble in a broad pH and Eh range. In this way, prior to the preliminary experiments using iron chloride as an additive in the flow-electrode, thermodynamical analyses were carried out to evaluate the stability window of soluble species containing iron. A total iron concentration of 500 mM was chosen for the analyses, higher than the iron concentration in the FCDI experiments. An Eh-pH diagram of the system Fe-H₂O is shown in Figure B.1.
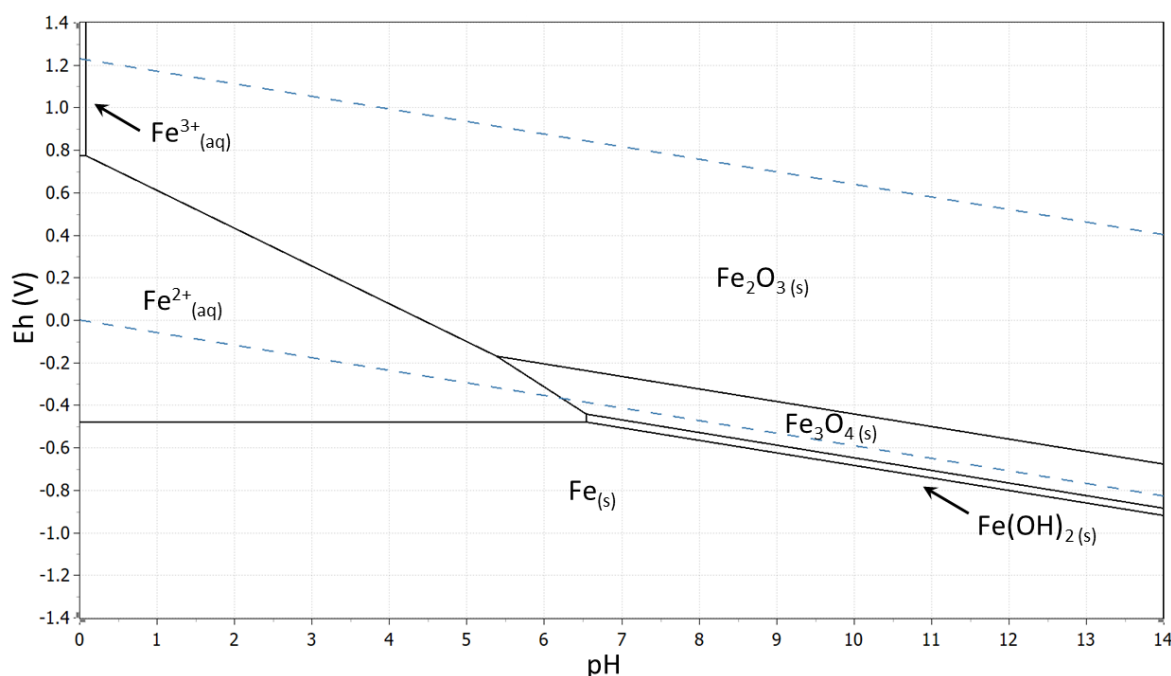

Figure B.1 – Eh-pH diagram of the system Fe-H₂O at 25 °C. The concentration of soluble iron in the system is 0.5 M (HSC v.9).

The diagram in Figure B.1 shows a small solubility region for the Fe^{3+}, approximately below pH 0.2. For practical application, that means that the flow-electrode must be kept below this pH in order to keep the redox pair Fe^{3+}/Fe^{2+} soluble. The species and their thermodynamical data used in the Eh-pH diagram are presented in Table B.1. All data was obtained in the study of (Gontijo et al., 2022).

Table B.1 – Standards Gibbs free energies of formation at 25°C of species used for Eh-pH diagram of the system Fe-H₂O.

Species	ΔG^0_f (kcal mol^{-1})	Species	ΔG^0_f (kcal mol^{-1})
Fe	0.014	$Fe^{3+}_{(aq)}$	-3.864
FeO	-58.358	$FeO^+_{(aq)}$	-53.093
Fe_2O_3	-177.900	$FeOH^+_{(aq)}$	-66.285
Fe_3O_4	-241.960	$FeOH^{2+}_{(aq)}$	-57.609
FeOOH	-116.989	$Fe(OH)_2^+_{(aq)}$	-109.731
$Fe(OH)_2$	-117.578	$Fe(OH)_3^-_{(aq)}$	-149.611
$Fe(OH)_3$	-168.610	$Fe(OH)_4^-_{(aq)}$	-201.361
$Fe^{2+}_{(aq)}$	-21.669	$Fe(OH)_4^{2-}_{(aq)}$	-185.823

The Eh-pH shown in Figure B.2 indicates that the most stable soluble Fe species at 0.5 M of Fe concentration and 1.5 M of Cl⁻ are $FeCl_2^+_{(aq)}$ – Fe^{III} – and $FeCl^+_{(aq)}$ – Fe^{II}. A much larger area of soluble species, especially for Fe^{III} species, is observed as chloride is added to the system. It can be concluded through this diagram that the flow-electrode pH can be increased up to pH 5 without precipitation of iron as Fe_2O_3. However, in our preliminary experiments, precipitation was observed starting from a pH of around 2.2. The chemical species used to calculate the diagram and their respective standards Gibbs free energies are presented in Table B.2.
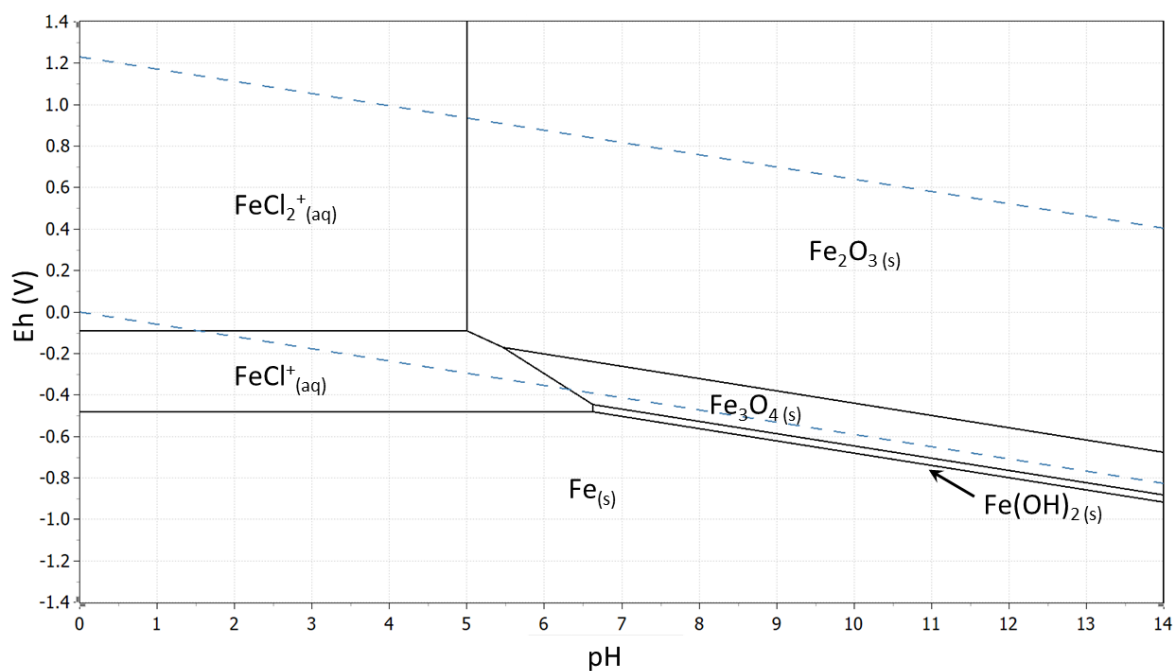
Figure B.2 – Eh-pH diagram of the system Fe-Cl-H₂O at 25 °C. The concentrations in the system are 0.5 M of soluble iron species and 1.5 M of free chlorine (HSC v.9).

Table B.2 – Standards Gibbs free energies of formation at 25°C of species used for Eh-pH diagram of the system Fe-Cl-H₂O. The data of containing chloride species was provided by the main data base of HSC chemistry v.9.

Species	ΔG^0_f (kcal mol^{-1})	Species	ΔG^0_f (kcal mol^{-1})
Fe	0.014	$Fe^{3+}_{(aq)}$	-3.864
$FeCl_2$	-72.145	$FeCl^+_{(aq)}$	-53.025
$FeCl_3$	-79.828	$FeCl^{+2}_{(aq)}$	-37.497
FeO	-58.358	$FeCl_2^+_{(aq)}$	-86.267
Fe_2O_3	-177.900	$FeO^+_{(aq)}$	-53.093
Fe_3O_4	-241.960	$FeOH^+_{(aq)}$	-66.285
FeOOH	-116.989	$FeOH^{2+}_{(aq)}$	-57.609
$Fe(OH)_2$	-117.578	$Fe(OH)_2^+_{(aq)}$	-109.731
$Fe(OH)_3$	-168.610	$Fe(OH)_3^-_{(aq)}$	-149.611
$Cl^-_{(aq)}$	-31.372	$Fe(OH)_4^-_{(aq)}$	-201.361
$Fe^{2+}_{(aq)}$	-21.669	$Fe(OH)_4^{2-}_{(aq)}$	-185.823

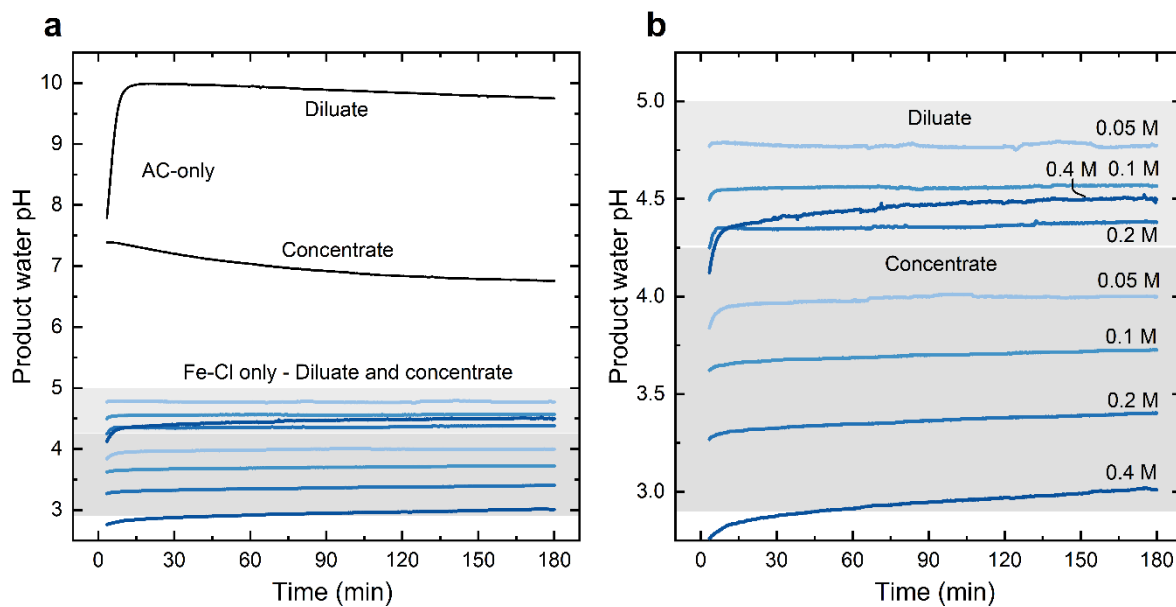# The pH of water streams in flow electrodes with AC-only and Fe-Cl-only

Figure B.3 – The pH of diluate and concentrate streams with flow electrodes with AC-only, and different concentrations of Fe-Cl-only. In (a), the pH of the AC-only system is compared to the pH of Fe-Cl-only. In (b), only the pH of Fe-Cl system is shown in detail.